Institute of Crop Science and Resource Conservation

Molecular Biology of the Rhizosphere

Linking spatial patterns of the rhizosphere microbiota with photosynthate dynamics in maize roots

Dissertation

zur Erlangung des Grades

Doktor der Agrarwissenschaften (Dr. agr.)

der Agrar-, Ernährungs- und Ingenieurwissenschaftlichen Fakultät

der Rheinischen Friedrich-Wilhelms-Universität Bonn

von

Sina Schultes

aus Haan, Deutschland

Bonn, 2025

Referentin: Prof. Dr. Claudia Knief

Korreferent: Prof. Dr. Michael Bonkowski

Tag der mündlichen Prüfung: 13.10.2025

Angefertigt mit der Genehmigung der Agrar-, Ernährungs- und Ingenieurwissenschaftlichen Fakultät der Rheinischen Friedrich-Wilhelms-Universität Bonn.

~ No amount of money ever bought a second of time ~

Tony Stark

Table of contents

List of abbreviations **1**

Summary **2**

Zusammenfassung **4**

1. Introduction **6**

1.1. Maize and its root system architecture 6

1.2. Recent advances in the phenotyping of roots 7

1.3. Photosynthate flux from the shoot to the root system and rhizosphere 8

1.4. The root system as a habitat for microorganisms 11

1.5. Mechanisms and spatial patterns of microbial colonization in the rhizosphere 13

1.6. Employing isotopic tracers to unravel the fate of photosynthates in roots and the rhizosphere (microbiota) 15

1.6.1. Radioactive isotopic tracers in plant sciences 15

1.6.2. Stable isotopic tracers in plant sciences 16

1.6.3. Stable isotopic tracers in microbial ecology 17

1.7. Aims and outline of the thesis 19

2. Results **22**

2.1. Soil texture and root system architecture impact the root-associated microbiota of maize 22

2.2. Photosynthate distribution determines spatial patterns in the rhizosphere microbiota of the maize root system 58

3. General discussion and conclusions **112**

3.1. Résumé 112

3.2. Root type and longitudinal section induce conserved spatial patterns in the rhizosphere microbiota 113

3.2.1. The root longitudinal section 113

3.2.2. Root types, their function, succession state and growth rate 114

3.2.3. Conserved spatial patterns point at robust mechanisms of rhizosphere organization 117

3.3. Photosynthates are heterogeneously distributed and released in the maize root system 118

3.4. Heterogeneous photosynthate distribution drives spatial patterns in the rhizosphere microbiota 121

3.5. Microbial microhabitats created by root morphology and photosynthate distribution 122

3.6. Additional factors contributing to microbial spatial variation 127

3.7. Practical relevance for plant breeding, microbiome engineering and modeling 128

3.8. Conclusion 130

4. Appendix **131**

4.1. Curriculum vitae 131

4.2. Danksagung 132

Bibliography **133**

List of abbreviations

AMF	Arbuscular mycorrhizal fungi
ASV	Amplicon sequence variant
bp	Base pair
CsCl	Cesium chloride
^{11}C	Carbon-11, an unstable, radioactive isotope of carbon
^{13}C	Carbon-13, a stable isotope of carbon
DNA/RNA-SIP	DNA/RNA stable isotope probing
db-RDA	Distance-based redundancy analysis
EA-IRMS	Elemental analyzer isotope ratio mass spectrometry
ITS	Internal transcribed spacer
LMM	Linear mixed model
MRI	Magnetic resonance imaging
PET	Positron emission tomography
MBq	Megabecquerel
mT/M	Millitesla per meter
NMDS	Non-metric multidimensional scaling
PERMANOVA	Permutational multivariate analysis of variance
SSU	Ribosomal small subunit
16S rRNA	16S ribosomal RNA, component of the prokaryotic SSU
18S rRNA	18S ribosomal RNA, component of the eukaryotic SSU

Summary

The rhizosphere serves as the boundary layer between plant roots and soil, enabling nutrient and water uptake while facilitating interactions with microorganisms through rhizodeposition. Despite its importance for plant health, the spatiotemporal dynamics of rhizodeposition and their effect on microbial community assembly in the rhizosphere remain poorly understood, particularly in functionally complex root systems. To bridge this gap, we investigated how spatial patterns of photosynthate distribution impact the assembly of prokaryotic, fungal, and cercozoan rhizosphere microbiomes in the maize rhizosphere.

Firstly, we explored small-scale spatial variation in the prokaryotic community within the maize rhizosphere, rhizoplane and endosphere. By combining the non-invasive root system monitoring technique magnetic resonance imaging (MRI) with 16S rRNA amplicon sequencing, we identified spatial patterns in prokaryotic diversity and community structure that varied sequentially across root types, along root longitudinal sections, as well as with root growth rates and root age. The consistency of these patterns across three different soil textures suggested the presence of conserved mechanisms governing microbiome spatial organization.

Secondly, we linked the spatial patterns of the rhizosphere microbiota to root photosynthate distribution. By labeling fresh photosynthates with the radioactive isotope ^{11}C and visualizing allocation via positron emission tomography (PET) and MRI, we found that photosynthate distribution is highly heterogeneous, varying between root types, along the root axis, and over time, with pronounced accumulations at young crown root tips. Corresponding labeling with and quantification of the stable isotope ^{13}C in root tissue and the rhizosphere revealed similar patterns, implying that root-internal photosynthate levels regulate rhizodeposition. Amplicon sequencing confirmed that these heterogeneities significantly shape prokaryotic, fungal and cercozoan rhizosphere communities, fueling colonization differences between root types and sections. Variability at root tips arose from heterogeneous photosynthate allocation and priority effects, while microbial patterns at root bases reflected succession during root maturation and shifting photosynthate distribution. Using DNA stable isotope probing (DNA-SIP), we identified prokaryotic, fungal and cercozoan consumers of ^{13}C-labeled photosynthates and found that specific consumer taxa profited in distinct regions with varying photosynthate allocation. This indicates that photosynthate heterogeneities, along with root architectural traits, drive microhabitat formation and thus niche differentiation, as well as microbial food web establishment in the complex root system of maize.

Overall, our findings highlight the critical role of spatially heterogeneous photosynthate allocation in shaping the rhizosphere microbiome. This introduces a new mechanism governing microbial colonization of the rhizosphere but also deepens our understanding of spatiotemporal rhizosphere organization, paving the way for future strategies to enhance plant health and resilience.

Zusammenfassung

Als Schnittstelle zwischen Wurzeln und Boden, ermöglicht die Rhizosphäre die Aufnahme von Wasser und Nährstoffen und die Interaktion mit Mikroorganismen durch Rhizodeposition. Trotz ihrer Bedeutung für die Pflanzengesundheit sind die raumzeitlichen Dynamiken der Rhizodeposition und deren Einfluss auf die mikrobielle Gemeinschaftsbildung in der Rhizosphäre, insbesondere in funktionell komplexen Wurzelsystemen, noch unzureichend erforscht. Darum untersuchten wir, wie räumliche Muster der Photoassimilatverteilung die prokaryotischen, pilzlichen und cercozoischen Gemeinschaften in der Mais Rhizosphäre beeinflussen.

Zunächst analysierten wir kleinräumige Variationen in der prokaryotischen Gemeinschaft innerhalb der Rhizosphäre, der Rhizoplane und der Endosphäre von Mais. Durch die Kombination von nicht-invasiver Magnetresonanztomographie (MRT) mit 16S-rRNA-Amplicon-Sequenzierung identifizierten wir räumliche Muster in der prokaryotischen Diversität und Gemeinschaftsstruktur. Diese variierten systematisch zwischen Wurzeltypen, entlang der Wurzellängsachse sowie in Abhängigkeit von Wachstumsraten und Wurzelalter. Die Konsistenz dieser Muster in drei verschiedenen Bodentexturen deutet auf fundamentale Mechanismen hin, die die räumliche Organisation des Mikrobioms steuern.

Darüber hinaus verknüpften wir die räumlichen Muster der Rhizosphärenmikrobiota mit der Verteilung von Assimilaten im Wurzelsystem. Durch Markierung frischer Assimilate mit dem radioaktiven Isotop ^{11}C und deren Visualisierung mittels Positronen-Emissions-Tomographie (PET) und MRT stellten wir fest, dass die Assimilatverteilung im Wurzelinneren hochgradig heterogen ist. Sie variiert zwischen Wurzeltypen, entlang der Wurzelachse und über die Zeit, mit ausgeprägten Anreicherungen an jungen Kronenwurzelspitzen. Eine entsprechende Markierung mit dem stabilen Isotop ^{13}C und dessen Quantifizierung in Wurzelgewebe und Rhizosphäre zeigten ähnliche Muster und legen nahe, dass die wurzelinterne Assimilatkonzentration die Rhizodeposition steuert. Amplicon-Sequenzierungen bestätigten, dass diese Heterogenitäten prokaryotische, pilzliche und cercozoische Gemeinschaften der Rhizosphäre maßgeblich prägen und Unterschiede in der Besiedlung zwischen Wurzeltypen und -abschnitten fördern. Variabilität an den Wurzelspitzen ergab sich aus heterogener Assimilatverteilung und Prioritätseffekten, während sie an Wurzelbasen auf die mikrobielle Sukzession während der Wurzelreifung und sich verändernde Assimilatverteilung zurückzuführen war. Mittels DNA stable isotope probing (DNA-SIP) identifizierten wir prokaryotische, pilzliche und cercozoische Konsumenten von ^{13}C-markierten Assimilaten und fanden heraus, dass bestimmte Assimilat konsumierende Arten in bestimmten Regionen mit unterschiedlicher Assimilatverteilung profitierten. Dies zeigt, dass Assimilatheterogenitäten zusammen mit strukturellen Wurzeleigenschaften die Bildung von Mikrohabitaten sowie den Aufbau des mikrobiellen Nahrungsnetzes im komplexen Wurzelsystem von Mais steuern.

Insgesamt unterstreichen unsere Ergebnisse die zentrale Rolle der räumlich heterogenen Assimilatverteilung bei der Strukturierung des Rhizosphärenmikrobioms. Dies offenbart einen neuen Mechanismus der mikrobiellen Gemeinschaftsbildung, vertieft aber auch unser Verständnis der raumzeitlichen Organisation der Rhizosphäre und ebnet den Weg für mögliche Strategien zur Förderung der Pflanzengesundheit und -resilienz.

1. Introduction

1.1. Maize and its root system architecture

Maize (*Zea mays*) is a commercially important cereal crop and, alongside rice and wheat, one of the world's three most important staple foods (Shiferaw et al., 2011). Its well-characterized genome and rich history of genetic studies covering a high intraspecific diversity (Chen et al., 2023), make maize a frequently used model organism in plant sciences. Insights from studying maize may be easily transferred to understand other members of the family Poaceae due to their physiological similarity.

Like other cereals, maize has a complex root system architecture comprising seed-borne, embryonic roots and shoot-borne, post-embryonic roots (Chapter 1 Fig. 1a). Extensive descriptions on maize root system architecture are provided by Hochholdinger et al. (2024) and briefly summarized here. The primary root is the first seed-borne root to emerge between 2-3 days after sowing and usually grows straight down into the substrate (Tai et al., 2016). The emergence of several seminal roots from the scutellar node completes the seed-borne root system, that mainly supports the plant during the early seedling stage (Hochholdinger & Tuberosa, 2009). At later developmental stages, the functions of the seed-borne root system are, in most cultivars, taken over by the shoot-borne root system that emerges from nodes above the mesocotyl. The shoot-borne root system comprises crown roots originating from around six consecutive belowground nodes (or whorls), and brace roots emerging from approximately three consecutive aboveground nodes (Tai et al., 2016). The first few belowground internodes do not elongate, resulting in a dense area of stacked nodes just above the mesocotyl (Hochholdinger, Woll, et al., 2004). Crown roots emerging from lower nodes are smaller in diameter, while crown roots emerging from higher nodes have a larger diameter and a steeper rooting angle. Generally, the number of shoot-borne roots increases from lower to higher nodes (Yu et al., 2014). While crown roots are primarily involved in nutrient and water absorption, brace roots mainly provide stability and lodging resistance. All roots except brace roots without soil contact form lateral roots. Lateral roots make up a major part of the root system's biomass and play a central role in nutrient and water uptake (Hochholdinger, Woll, et al., 2004).

While being largely conserved within species and cultivars, root system architecture still shows a high plasticity in response to soil conditions. Examples include responses to water availability like drought or flooding (Ceolin et al., 2024), nutrient deficiencies (Lopez et al., 2023), salinity stress (Zou et al., 2022) or mechanical impedance like soil compaction (Pandey & Bennett, 2024). Therefore,

monitoring root system dynamics is vital to understand plant-soil interactions. These measurements are, however, complicated by the opaque nature of soil.

1.2. Recent advances in the phenotyping of roots

The most simple and classical approach of root phenotyping is root excavation and root washing followed by manual scoring of root traits; a precise but time-intensive method called “shovelomics”. Although the shovelomics approach is useful in field experiments (Trachsel et al., 2011) and can be extended by computational image analysis (e.g. WinRHIZO), it remains a destructive approach that does not allow to monitor the root growth of an individual plant over an extended period of time. This problem is at least partially solved by rhizotrons/rhizoboxes (Nagel et al., 2012), i.e. flat, transparent containers filled with soil or a transparent medium allowing for camera-based, continuous measurement of root development. Even more promising for non-invasive, 3D monitoring of root growth are magnetic resonance imaging (MRI) and X-ray computed tomography (X-ray CT) (Atkinson et al., 2019). In contrast to rhizoboxes/rhizotrons, a complete root tree model can be extracted for plants scanned using MRI or X-ray CT. MRI relies on magnetic fields and radiofrequency pulses to manipulate the magnetic spin of protons in hydrogen atoms, creating detailed images of water-holding tissues. In contrast, X-ray CT involves passing an X-ray beam through a sample and measuring the beam’s attenuation, which highly depends on sample density (Metzner et al., 2015). Due to these differing physical principles, the two techniques are suited to different types of samples. X-ray CT, especially synchrotron X-ray CT is particularly useful for analyzing detailed root structures (e.g. fine roots, root hairs) in physically small samples (Keyes et al., 2017), whereas MRI is more advantageous for larger pots and studies involving a higher soil water content, with the option to explore water mobility within roots and in the soil (Metzner et al., 2015). While both non-invasive, 3D imaging methods can provide valuable insights into root system plasticity, they do not offer the possibility of investigating an essential interaction between roots and their surroundings: rhizodeposition.

1.3. Photosynthate flux from the shoot to the root system and rhizosphere

Plant photosynthates refer to all organic compounds assimilated by plants during the process of photosynthesis. In plants performing C3 and C4 photosynthesis, photosynthates are primarily produced during daylight hours, while this process may take place overnight in plants performing CAM photosynthesis. Mature green leaves are the main site of photosynthate production, although some other green tissues can, to some extent, contribute to their assimilation. Glucose molecules synthesized in the chloroplasts are generally converted into sucrose before being transported to sink plant tissues. Sucrose is then transferred to specialized parenchyma cells, i.e. companion cells adjacent to the phloem and enters the phloem for long-distance transport. The driving force of sucrose transport in the phloem is a combination of osmotic and hydrostatic pressure differences between the source and sink tissues. In source tissues, the osmotic potential caused by the high concentration of sucrose leads to a water inflow from surrounding cells into the phloem, where the increased water pressure then powers the flow towards the sinks (Gamalei, 2002). In sink tissues, sucrose is unloaded and actively metabolized or stored as starch. The proportion in which photosynthates are allocated to the various sink tissues highly depends on the plant species, the plant's developmental stage and on environmental conditions.

A considerable sink for photosynthates is the root system. In cereals, up to 20-30% of assimilated photosynthates are allocated into the root system (Kuzyakov et al., 2000), where they are stored, used as an energy source for root growth, for water and nutrient acquisition or secreted into the surrounding soil. Generally, annual crops allocate more assimilated carbon to the shoot and less to the roots than perennials, with belowground allocation peaking in the first two months of growth (Pausch & Kuzyakov, 2018). In addition to photosynthates that are mostly excreted in the form of simple sugars, plant roots also release a variety of other primary (e.g. amino acids, proteins, organic acids) and secondary metabolites (e.g. terpenoids, phenolics) (Philippot et al., 2013). These compounds are released by different mechanisms of rhizodeposition (Chapter 1 Fig. 1b), such as root exudation, mucilage secretion, and the shedding of root cap cells (Nguyen, 2003). Other sources also count volatile compounds, the direct loss of photosynthates to symbionts and cell debris, e.g. from damaged root hairs to the processes of rhizodeposition (Jones et al., 2009; Oburger & Jones, 2018). Root exudation is primarily fueled by passive diffusion due to an osmotic gradient from the cytoplasm to the soil matrix; but can be accelerated by passive or active transport through membrane channels (Oburger & Jones, 2018). In maize, 79% of the root exudates were found to be water-soluble and mainly consisted of carbohydrates (64%), amino acids (22%) and organic acids (14%) (Hütsch et al., 2002). As low molecular weight compounds (< 1000 Da), recently assimilated photosynthates

contribute considerably to root exudation in quantitative terms (Badri & Vivanco, 2009; Farrar et al., 2003; Oburger & Jones, 2018). In contrast, mucilage mainly consists of high molecular weight compounds (> 1000 Da), i.e. polysaccharides and up to 6% proteins (Jones et al., 2009). After being synthesized in the Golgi apparatus of root cap cells, mucilage is transported to the cell membrane in vesicles and actively secreted by exocytosis (Nguyen, 2003). Root cap cells are continuously renewed as the root tip moves through the soil, resulting in their continuous shedding as another release mechanism of high molecular weight compounds (Farrar et al., 2003). When compared to root exudation and mucilage secretion, root cap cell shedding only makes up a small proportion of root carbon loss (Jones et al., 2009). The rate of exudation is typically higher in seedlings and decreases with increasing plant age, which emphasizes temporal dynamics (Hütsch et al., 2002). While mucilage secretion and root cap cell shedding are processes that can be easily localized to the root tip (Jones et al., 2009), the spatial patterns of root exudation are less clearly resolved. It is generally accepted that root tips and the elongation zone are hotspots of root exudation (Doan et al., 2017; Sasse et al., 2018). However, root areas where lateral roots emerge are also recognized sites of exudate loss. Particularly in complex root systems, the localization of the different rhizodeposition processes is not yet fully charted. In experimental practice, it remains difficult to distinguish between root exudates and other rhizodeposits.

Overall, rhizodeposition of photosynthates and various other organic compounds into the surrounding soil serves different purposes: nutrient mobilization, lubing and protecting root tips during growth, influencing soil properties such as aggregation and facilitating plant-microbe interactions. For root-associated microorganisms, rhizodeposition is a major source of organic carbon, which is generally limited in the bulk soil. It is estimated that between 64 and 86% of the excreted carbon is rapidly metabolized by root-associated microorganisms (Hütsch et al., 2002).

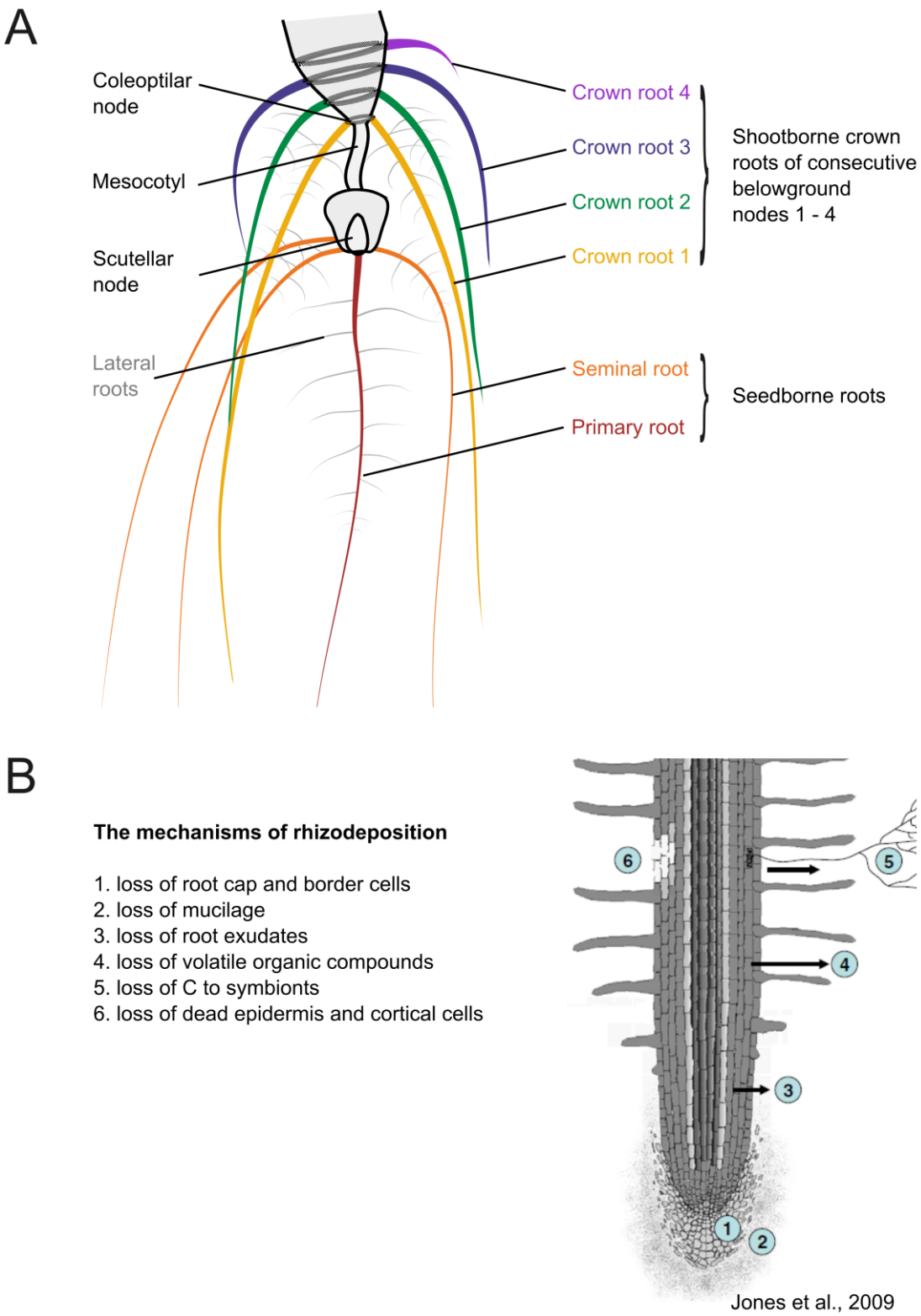

Fig. 1 Schematic overview of the maize root system at ~3 weeks after sowing **(a)** and the mechanisms of rhizodeposition **(b)** as adapted from Jones et al. (2009).

1.4. The root system as a habitat for microorganisms

As nutrients in the bulk soil are often limited, soil microorganisms mainly reside in microbial hotspots (Kuzyakov & Blagodatskaya, 2015), e.g. associated to plant roots, in the detritusphere, on aggregate surfaces or in biopores created by soil fauna and decaying plant roots (Wendel et al., 2022). Microorganisms associated with plant roots are distributed across three main habitats: the rhizosphere, rhizoplane, and endosphere. Microorganisms found in these habitats include bacteria, archaea, fungi, protists, algae and viruses (Mendes et al., 2013).

The rhizosphere is defined as the soil area directly adjacent to the roots. Its precise extension is continuously discussed, as it can vary with soil parameters like compaction, aggregation, and soil moisture content (Kuzyakov & Razavi, 2019). However, it is generally confined to the lower millimeter scale (Razavi et al., 2016). A good rule of thumb for experimental scientists is that the rhizosphere is the soil portion that is still adhering to the roots when a plant is dug up and gently shaken. In contrast to the bulk soil, the rhizosphere is rich in organic carbon due to rhizodeposition processes (Schimel & Weintraub, 2003) and thus more densely populated by microorganisms (Watt, Hugenholtz, et al., 2006). At the same time, prokaryotic alpha diversity declines in the rhizosphere as compared to the bulk soil (Ling et al., 2022). However, microbial activity and nutrient turnover are generally higher in the rhizosphere than in the bulk soil (Kuzyakov & Blagodatskaya, 2015). Typically, bacteria of the phylum Proteobacteria are enriched in the maize rhizosphere as compared to the bulk soil, while phyla Acidobacteria, Planctomycetes and Verrucomicrobia are more abundant in the bulk soil (Peiffer et al., 2013). Bacteria encountered in the maize rhizosphere frequently belong to the genera *Burkholderia, Sphingobium, Arthrobacter, Bradyrhizobium, Massilia, Bacillus, Dyella, Azospirillium and Ralstonia* (Hünninghaus et al., 2019; Li et al., 2014). While some species (*Bacillus spp., Azospirillum spp. and Pseudomonas spp.*) may promote plant growth by their ability to stimulate root growth, solubilize nutrients or produce growth promoting substances, other genera contain potential pathogens to maize (e.g. *Ralstonia*). Dominant fungi in the maize rhizosphere mostly belong to the Ascomycota, Basidiomycota and Glomeromycota (Hünninghaus et al., 2019; Kong et al., 2020). Some commonly encountered genera are *Aspergillus, Trichoderma, Fusarium, Mucor, Rhizoctonia, Penicillium* and *Cladosporium* (Cavaglieri et al., 2009)*;* some of which contain strains that can exhibit plant growth promoting properties (Adedayo & Babalola, 2023). Protists are a diverse group of mostly unicellular eukaryotes (Dumack & Bonkowski, 2021). They are polyphyletic, i.e. they are grouped based on shared characteristics rather than shared ancestry, which complicates the analysis of their community structure by 18S amplicon sequencing. Many protists follow a predatory life style, with predatory protist populations typically increasing in the rhizosphere as

compared to the bulk soil (Bonkowski et al., 2021). The Cercozoa and Endomyxa within the Rhizaria are dominant protist phyla in soil environments (Dumack et al., 2020; Khanipour Roshan et al., 2021). Within the Cercozoa of the maize rhizosphere, bacterivore and eukaryvore Glissomonadida and bacterivore and omnivore Cercomonadida are especially common (Rüger et al., 2022; Yim et al., 2022), as well as the cercozoan families Allapsidae and Paracercomonadidae and the Amoebozoan family Filamoebidae (Taerum et al., 2022), while the bulk soil is colonized by mostly bacterivore Thaumatomonadida (Cercozoa) (Rüger et al., 2022). The selective pressure of predation by protists, which are often specialized grazers, significantly shapes the community composition of their bacterial prey (Trap et al., 2016). Additionally, through predation on other microorganisms, protists release significant amounts of nutrients, especially nitrogen, back into the rhizosphere (Bonkowski, 2004). This mobilization of nitrogen increases the transport of N by arbuscular mycorrhizal fungi (AMF) and thus, indirectly, benefits plant health (Koller et al., 2013).

The rhizoplane is defined as the root surface. Microbial inhabitants of the rhizoplane directly attach to the root surface using structures like pili or fimbriae (Wheatley & Poole, 2018) and can form mutualistic relationships with the plant host, e.g. for nutrient acquisition, plant growth promotion or pathogen suppression. Since the rhizoplane functions as a boundary layer between the rhizosphere and endosphere, its microbial community often is a blend of rhizosphere and endosphere communities. For instance, endophytes not already present in the seed must enter the endosphere via the root surface, mostly through cracks formed during lateral root development (Monteiro et al., 2008). Thus, they temporarily become a part of the rhizoplane community.

The endosphere refers to the root interior, where microorganisms mostly reside in the intercellular space or the vascular vessels (Liu et al., 2006). An extensive overview on the endophytes of maize is provided by Wallace and May (2018) and briefly summarized here. Highly abundant bacterial phyla in the overall maize endosphere include the Proteobacteria, Bacteroidetes, Chloroflexi, Firmicutes and Actinobacteria, with over 90% belonging to Proteobacteria or Firmicutes (Beirinckx et al., 2020; Wallace & May, 2018). Beirinckx et al. (2020) identified 12 main families enriched in the endosphere of maize roots across experiments, amongst them the Caulobacteraceae, Comamonadaceae, Flavobacteriaceae, Oxalobacteraceae, Rhizobiaceae and Streptomycetaceae. Some genera are known for plant growth-promoting activities, such as the ability to fix nitrogen or solubilize phosphates, e.g. the genera *Azospirillum*, *Herbaspirillum* and *Burkholderia* (Wallace & May, 2018). Most fungal inhabitants of the maize endosphere belong to the Ascomycota in the classes Dothideomycetes and Sordariomycetes. Some commonly found genera include pathogens like *Alternaria*, *Fusarium*, and *Acremonium*, but also beneficial organisms such as *Trichoderma* or AMF (Wallace & May, 2018). AMF (phylum Glomeromycotina) form mutualistic relationships with maize

in which the fungus enhances plant nutrient uptake and receives photosynthates in return (Sasvári et al., 2011). Although protists may indirectly modify the endosphere bacterial community composition by grazing in the rhizosphere, predatory protists are not known to colonize the root endosphere (Asiloglu et al., 2024).

Even though the rhizosphere, rhizoplane and endosphere are habitats with distinct characteristics, their microbial communities are not unique and often overlap when microorganisms migrate between layers, e.g. during the establishment of the endosphere microbial community. While the process of community establishment in the endosphere is often based on host selection of those microorganisms already present in the rhizosphere and those inherited via the seed, there are more factors to be considered in the community assembly in the rhizosphere. Especially in complex root systems with high spatial heterogeneity, the process of microbial community assembly is not yet well understood.

1.5. Mechanisms and spatial patterns of microbial colonization in the rhizosphere

Like with every other ecological community, the assembly of the rhizosphere microbial community is influenced by a multitude of factors, including abiotic conditions as well as the biotic interactions between microorganisms and between the plant host and microorganisms. Central abiotic determinants include the soil type, soil aggregation, soil water content, pH and nutrient availability (Yim et al., 2022). Typical biotic interactions are the selection by the plant host, the deterministic top-down control of microorganisms by secondary consumers (e.g. the aforementioned grazing protists but also predatory bacteria), the bottom-up control by the availability of primary consumers and rhizodeposits, and the competition for resources between species of the same niche (Gao et al., 2018). Soil traits have a particularly high impact on the rhizosphere microbial community composition (Marschner et al., 2001; Yim et al., 2022), as they determine which microorganisms can be recruited from the “seed bank” of the bulk soil (Lennon & Jones, 2011). Soil types differ in pore size and habitat connectivity (Hemkemeyer et al., 2018; Seaton et al., 2020). Clay has the smallest pore size, followed by silt and sand. Loam, which is a mixture of sand, silt, and clay, has larger pore spaces than pure clay or silt. Soil types with smaller pore size generally have a higher water retention and cation exchange capacity as well as a low connectivity, traits which were observed to increase bacterial diversity (Hemkemeyer et al., 2018; Seaton et al., 2020).

1. Introduction

In root-associated habitats, the plant host plays a central role in shaping the composition of the microbial community. Through rhizodeposition and physical root characteristics, plant hosts provide an environment that selects for specific microbial species, which is why the rhizosphere microbiota is distinct from bulk soil and between plant species (Berg & Smalla, 2009). Generally, the rhizosphere is a habitat with high spatial heterogeneity, where gradients of nutrient and water availability, pH and soil aggregation vary both with the distance from roots and along roots. A rough concept of microbiome assembly along the radial root axis is already generally accepted (Bulgarelli et al., 2013). Through an exponential increase in rhizodeposit concentration with increasing vicinity to the root (Gao et al., 2011; Hafner et al., 2014; Jones et al., 2004), microorganisms are recruited from the bulk soil, where carbon sources are generally limiting (Liu et al., 2022). This is followed by a selection of root endosphere microorganisms, largely controlled by host genotypic factors (Bulgarelli et al., 2013). This is demonstrated by a microbial diversity decrease in the rhizosphere, which decreases even further in the rhizoplane and especially in the endosphere (Becker et al., 2022). Additionally, there is increasing evidence for community recruitment processes along the longitudinal root axis. Along roots, different root zones such as the root tip, elongation zone, root hair zone and mature root regions produce distinct blends of rhizodeposits that have been observed to shape microbial communities (Aulakh et al., 2001; Chaparro et al., 2014). Root tips are often colonized by copiotrophic bacteria due to their capability to rapidly exploit nutrient-rich exudates (Ho et al., 2017; Maloney et al., 1997). The root tip and elongation zone are considered the root sections harboring the highest numbers of microorganisms (DeAngelis et al., 2009; Jaeger et al., 1999; Massalha et al., 2017). In contrast, microfaunal populations in the rhizosphere tend to reach a maximum in the older regions of the root system rather than at the root-tip (Griffiths et al., 2007). Older roots and basal root regions often harbor a distinct microbial community than root tips. Authors observed clear differences in bacterial and archaean community composition between the root tip, root hair and the mature root zone (DeAngelis et al., 2009) and in prokaryotic and protistan community composition from the root tip along the root hair zone to the primordia and lateral roots (Rüger et al., 2021). Nevertheless, drawing conclusions about how biotic interactions between microorganisms potentially contribute to colonization patterns remains difficult, as no study has yet examined all prokaryotic, fungal and cercozoan communities on the same model plant.

How microbial assembly processes differ between root types is, however, less resolved. Here, several processes might contribute to microbial spatial variation. Zai et al. (2021) found that root diameter is linked to microbial community composition. At the same time, different blends of root exudates between root types are also reported to influence microbial community composition (Kawasaki et al., 2016). Yu et al. (2018) observed differences in AMF colonization between maize

axial and lateral roots. Also, roots with a longer residence time in soil might harbor a different microbial community than very young roots (Watt, Silk, et al., 2006).

Researching spatial patterns of photosynthates in the root system and rhizosphere and in association with their uptake by rhizosphere microorganisms has proven challenging. Destructive rhizodeposit sampling in soil is problematic as soluble rhizodeposits are quickly absorbed by the solid phase or metabolized by the rhizosphere microbiome (Oburger & Jones, 2018). Attempts to characterize the microbial photosynthate consumers by small-scale sampling are heavily biased as the community also contains inactive microorganisms and members that are rather involved in soil organic matter breakdown than photosynthate consumption. Fortunately, isotopic labeling techniques present a helpful tool to trace photosynthates in the root-soil-microorganism continuum.

1.6. Employing isotopic tracers to unravel the fate of photosynthates in roots and the rhizosphere (microbiota)

1.6.1. Radioactive isotopic tracers in plant sciences

A radioactive isotope is an unstable form of an element with the same number of protons but a different number of neutrons, causing it to decay over time and release energy in the form of radiation. In plant sciences, radioactive isotopes are valuable tools to track and quantify molecules throughout plant metabolic processes, as their radioactive emissions can be detected. Two of the most commonly applied radioactive isotopes in plant sciences are ^{32}P (Yamawaki et al., 2011) and ^{14}C (Pausch & Kuzyakov, 2011). While ^{32}P is used to investigate phosphorus uptake and transport in plants, ^{14}C is used to study carbon assimilation during photosynthesis and its allocation to different sinks. Labeling can either be conducted for a short period of time (pulse labeling) or for the whole plant growth period (continuous labeling). ^{14}C pulse labeling is mainly used to trace the fate of recently assimilated photosynthates in a specific growth stage, while continuous labeling is better suited to estimate the partitioning of total plant derived carbon throughout a whole growth period (Kuzyakov et al., 2000). Studies aiming to investigate root photosynthate partitioning with ^{14}C typically grow plants in rhizoboxes and label them in an atmosphere containing $^{14}CO_2$ for a few hours. This is then followed by either placing a phosphor imaging plate directly onto the rhizobox sample or onto a filter paper that previously captured the sample's root exudates (Holz et al., 2019). While ^{14}C labeling and phosphor imaging represent a valuable tool to investigate and quantify ^{14}C allocation in roots and exudates, it also comes with limitations. The long half-life of ~5700 years makes ^{14}C suitable for both, continuous and pulse labeling, but also complicates the application of independent

^{14}C pulses throughout plant growth. Additionally, the plant growth in rhizoboxes only enables imaging of a part of the root system at the same time (Kuzyakov et al., 2000). For pulse labeling studies, the carbon isotope ^{11}C is advantageous, as its short half-life (20.4 min) allows the application of independent pulses throughout plant life and its high detection limit enables the labeling of a leaf part only while still being able to trace the label throughout the plant (Kuzyakov et al., 2000). In combination with positron emission tomography (PET), $^{11}CO_2$ labeling even allows for 3D non-invasive imaging and quantification of photosynthate allocation in the shoot and root system (Hubeau & Steppe, 2015) with a spatial resolution of below 2 mm (Hinz et al., 2024). During an experiment applying $^{11}CO_2$ labeling and PET, plants are pulse labeled with radioactive $^{11}CO_2$ for several minutes, which is then assimilated, converted into labeled photosynthates and transported into plant tissues. In the following ~2.5 hours, the transport and allocation of labeled photosynthates can be non-invasively imaged and quantified by PET. For imaging, PET relies on the β^+ decay of ^{11}C, during which a proton is converted into a positron, a neutron and an electron neutrino. Once the positron meets an electron within the plant tissue, two γ-rays are emitted in an antiparallel way during a process called annihilation. These γ-rays are then detected by scintillators and photodetectors (Hubeau & Steppe, 2015; Waarde, 2012). In combination with root phenotyping methods like MRI or X-ray CT, PET represents a great tool to investigate belowground carbon flow in correlation with root structure and growth speed (or water flow after labeling with ^{15}O). An important limitation of PET in the investigation of the fate of belowground photosynthates is, however, the inability to discriminate between root-internal labeled photosynthates and labeled photosynthates that have been secreted into the rhizosphere. Here, employing complementary stable isotope analyses poses a better alternative.

1.6.2. Stable isotopic tracers in plant sciences

A stable isotope is a version of an element that has the same number of protons but a different number of neutrons. Unlike radioactive isotopes, stable isotopes do not undergo radioactive decay over time, as their combination of protons and neutrons form a nucleus with a balanced energy state. In plant sciences, stable isotopes are used to measure photosynthesis efficiency (e.g. by ^{18}O) and trace plant nutrient flows (e.g. by ^{15}N). The carbon isotope ^{13}C can be used to explore the allocation of photosynthates within plant tissues and into the soil. During ^{13}C labeling experiments, the plants are placed in an atmosphere containing $^{13}CO_2$, which is then assimilated, converted into labeled photosynthates and transported into plant tissues and into the soil, where it can be easily differentiated from unlabeled soil organic matter. As with radioactive ^{14}C, ^{13}C labeling can either be

conducted for a short period (pulse labeling) or for the whole plant growth period (continuous labeling).

A powerful technique to measure $^{13}C/^{12}C$ (or $^{15}N/^{14}N$) isotopic ratios in plant or soil samples from labeling studies is EA-IRMS, a combination of an elemental analyzer (EA) with an isotope ratio mass spectrometer (IRMS). During an EA-IRMS measurement, dried and ground samples are first combusted in the EA, yielding CO_2 and N_2, which are then separated on a gas chromatography column (Ogawa 2010). Gases are then introduced into the IRMS, where they are ionized, accelerated and separated according to their mass-to-charge ratio, where heavier particles have a higher radius in a magnetic field than lighter particles. Stable isotope studies using IRMS have already significantly contributed to the understanding of carbon partitioning between plant shoots and roots, microorganisms and soil organic matter (Blagodatskaya et al., 2011; Werth & Kuzyakov, 2006, 2010). In their meta-study, Kuzyakov et al. estimated that in wheat, 50% of the total amount of assimilated carbon is retained in the shoot, while 25% is lost by shoot respiration and 25% is transferred belowground. Of the belowground carbon, 36% is lost by root respiration, while 52% is retained in the roots and 12% in the soil and its microbiome (Kuzyakov et al., 2000). However, despite the possibility of stable isotope labeling, photosynthate partitioning into the root system and rhizosphere has not yet been systematically measured at a small scale, i.e. along the root axis of functionally different root types.

1.6.3. Stable isotopic tracers in microbial ecology

A microbial ecology, stable isotopes are valuable tools to investigate nutrient cycling and microbial activity. Labeling studies with stable isotope substrates such as ^{13}C, ^{18}O or ^{15}N enable the identification of microorganisms that actively incorporate these substrates, thereby helping to understand the metabolic activity of microbial taxa. This allows for the qualitative and quantitative assessment of taxon function in processes such as the soil organic carbon cycle, N fixation or decomposition of soil organic matter. Additionally, labeling studies can give insights into the food web position of microbial taxa and their role as primary or secondary consumers of substrates. Amongst the many stable isotope-based molecular and imaging techniques that are extensively reviewed elsewhere (Pett-Ridge & Firestone, 2017), two central techniques to identify microbial photosynthate consumers stand out. Traditionally, ^{13}C labeling experiments have been coupled to stable isotope probing based on phospholipid fatty acid analyses (PLFA-SIP), which rely on differences in PLFA membrane composition between microbial groups (Yao et al., 2015). Once microorganisms incorporate the ^{13}C label into their phospholipids, the PLFAs can be extracted,

methylated to form volatile fatty acid methyl esters that can then be identified and quantified by gas chromatography combustion IRMS (Yao et al., 2015). A more recent method allowing for the taxonomically precise identification of microbial label incorporators is nucleic acid based stable isotope probing (DNA- or RNA-SIP). During a SIP study, environmental samples are incubated with a ^{13}C-, ^{18}O- or ^{15}N-labeled substrate and nucleic acids are extracted. The isotopically labeled nucleic acids are then subjected to ultracentrifugation in high purity caesium salts: caesium chloride for DNA and caesium trifluoroacetate for RNA, respectively (Lueders, 2010). Due to the high speed (120.000 – 180.000 x g) and long spinning time (36 – 65 h) of ultracentrifugation, a density gradient forms in the caesium salt medium. As labeled and unlabeled nucleic acids differ in weight, they are separated along the gradient and can be retrieved by gradient fractionation, i.e. the stepwise removal of medium from the gradient (Neufeld et al., 2007). Thereby, fractions from the bottom of the gradient will contain a high proportion of the heavier, isotopically labeled nucleic acids. The purified nucleic acids can then be further processed for amplicon sequencing, metagenome sequencing or meta transcriptomics (Dunford & Neufeld, 2010).

Past ^{13}C labeling studies have significantly advanced our knowledge about the fate of photosynthates in the rhizosphere microbiome. Paterson et al. (2007) used PLFA-SIP to demonstrate microbial specificity in exudate consumption. In an artificial root experiment, they showed that ^{13}C-labeled glucose and fumaric acid were incorporated by a wider group of microorganisms than glycine. el Zahar Haichar et al. (2008) observed that microbial photosynthate consumers differed between plant species in their DNA-SIP study, while Drigo et al. (2010) used both RNA- and PLFA-SIP to investigate the crucial role of arbuscular mycorrhizal fungi (AMF) in redistributing root derived carbon to other microorganisms. The central role of AMF (Glomeromycota) in photosynthate uptake is emphasized by RNA-SIP results from Hünninghaus et al. (2019), who also identified the bacteria *Azospirillum*, *Arhtrobacter* and *Massilia* and protistan flagellates within the Thaumatomonadida (Cercozoa) and Apusozoa (Rhizaria), and of the Leptomyxida (Amoebozoa) as prime photosynthate consumers. Their study is one of the few SIP studies of the rhizosphere that spatially resolved the colonization of the maize root system with bacterial, fungal, and protistan photosynthate consumers. However, it did not differentiate between individual roots or root types.

1.7. Aims and outline of the thesis

As highlighted above, the underlying mechanisms driving spatial pattern formation in the rhizosphere microbiota are poorly understood. The allocation of photosynthates into the root system and their release into the surrounding soil shapes the rhizosphere environment and supports microbial life. However, it remains unclear how the spatial distribution of photosynthates in a complex root system impacts microbiome assembly and direct consumers of rhizodeposits on a small scale. Especially in root systems like that of maize, featuring diverse functionally different root types, the following questions are yet unanswered:

1. *How does the complex root system architecture of maize affect the spatial variation of the rhizosphere, rhizoplane and endosphere microbiota and are these effects altered in response to soil texture?* (Chapter 2.1)
2. *Where are photosynthates allocated within a complex root system and where are they released into the rhizosphere?* (Chapter 2.2)
3. *To what extent do heterogeneous patterns in photosynthate distribution affect spatial variation in the rhizosphere microbiota and its photosynthate consumers?* (Chapter 2.2)

The DFG-funded programme *"Rhizosphere Spatiotemporal Organisation – a Key to Rhizosphere Functions"* (SPP2089) aimed to elucidate spatial patterns and their underlying mechanisms in the rhizosphere of maize, on single root to root system scale. Within the project, this research focused on linking spatial patterns of root photosynthate distribution to the assembly of prokaryotic, fungal, and cercozoan microbiomes. To address the above research questions, we employed stable and radioactive carbon tracer techniques along with non-invasive imaging technology and profiling of the prokaryotic, fungal and protistan (cercozoan) microbial communities. To capture microbial variation on a small scale, we established a detailed rhizosphere sampling scheme that differentiated between the different root types and sections of maize, while considering the different residence times of each root in the soil. This was aided by non-invasive imaging of root development using magnetic resonance imaging. Photosynthate distribution within the roots was imaged using radioactive $^{11}CO_2$ labeling coupled with positron emission tomography and MRI. Excretion of photosynthates into the rhizosphere was tracked by pulse labeling with stable $^{13}CO_2$ followed by EA-IRMS to measure ^{13}C-labeled photosynthates in the root tissue and rhizosphere soil. Microbial photosynthate consumers that incorporated the ^{13}C-labeled photosynthates were identified by DNA stable isotope probing and amplicon sequencing. Altogether, we aimed to deliver a holistic picture of the allocation of recently assimilated photosynthates in the maize root system and its impact on the (photosynthate-consuming) rhizosphere microbiota.

Chapter 2.1 (Experiment I.)

In experiment I, we explored the effect of different soil textures on the microbiota assembly in maize, while focusing on small-scale spatial patterns associated with the root system architecture. Fifteen maize plants were grown in a loamy, a sandy and a silty sand substrate and root development was regularly monitored by MRI. After three weeks, the rhizosphere, rhizoplane and endosphere prokaryotic community was profiled by amplicon sequencing of the 16S rRNA gene and the observed spatial variation in community composition was related to the root architectural parameters measured by MRI. This experiment also allowed us to establish our sampling scheme and identify a substrate suitable for the following experiments.

Chapter 2.2 (Experiments II. + III.)

Experiments II and III focused on measuring photosynthate distribution and relating it to spatial patterns of the microbiota in the root system. In experiment II, we visualized root-internal photosynthates by radioactive $^{11}CO_2$ labeling with subsequent PET-MRI. Then, we analyzed the variation in the prokaryotic, fungal and cercozoan rhizosphere communities in dependence on the observed photosynthate patterns within the root system. Experiment III aimed to relate spatial variation in the microbiota to both, root-internal and rhizosphere photosynthate distribution. For that, the $^{11}CO_2$ labeling approach from experiment II was complemented by stable $^{13}CO_2$ labeling of the same plants. This allowed us to quantify labeled photosynthates in specific root tissue samples and corresponding rhizosphere samples by EA-IRMS and identify prokaryotic, fungal and cercozoan consumers of labeled photosynthates by DNA-SIP in these samples.

2. Results

2.1. Soil texture and root system architecture impact the root-associated microbiota of maize

Sina R. Schultes[1, 2], Daniel Pflugfelder[2], Dagmar van Dusschoten[2], Michelle Watt [3], Robert Koller[2], Claudia Knief[1]

[1]Institute for Crop Science and Resource Conservation (INRES), Molecular Biology of the Rhizosphere, University of Bonn, Bonn, Germany

[2]Institute of Bio- and Geosciences, IBG 2: Plant Sciences, Forschungszentrum Jülich, Jülich, Germany

[3]Chair of Botany, School of BioSciences, Faculty of Science, University of Melbourne, Melbourne, Australia

Abstract

A substantial part of the root microbiome is recruited from the surrounding soil, making soil properties a major impact factor in root microbiome assembly. Here, we explore the effect of different soil textures on the bacterial community in the rhizosphere, rhizoplane and endosphere of maize, while focusing on small-scale spatial patterns associated with root system architecture. For this, we combined the non-invasive 3D imaging technique magnetic resonance imaging (MRI) with image-guided sampling of selected roots. Imaging illustrated that the root length and growth rate of axial roots differed only slightly between substrates, suggesting that the maize axial root system has a high capacity to compensate for different soil textures. 16S amplicon sequencing of the rhizosphere, rhizoplane and endosphere bacterial communities revealed that soil texture, followed by the root architectural traits root type and root longitudinal section were the main explanatory factors for variation in the bacterial community in all compartments. Soil texture predominantly influenced bacterial diversity and community composition within the rhizosphere while losing impact with closer proximity to the roots, implying a stronger host selection. Patterns of bacterial alpha and beta diversity along the root longitudinal axis were consistently observed across substrates, suggesting the existence of universal mechanisms driving community assembly along the root. In contrast, sequential patterns linked to root types and their emergence time were consistently observed but varied in their extent between substrates, e.g. by exerting a significantly greater influence on community composition in sandy soils compared to loam. This highlights how soil properties, such as texture, can alter the magnitude of root-associated microbial colonization processes even in the absence of direct effects on root system architecture.

Introduction

In recent years, approaches using plant-associated microbiota to improve crop performance have been increasingly pursued (Sible et al., 2021). However, their success can vary considerably depending on the soil type (Li et al., 2022). Numerous studies have already established that soil properties are amongst the central determinants of root microbiome assembly (Berg & Smalla, 2009), a process that remains poorly understood. Notable soil properties influencing microbiome assembly include soil pH, soil organic C content, soil redox status, soil moisture, N/P availability, soil texture and soil temperature (Delgado-Baquerizo et al., 2018; Fierer, 2017). Among these, soil texture stands out as one of the more complex and less understood determinants of soil microbial community structure.

Soil texture is defined by the proportion of sand (0.05 - 2.0 mm), silt (0.002 - 0.05 mm) and clay (<0.002 mm) particles in a substrate (USDA, 2017). Different soil textures have been shown to directly influence microbial diversity and community composition in both rhizosphere and bulk soil (Hartmann & Six, 2023). This can e.g. be attributed to different pore size distribution, pore connectivity and sorption capacity (Xia et al., 2020; Yim et al., 2022) as well as to different particle and aggregate sizes (Biesgen et al., 2020; Hemkemeyer et al., 2018). However, soil texture might also affect the microbial small-scale colonization of the root system and rhizosphere, as it can fundamentally alter root system architecture (Lippold et al., 2021; Rich & Watt, 2013; Rogers et al., 2016). The root system of maize is already highly complex (Hochholdinger & Tuberosa, 2009), consisting of seed-borne (primary and seminal) and shoot-borne (crown) root types that create various habitats for different microbial communities (Kawasaki et al., 2021). Similarly, complex patterns of microbial community assembly along the longitudinal axis of maize roots were detected (Rüger et al., 2021). Different soil textures have not only been observed to impact root system architecture (Rüger et al., 2022), but also root gene expression (Ganther et al., 2021) and rhizodeposition (Fischer et al., 2010; Nguyen, 2009), which might additionally feedback on small-scale microbiome assembly in the rhizosphere and root system. Here, we investigate how different soil textures affect the maize bacteriota in the rhizosphere, rhizoplane and endosphere, with a focus on how small-scale colonization patterns associated with root system architecture are altered by soil texture. Based on the findings of former studies using the same substrates (Lippold et al., 2021; Rüger et al., 2022), we expect that soil texture affects root system architecture. We further hypothesize, that 1) the impact of soil texture on the microbiota exceeds the small-scale heterogeneity induced by root system architecture; 2) soil texture affects the bacterial community more severely in the

rhizosphere than in the rhizoplane and least in the endosphere; and 3) the effects of root system architecture on the microbiota differs in dependence on texture.

We cultivated maize plants in three substrates with differing soil textures (loam/sand/silty sand) for three weeks. Thereby, the loam and sand substrate shared a microbiome, while the silty sand was included as a control featuring a sandy texture but a differing microbiome. We non-invasively monitored root system development over time by magnetic resonance imaging (MRI). Guided by the MRI scans, we sampled specific roots of different root types and developmental stages on day 21 after sowing. Variation in bacterial community structure in the rhizosphere, rhizoplane and endosphere was examined by LNA-primer assisted 16S amplicon sequencing.

Material and methods

Soil preparation and plant growth

This study was performed using a standardized protocol for soil column experiments and two substrates, loam and sand (Vetterlein et al., 2021). The substrate loam was derived from a Haplic Phaeozem (Schladebach, Germany). To obtain the substrate sand with a differing texture but largely the same initial microbiome, 16.7% of the loam soil was mixed with 83.3% quartz sand from WF33, Quarzwerke GmbH (Frechen, Germany). Differences in nutrient availability between the loam and the sand substrate were compensated by a tailored fertilization scheme (Vetterlein et al., 2021). The third substrate, a silty sand, had a different microbiome and was derived from the Landwirtschaftliche Untersuchungs- und Forschungsanstalt (LUFA, Speyer, Germany). More information on the substrates can be found in Table S1. All substrates were fertilized, dried to constant weight and sieved to <1mm prior to homogeneously filling the columns (30 cm height, 8 cm diameter). Substrates were then compacted to a bulk density of 1.26 g cm^{-3} (loam) and 1.47 g cm^{-3} (sand and silty sand). Fifteen *Zea mays* seeds (line B73) were surface sterilized in 10% H_2O_2 for 10 min, primed in a saturated $CaSO_4$ solution for 3 h and sown at 1 cm depth. Five plants per substrate were grown in a climate chamber for 21 days as previously described (Vetterlein et al., 2021). Plants were watered to uphold a volumetric water content of 22% (loam) and 18% (sand, silty sand).

MRI scanning and collection of root growth data

All plants were scanned by MRI on days 6, 9, 13 15 and 20 after sowing in order to non-invasively monitor root system architecture and root development. We used a 4.7-T vertical bore magnet (Magnex Scientific, Oxford, United Kingdom) equipped with a 21-cm gradient system up to 400 mT/M (MR Solutions, Guildford, United Kingdom) as previously described by van Dusschoten et al. (2016) with minor adjustments: To counter the strong imaging artefacts observed in the soils, the spectral width of the MRI acquisition was increased to 400 kHz. To amend the resulting decrease in signal-to-noise ratio, the imaging time was doubled for the loam and the sand. MRI data were analysed using the program NMRooting (Pflugfelder et al., 2017; van Dusschoten et al., 2016). We restricted root tree analysis to the axial roots, i.e. the primary root, the seminal roots and the crown roots originating from the first three consecutive belowground nodes of origin (crown 1 – 3), as these roots could be detected without technical limitations in all substrates (Fig. 1, S1). Lateral roots were excluded from the analyses. Root types were manually assigned. The length of individual root types as well as the summed length of all axial roots was measured at each timepoint. Per plant, one root of each root type was selected for sampling and the more elaborate root analyses. The age of each

sampled root was estimated according to its first appearance in an MRI image. Additionally, the growth rate of the sampled roots was calculated from the difference in root length between two measuring timepoints. Normality and homogeneity of variances of the data was verified using a Shapiro-Wilk test and a Levene's test on each measurement timepoint subset. The significance of differences between substrates was determined by a separate ANOVA and Tukey HSD posthoc test for each measurement timepoint subset (Fig. 2).

Image-guided sampling

Destructive sampling occurred on day 21 after sowing, one day after the last MRI image analysis, which allowed to identify representative roots per root type from each plant individual and to use the information about their localization in the soil column during the harvesting procedure. Before sampling, the soil was brought to the targeted volumetric water content to ensure a comparable extension of the rhizosphere. Soil cores were pushed out of the pots and carefully dissected. Per plant, one root of each root type was collected. Additionally, bulk soil samples were taken from the unrooted soil in the middle of each soil column. From each root, a root tip sample of about 2 cm in length and a root base sample of about 10 cm in length were cut. Lateral roots were cut off the root base samples to avoid mixed root type signals. As crown roots of the third node were very small on day 21, only root tip samples were taken from this root type. Rhizosphere samples were obtained by dipping each root piece into 0.3% sterile NaCl solution. Rhizoplane samples were obtained afterwards by vortexing the same root piece in 0.3% sterile NaCl for 15 seconds. The remaining root piece then constituted the endosphere sample. Rhizosphere and rhizoplane samples were centrifuged at 5000 x g and 4 °C for 30 min in a swing-out rotor, and the pellets were stored at -20 °C. Endosphere samples were hand-ground in liquid nitrogen and stored at -20 °C.

DNA extraction and amplicon sequencing

DNA was extracted using the FastDNA™ SPIN Kit For Soil (MP Biomedicals™, Santa Ana, Canada) following the protocol of Tournier et al. (2015) with minor alterations (2 x 45 s homogenization). 16S rRNA gene amplicons were generated following an LNA PCR protocol (Table S2, S3) to suppress the amplification of plant organelle-derived 16S rRNA genes (Ikenaga & Sakai, 2014). An initial PCR using the modified primer set 63f-1492r was performed in triplicates and was followed by a nested PCR using primer set 515f-806r (Caporaso et al., 2011) targeting the V4-V5 region of the 16S SSU rRNA gene with previously published barcodes (Frindte et al., 2019). Amplification products were quantified using the QuantiFluor dsDNA System (Promega, Fitchburg, Wisconsin, USA) on a Qubit®

2.0 Fluorometer (Invitrogen, Carlsbad, California, USA) and pooled at equimolar concentrations. Pooled PCR products were purified with the CleanNA magnetic bead system (GC-Biotech, Waddinxveen, the Netherlands). Library preparation and sequencing of the 16S rRNA gene amplicons was performed by the Max Planck-Genome-centre Cologne on a HiSeq2500 instrument (Illumina, San Diego, Canada) generating 2x250 bp paired-end reads.

Sequence data analysis

Data from sequencing on two HiSeq runs were combined as the first analysis did not provide sufficient read counts. The raw 16S rRNA gene sequence reads were preprocessed using a customized bash script with Cutadapt version 3.0 to demultiplex the samples (Martin, 2011). Primer trimming was performed using QIIME 2, version 2020.11 (Bolyen et al., 2019) and denoised amplicon sequence variants (ASVs) were created using the DADA2 pipeline (Callahan et al., 2016). The denoising step also comprised forward and reverse read merging and chimera removal. Sequence alignment was performed using the MAFFT software (Katoh & Standley, 2013). The SILVA database (version 138) was used for bacterial taxonomy assignment (Quast et al., 2012).

Statistical data analysis

Data were exported into R (version 4.2.2) and analyzed with the packages *phyloseq* (McMurdie & Holmes, 2013) , *vegan* (Dixon, 2003) and *lmerTest* (Kuznetsova et al., 2013). Figures were created using the package *ggplot2* (Wickham, 2016). Singletons, reads unidentified above class level, chloroplasts and mitochondria were removed from the data set. Samples below 5000 reads were removed. The ASV tables were rarefied onto the lowest number of reads per sample for all alpha diversity analyses.

Alpha diversity was reported as Shannon diversity index. Differences in alpha diversity between groups of samples were assessed independently for each compartment using linear mixed effect models (LMMs) using the *lmer()* function of package *lmerTest*. The fixed effects substrate, root type, root section, root age and growth rate between the last imaging timepoint (day 15) and the sampling timepoint (day 20) were considered for the maximum model. Prior to model fitting, possible multicollinearity between fixed effects was checked in each subset using the *corvif()* function of the package *AED* (Zuur et al., 2009). The predictor root age was excluded from further model fitting due to its high collinearity with root type, but Shannon diversity in dependence on root age is nonetheless included in the supplements (Fig. S2). For each subset, the *step()* function of package *lmerTest* was used to back-fit a “maximum” LMM containing all remaining candidate fixed effects and their

interaction with the fixed effect substrate, while retaining the random effect plant individual. Back-fitting resulted in an identical model for the analysis of data from the rhizoplane and endosphere, and in a slightly different model for the rhizosphere data in which growth rate was retained as a fixed effect in contrast to the other models (Table S4). The significance of fixed effects was assessed by the *anova()* function of the *stats* package and pairwise comparisons of the categorical fixed effects were performed using the *emmeans()* function of the *emmeans* package (Lenth, 2022). The correlation between Shannon diversity indices and root growth rates was tested using Spearman's rank correlation.

For the downstream analysis of beta diversity, a Bray-Curtis distance matrix was constructed. Variation in community composition was analysed using unconstrained ordination in non-metric multidimensional scaling (NMDS) plots, using k=2 dimensions. The significance of the individual variables and their interactions was analysed by a permutational multivariate analysis of variance (PERMANOVA) using function *adonis2()* of the package *vegan*. For a more targeted analysis of community composition in relation to root traits, we used distance-based redundancy analysis (db-RDA)-based backwards variable selection to select for the most meaningful root parameters in each soil substrate using the functions *capscale()* and *ordistep()* of the package *vegan*. The significance of the resulting model and individual model terms was then tested using *anova()* function of the *stats* package on the model results. The contribution of individual variables to variation in community composition was analysed by variation partitioning using the function *varpar()* of the package *vegan*.

Results

Root system architecture and root development in different soil substrates

The root systems of all plants were imaged by MRI on days 6, 9, 13, 15 and 20 after sowing to non-invasively visualize root growth upon plant cultivation in the different soil substrates by NMRooting (Fig. 1). Quantitative root growth data were extracted from the MRI scans and revealed that the total root length of the root systems did not differ significantly between substrates at any timepoint, although the data suggest a slightly shorter total root length for plants in the loam substrate compared to sand and silty sand and increasing variation over time for roots grown in silty sand (Fig. 2a). A closer look at the individual root types did, however, reveal some variation in root length in dependence on the soil substrates (Fig. 2b). The observed differences in root length usually persisted throughout the measurement timepoints but were not always significant. Most consistent differences were observed for primary roots, which were significantly longer in silty sand than in the other two substrates or at least in the sandy soil at measurement days 9, 13 and 20 (Fig. 2b). Seminal roots were slightly longer in sandy substrates than in loam with confirmed significance at day 9. Growth speed data were only generated for sampled roots to later relate growth rate with microbial colonization. The growth rates of the sampled roots showed that the growth rate of the primary decreased over time, whereas the growth rate of the seminal roots decreased after an initial increase. The recently emerged crown roots of the second generation showed increasing growth rates (Fig. 2c). There were no significant differences observed related to the substrates, except for a significantly increased growth rate of seminal roots in silty sand between day 6 and 9 and as well as crown roots of the first generation between day 13 and 15, i.e. in both cases the phase with highest root growth rates.

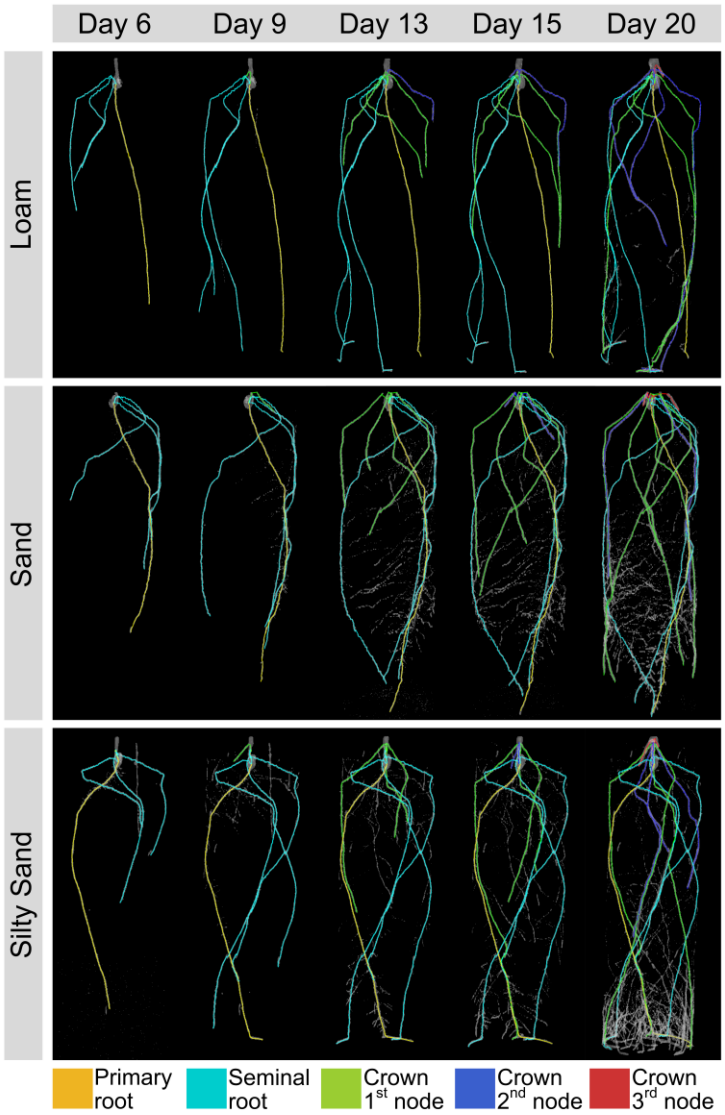

Fig. 1 Development of three exemplarily selected maize root systems in three soil substrates over time, non-invasively scanned by MRI. Root types (colored) were annotated using the program NMRooting. Differences in the visibility of lateral roots (white) are related to substrate properties.

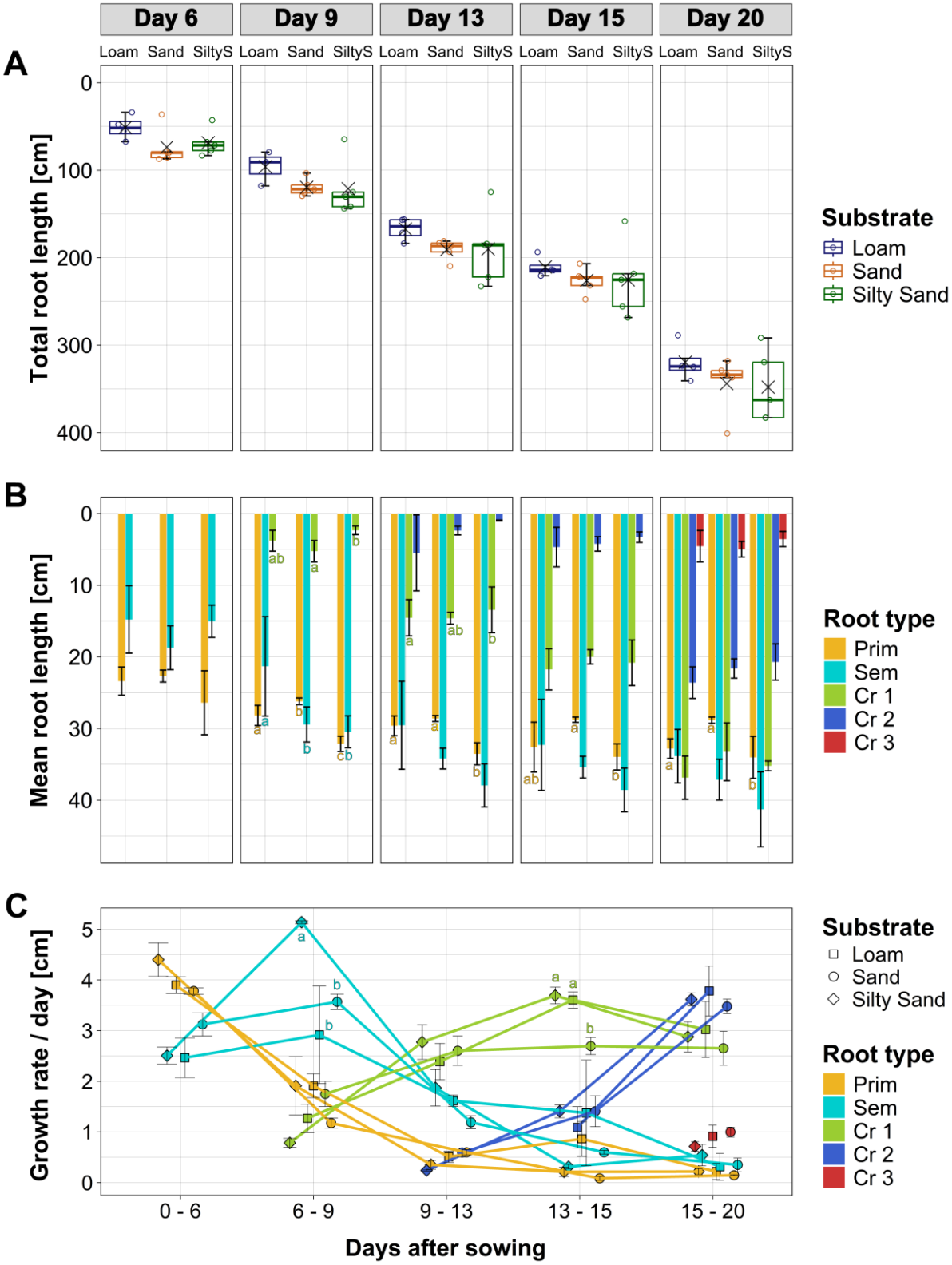

Fig. 2 Quantitative root data derived from MRI scans. (a) Total root length of the whole root system, excluding lateral roots. The mean is plotted as X. **(b)** Mean root length per root type by substrate at different days after sowing. Prim = primary root, Sem = seminal root, Cr1 = crown root of first whorl, Cr2 = crown root of second whorl, Cr3 = Crown root of third whorl. Root type length was averaged for each plant. Errorbars indicate the standard deviation between individual plants. Differences in root length in dependence on substrate were evaluated by ANOVAs for each root type at each

timepoint. Distinct lowercase letters indicate significant differences in root length in dependence on soil substrate, as determined by Tukey HSD posthoc tests (threshold $p<0.05$). **(c)** Growth rate of sampled roots, generated from the difference in root lengths between measuring timepoints. Error bars indicate the standard error of mean between plant individuals. Significance of differences was tested by separate ANOVAs for each root type at each timepoint. Distinct lowercase letters indicate significant differences of growth rates between substrates, as determined by Tukey HSD posthoc tests (threshold $p<0.05$).

Effects of substrate and root properties on bacterial alpha diversity in root-associated compartments

Variation in alpha diversity of the maize root-associated bacterial community was evaluated independently in the rhizosphere, rhizoplane and endosphere based on the Shannon diversity index. To identify relevant influence factors, back-fitted individual linear mixed effects models were set up for each compartment. This revealed that substrate, root type and root section significantly affected Shannon diversity in all compartments. The effect of root growth rate and its interaction with substrate was only significant for bacterial diversity in the rhizosphere, and the interaction between substrate and root type was only significant in the rhizoplane and endosphere models (Table 1).

Table 1 Effects of substrate and root parameters on Shannon diversity within each root-associated compartment according to a linear mixed effect model (LMM).

	Fixed effect	F	*p*
Rhizosphere model	Substrate	9.056	<0.001
	Root type	5.081	<0.001
	Root section	14.857	<0.001
	Growth rate	4.770	<0.05
	Substrate:Growth rate	6.035	<0.01
Rhizoplane model	Substrate	11.766	<0.001
	Root type	18.838	<0.001
	Root section	28.327	<0.001
	Substrate:Root type	3.317	<0.01
Endosphere model	Substrate	5.859	<0.05
	Root type	15.943	<0.001
	Root section	15.354	<0.001
	Substrate:Root type	4.363	<0.001

Pairwise comparisons of marginal means estimated by the LMMs showed that bacterial Shannon diversity in the rhizosphere and rhizoplane of plants grown in loam was significantly higher than that of plants grown in the sandy substrates (Fig. 3a). Root growth in sand resulted in the lowest bacterial diversity estimate in the rhizosphere, whereas the lowest diversity in the endosphere was observed upon growth in silty sand (Fig. 3a). In the bulk soil, only slight differences in Shannon diversity were encountered between substrates (Fig. S3).

The bacterial communities that were associated with different root types showed a declining pattern in alpha diversity from the older primary roots to the more recently developed crown roots in all soil substrates and compartments (Fig. 3b), an effect that could likewise be observed for root base and root tip samples (Fig. S4). Pairwise comparisons confirmed that bacterial diversity was significantly lower in communities associated with crown 3 roots compared to primary roots in all compartments and regardless of the soil substrate, though with the endosphere community upon root growth in sand soil as only exception. In contrast to the other compartment models, the rhizosphere LMM did not feature an interaction term between substrate and root type (Table S4), i.e. the root type's effect on Shannon diversity did not depend on the substrate present. This resulted in identical statistical results for all substrates in the rhizosphere (Fig. 3b). In the rhizoplane, we

observed a significant reduction in bacterial diversity from primary to seminal roots in the two sand substrates. In the endosphere bacterial community, significant but contrasting differences in diversity estimates were observed between crown roots in loam and silty sand. Meanwhile, all root type-associated differences in bacterial alpha diversity were mitigated when roots grew in sand soil.

Root section emerged as the most influential factor explaining variation in bacterial alpha diversity (Table 1). Bacterial Shannon diversity was lower at root tips compared to root bases, a pattern that remained consistent across substrates and compartments (Fig. 3c). This consistency is further supported by the absence of an interaction term between substrate and root section in all three LMMs, indicating that the effect of root section on Shannon diversity is not dependent on the substrate. Since pairwise comparisons of marginal means using the *emmeans()* function cannot be applied to numeric predictors, the relationship between Shannon diversity and root growth rate was analyzed using Spearman's rank correlation (Fig. 4). The analysis revealed a significant decrease in Shannon diversity with increasing root growth rate across all compartments in sand and silty sand (Fig. 4). However, no significant correlation between diversity and growth rate was observed in any compartment within the loam substrate.

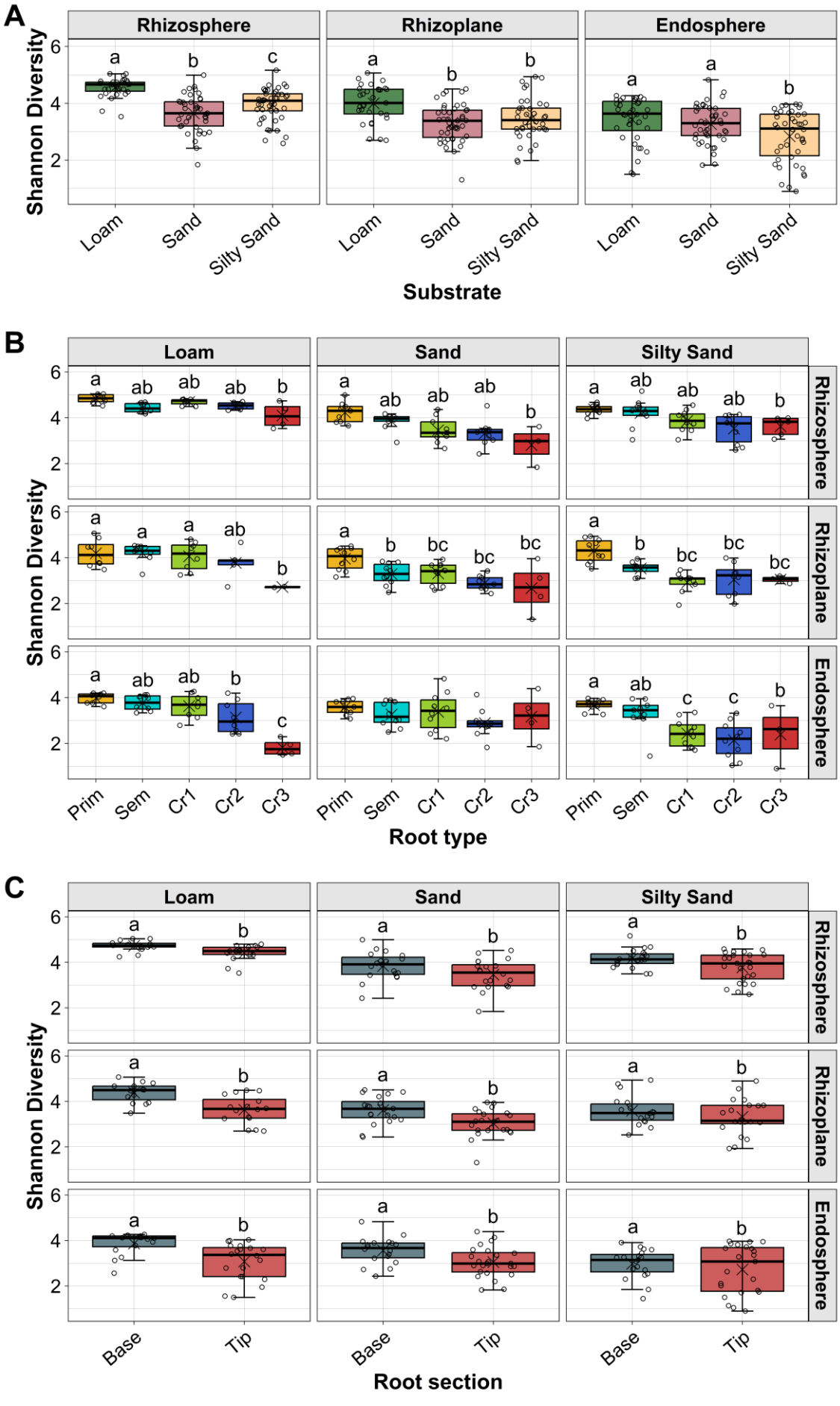
A
Rhizosphere
Rhizoplane
Endosphere
Shannon Diversity
Loam
Sand
Silty Sand
Substrate
B
Loam
Sand
Silty Sand
Rhizosphere
Rhizoplane
Endosphere
Shannon Diversity
Prim
Sem
Cr1
Cr2
Cr3
Root type
C
Loam
Sand
Silty Sand
Rhizosphere
Rhizoplane
Endosphere
Shannon Diversity
Base
Tip
Root section

Fig. 3 Variation in bacterial alpha diversity in the three substrates and root-associated compartments in dependence on **(a)** substrate, **(b)** root type and **(c)** root longitudinal section, evaluated based on the Shannon diversity index. The mean is plotted as X. Distinct lowercase letters indicate significant differences within each substrate and compartment, as determined by pairwise comparisons of marginal means estimated by a linear mixed effect model (LMM) for each compartment (Table S5-S7). Prim = primary root, Sem = seminal root, Cr1 = crown root of first whorl, Cr2 = crown root of second whorl, Cr3 = Crown root of third whorl.

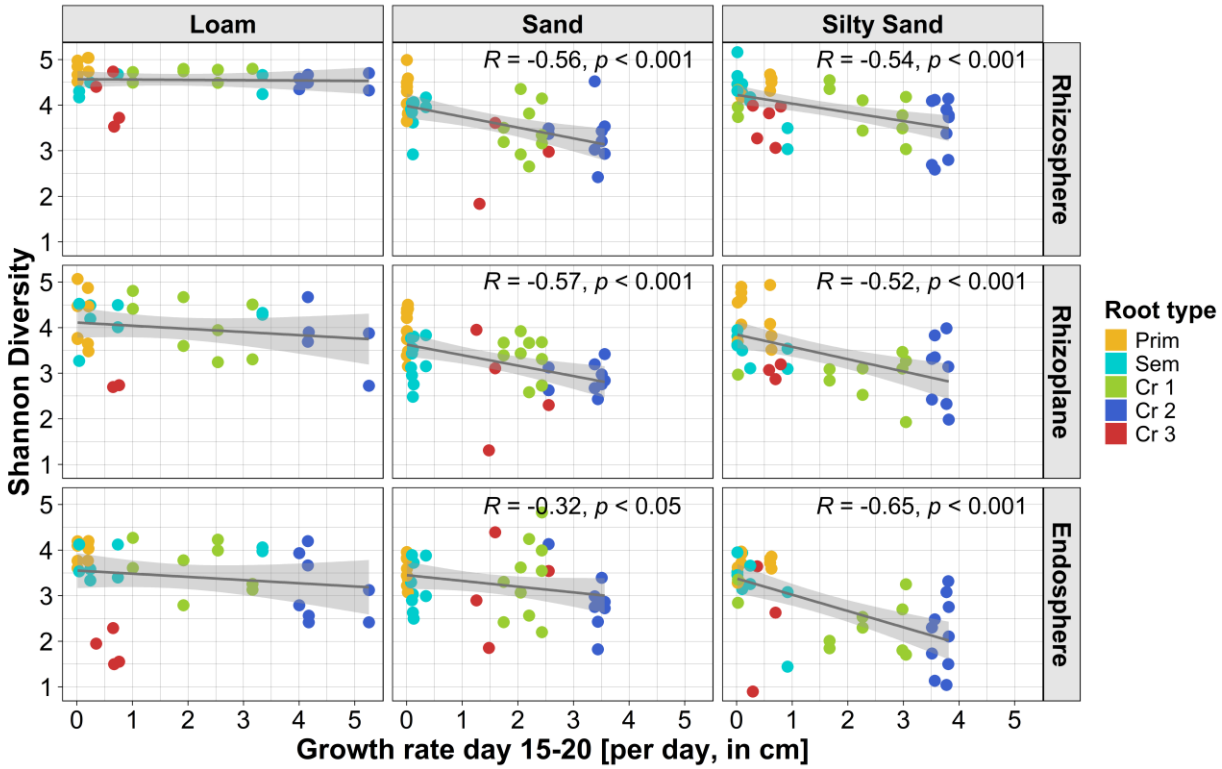

Fig. 4 The effect of root growth rate between day 15 and 20 on Shannon diversity. Correlation between growth rate and Shannon diversity was tested using Spearman's rank correlation, observations are coloured according to root type. Gray-shaded areas indicate the 95% confidence interval of the linear regression model fitted to the data. Prim = primary root, Sem = seminal root, Cr1 = crown root of first whorl, Cr2 = crown root of second whorl, Cr3 = Crown root of third whorl.

2.1. Results

Effects of substrate and root properties on bacterial beta diversity in root-associated compartments

For an initial exploration, patterns in bacterial beta diversity were illustrated by NMDS plots based on Bray-Curtis dissimilarities, with one plot for each compartment in each substrate (Fig. 5). Generally, patterns according to root type and root section were most pronounced in the endosphere of plants grown in the loam and sand soil. The sequential clustering according to root type could be observed for both, root tip and root base samples. Interestingly, root base samples clustered slightly closer together than root tip samples, across all soils and compartments. Permutational multivariate analysis of variance (PERMANOVA) verified the effects of the individual categorical factors on community composition but also revealed significant interactions between root type and root section in the sand substrate (Table 2).

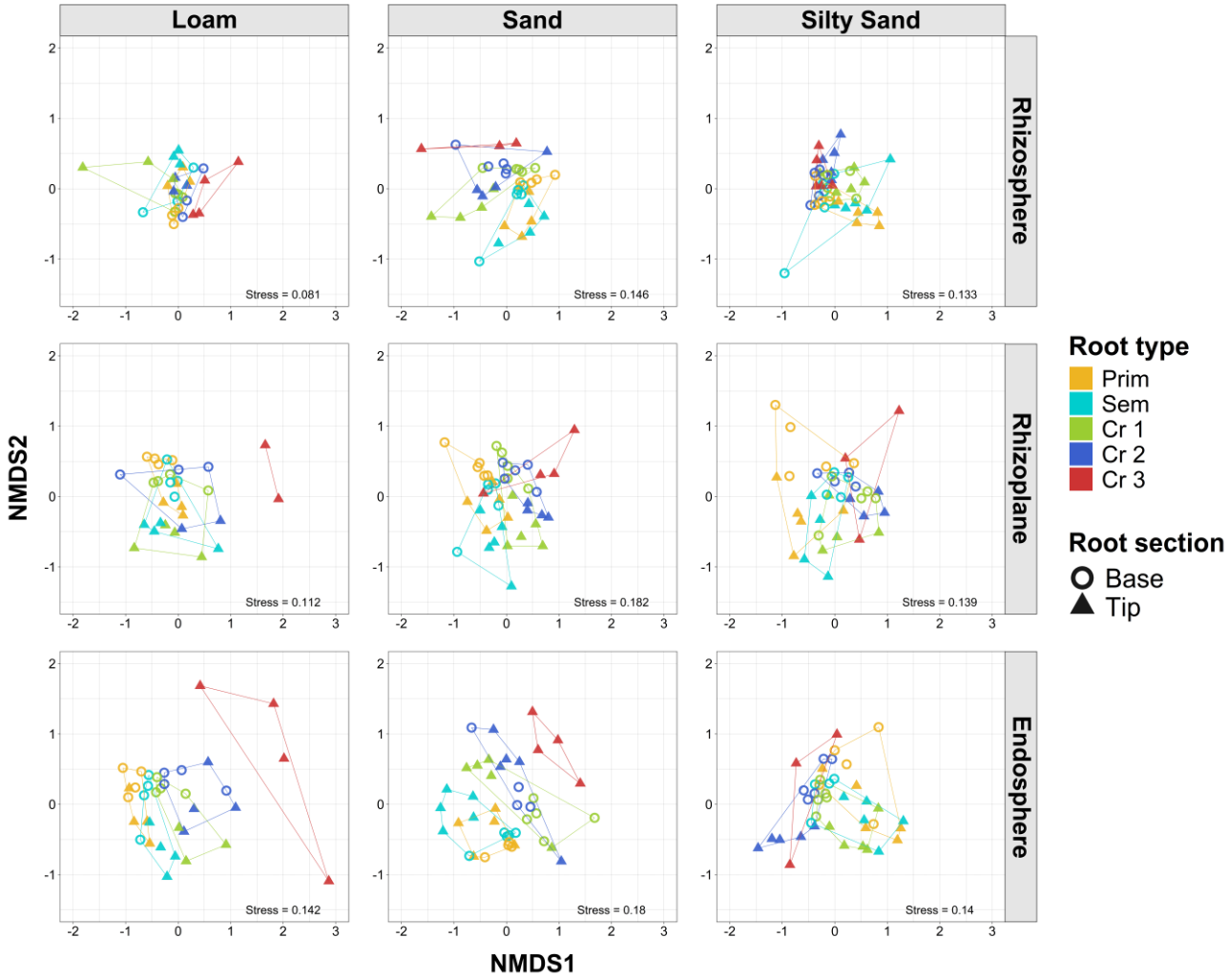

Fig. 5 Unconstrained ordination visualized by non-metric multidimensional scaling (NMDS) plots based on Bray-Curtis dissimilarities. Prim = primary root, Sem = seminal root, Cr1 = crown root of first whorl, Cr2 = crown root of second whorl, Cr3 = Crown root of third whorl.

Table 2 The effect of root type, root section and their interaction on bacterial community composition in three compartments and three substrates, as analysed by permutational multivariate analysis of variance (PERMANOVA). The significance of R^2 values is illustrated as follows: *** = $p < 0.001$, ** = $p < 0.01$, * = $p < 0.05$.

	Variable	Loam	Sand	Silty Sand
Rhizosphere	Root type	0.229 ***	0.225 ***	0.222 ***
	Root section	0.108 ***	0.116 ***	0.122 ***
	Interaction	0.108	0.111 ***	0.107 **
Rhizoplane	Root type	0.281 ***	0.254 ***	0.192 ***
	Root section	0.141***	0.118 ***	0.101 ***
	Interaction	0.073	0.095 **	0.064
Endosphere	Root type	0.355 ***	0.261 ***	0.228 ***
	Root section	0.096 ***	0.128 ***	0.126 ***
	Interaction	0.063	0.073 *	0.072

We used db-RDA as a constrained ordination analysis to evaluate whether root type, root section, compartment, root growth rate or root age were the most meaningful parameters influencing microbial beta diversity. The stepwise selection retained compartment, root type and root section as significant predictors of bacterial beta diversity (Table S8). The overall models together explained 41.16% of variance in the loam, 32.80% of variance in the sand and 34.04% of variance in the silty sand. In the db-RDA ordination plot of the loam substrate, samples were strongly separated by compartment along the first axis and by root type along the second axis (Fig. 6). In contrast, in the sandy substrates, root type clustered strongly along the first axis while root section clusters most strongly along the second axis; with the different compartments overlapping more. In loam, rhizosphere samples clustered more closely together than rhizoplane and endosphere samples, a pattern that was also partially visible in a compartment-based db-RDA analysis (Fig. S5, Table S9).

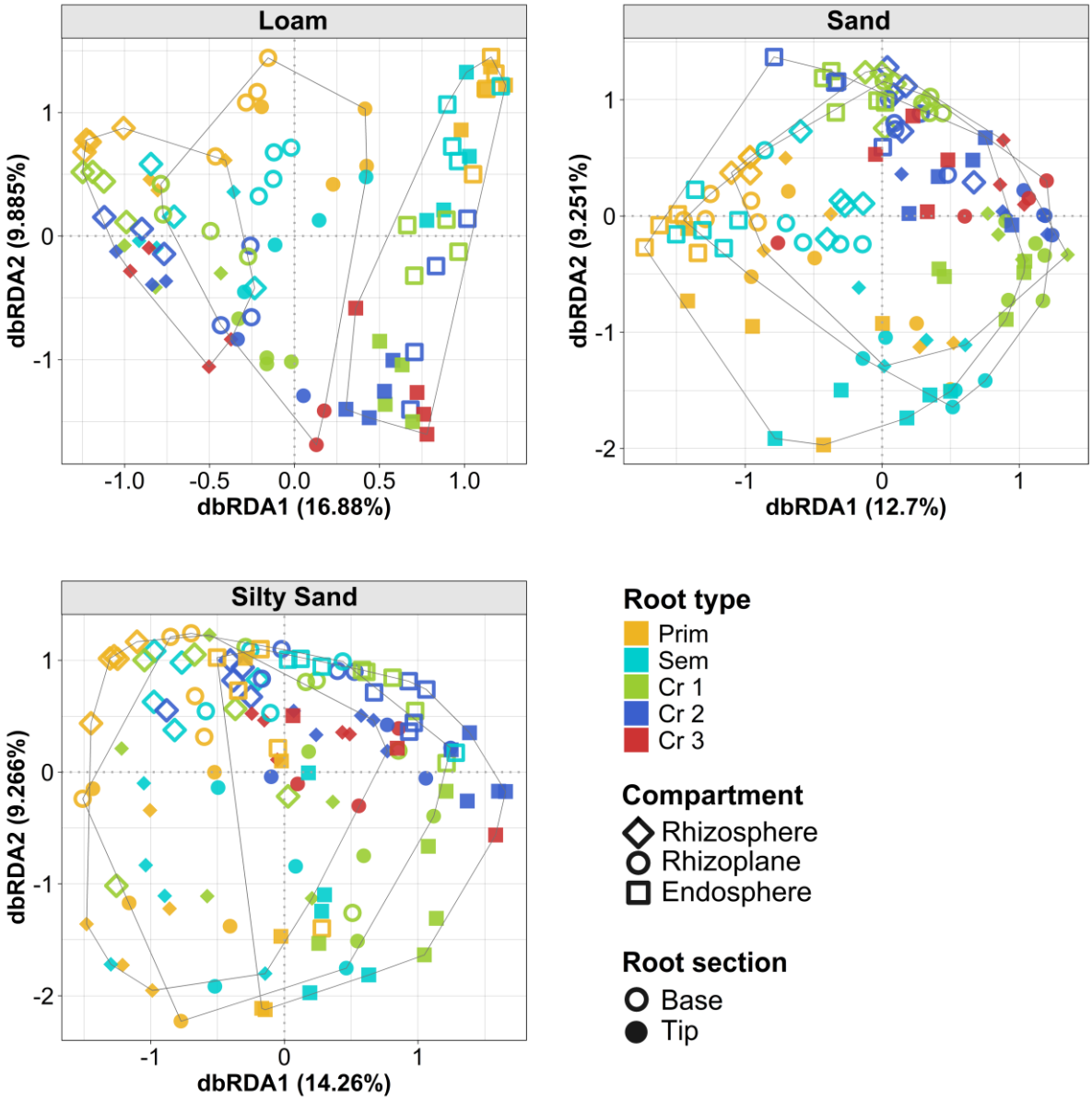

Fig. 6 Ordination via distance-based redundancy analysis (db-RDA) for the three soil substrates loam, sand and silty sand. Samples are colored by root type and sample shapes correspond to different compartments. Filled and unfilled shapes represent different root sections.

To explore the individual contributions of variables to variation in beta diversity more closely, a variation partitioning analysis was performed (Table 3). Compartment explained most variance (18.64%) in the loam substrate, while root type explained most variance in the two sandy substrates (13.50-16.03%). Meanwhile, the effect of compartment was reduced in sand by more than 60% as compared to the loam substrate. Shared variation was negligible in all soil substrates.

Table 3 Partitioning of the variation observed in community composition.

	Loam	Sand	Silty Sand
Compartment	0.1864	0.0652	0.1130
Root type	0.1439	0.1603	0.1350
Root section	0.0647	0.0988	0.0902
Shared variation	0.0000	0.0003	0.0000
Residuals	0.6242	0.6928	0.6767

Discussion

The axial root system shows a high architectural robustness in different substrates

MRI enabled us to observe maize root growth in different substrates over time and to non-invasively measure root traits. The effect of different soil textures on the development of the axial root system was however less pronounced than expected. The total length of the axial root system was slightly shorter in loam compared to the sandy substrates (Fig. 2a), even though mechanical impedance induced by high bulk densities such as that in sand was previously reported to cause a proportionally reduced (axial) root length in maize (Rüger et al., 2022; Vanhees et al., 2022). Significant differences in the length and growth rate of individual root types occurred only transiently and were restricted to the primary, seminal and crown 1 roots. This indicates that the maize axial root system has a high capacity to continuously compensate for different soil textures during various growth stages. More variation according to soil properties is often observed in lateral roots as they make up the largest part of root system plasticity (Yu et al., 2019). Additionally, root diameter is another central factor affected by soil texture. Root diameter reportedly increased in sand substrate with higher bulk density as opposed to loam substrate (Jorda et al., 2022; Lippold et al., 2021). Root diameter and lateral roots can, however, not yet be accurately measured using MRI in our loam and sand substrates.

Soil texture affects bacterial alpha and beta diversity more in the rhizosphere than in the endosphere

Alpha diversity in sand was significantly reduced compared to loam in the rhizosphere and rhizoplane, but this difference was largely mitigated in the endosphere. Similarly, differences in variance between loam and sand samples were reduced in the endosphere as opposed to the rhizosphere (Fig. 3a). In our study, differences between sand and loam can be attributed to different soil textures, while silty sand additionally had a different initial inoculum. Thus, the decreased difference between alpha diversity of loam and sand can likely be attributed to the strong filtering of the endosphere microbiome by the host and the higher exposure of the rhizosphere microbiome to soil properties (Brown et al., 2020; Bulgarelli et al., 2013; Veach et al., 2019). In contrast, alpha diversity of silty sand was still significantly different from the other substrates in the endosphere (Fig. 3a); indicating that the endosphere microbiome is, for a large part, recruited from the rhizosphere microbiome as a source (Edwards et al., 2015). A db-RDA analysis of beta diversity in the different compartment subsets supports these assumptions (Fig. S5). Loam and sand samples increasingly overlapped with decreasing distance to the root, where soil texture effects lose impact. Meanwhile, silty sand samples still clustered separately in the endosphere due to their distinct microbiome (Fig.

S5). Variation partitioning revealed that, as hypothesized, substrate had the largest effect on microbial community composition and exceeded the influence of the root-associated factors root type and root section in all compartments (Table S10). Variation partitioning also confirmed that the influence of substrate was more prominent in the rhizosphere than in the endosphere, with the effect of substrate declining by almost half with increasing proximity to the root (Table S10). In contrast, a slightly increased impact of root type and root section was observed with increasing proximity to the root, where microbiome selection by host traits is gaining importance

A decrease in alpha diversity in sand as opposed to loam has already been observed in the maize rhizosphere (Yim et al., 2022). We can now verify that this is also the case in the rhizoplane, but not in the endosphere (Fig. 3a). Lower alpha diversity in the sand fraction was previously explained by a higher pore connectivity between larger particles which enables microbes to move more freely (Carson et al., 2010). This effect was however shown to strongly depend on soil moisture content (Chau et al., 2011; Xia et al., 2020). In contrast, loam with its higher proportion of fine particles might have a better nutrient availability and offers protection through exclusion of predators like protists, thereby increasing the bacterial alpha-diversity (Sessitsch et al., 2001). Interestingly, the difference between alpha diversity in loam and sand was more pronounced in the rhizosphere than in the bulk soil (Fig. S3). This suggests that in comparison to bulk soil, the impact of soil texture-dependent conditions like water retention or porosity might be amplified in the rhizosphere due to rhizosphere-specific factors like root exudation. Meanwhile, soil texture-dependent conditions gradually lose impact in the rhizoplane and endosphere.

Root age and growth rate have less impact than expected

Root parameters measured by MRI were used to test how the bacterial community responds to root system architecture in different substrates. The selection of the most meaningful drivers of alpha diversity by a back-fitted LMM revealed substrate, root type and root section as significant factors in all compartments, while root growth rate was only significant in the rhizosphere model (Table 1). Similarly, db-RDA followed by variation partitioning revealed that substrate, root type and root section contributed most to the variation in community composition in each compartment (Fig. S5, Table S10). Even though root growth rate impacts on rhizodeposition (Landl et al., 2021) and colonization differences in aging root systems have been demonstrated (Wagner et al., 2016), both factors did not rank among the most influential determinants or were totally excluded by our models of bacterial alpha and beta diversity. The exclusion of these quantitative predictors can have several explanations. Firstly, root type might have explained much of the same variation as root age and root growth rate, rendering the quantitative factors redundant. Indeed, very similar patterns in alpha

diversity were observed for root type and root age (Fig. 3b, S2), and root age was excluded during fitting of the LMM due to its high collinearity with root type. Different root types also showed different growth rates (Fig. 2), thus correlation might have led to the exclusion of growth rate from most LMMs as well, even though a significantly decreased alpha diversity with increasing growth rate was observed in the sandy substrates (Fig. 4). Also, a reduced impact of growth rate at root base areas and in the rhizoplane and endosphere compartments where microorganisms are tightly attached needs to be considered. Generally, the categorical parameters root type and root section represent functional niches that might better fit the microbial community colonization patterns than quantitative factors.

Root section patterns are largely conserved between soil substrates

The decrease of bacterial alpha diversity in root tips as compared to root bases was highly comparable between all substrates (Fig. 3c). Root section significantly affected alpha diversity in all compartments and did not show an interaction with substrate in our LMM, indicating that its effect on alpha diversity is consistent in different substrates (Table 1). Similarly, the shift in community composition along the root longitudinal axis was highly comparable between substrates and compartments (Fig. 5, Table 2). A constrained ordination analysis confirmed that root section significantly affected community composition in all substrates (Table S8) and explained 6.47 – 9.88% of the variation (Table 3). These observations suggest that robust underlying mechanisms steer the colonization along the root longitudinal axis, mechanisms which are consistent between different soil substrates. Rhizodeposition by plant roots is such a mechanism. The amount of rhizodeposits is higher at root tips than at root bases (Holz et al., 2019), making root tips hotspots of microbial colonisation (Kuzyakov & Blagodatskaya, 2015). In line with our results, root tips have been previously reported to harbour a lower bacterial diversity than root bases (Kawasaki et al., 2021; Rüger et al., 2021) which is possibly due to an enrichment of competitive taxa that can readily metabolize the labile C at the tip (Dennis et al., 2010). However, the separate clustering of root tip samples in our ordination plots also suggest a higher degree of random colonization at root tips than at root bases. In addition to a varying rhizodeposition along the maize root longitudinal axis, differential gene expression patterns were encountered along the root longitudinal axis (Stelpflug et al., 2016), which can in turn influence the microbial assembly.

Root type sequential patterns vary in their extent between substrates

Analyses of alpha and beta diversity both revealed sequential patterns in the bacterial colonization of different root types. Alpha diversity significantly decreased in younger crown roots as compared to the primary root in all compartments and soil substrates except in the endosphere of plants grown in the sand substrate (Fig. 3b). We found that root type patterns in alpha diversity strongly covaried with root age patterns (Fig. S2), which hints at the importance of the residence time of a root in soil and therewith the age of the rhizosphere for microbiome assembly. Similarly, both unconstrained (Fig. 5) and constrained (Fig. 6) analyses of community composition revealed sequential patterns that corresponded to the emergence time of root types, across substrates. The sequential clustering according to root type could be observed for both, root tip and root base samples, indicating that factors causing root-type specific colonization are already present at the newly developed root tip (Fig. 5, 6, S4). Differences in rhizodeposition could be a viable explanation. Recent studies demonstrate that the amount of root exudates (Kawasaki et al., 2018), as well as the properties of mucilage (Werner et al., 2022) differ between root types of cereals and that different maize root types show different physiological traits (Ahmed et al., 2018). Furthermore, different maize root types showed different gene expression patterns (Tai et al., 2016), which can in turn influence the microbial assembly (Kawasaki et al., 2016; Yu et al., 2018).

When different soil substrates were compared, root-type associated patterns in alpha diversity slightly varied between substrates and compartments. In the LMMs, the significant interactions between substrate and root type indicate that alpha diversity is jointly determined by a substrate-dependent source community and potential host filtering that differs across root types. Variation partitioning analyses revealed that in sandy substrates, root type surpasses compartment as main driver of bacterial community composition (Table 3). This becomes especially apparent in the db-RDA ordination plots, where in loam, samples were strongly separated by compartment along the first axis while in sandy substrates root type clustered strongly along the first axis and samples from different compartments largely overlapped (Fig. 6). This is in line with previous results of Kawasaki et al. who found that the variation between different root types and along individual roots of wheat and rice was comparable in magnitude with the variation detected between different plant species (Kawasaki et al., 2021). We found that root type-dependent variation in sandy substrates was comparable in magnitude with compartment differences in loam soil (Table 3). The high impact of root type on bacterial community composition in sandy substrates might be due to a greater dependence on root-derived resources in sandy substrates. The sand substrate was lower in organic carbon than the loam substrate (Vetterlein et al., 2021) and the greater porosity of sand further reduces the availability of microbial habitats, leading to an enhanced importance of root resources

and an amplification of root type-dependent variation. Also, although we did not detect root architecture modifications due to soil substrate, the root's exudation profile might still be modified as adaptation to sandy substrates in comparison to loam.

Conclusion

Our study illustrates that the root-associated bacterial microbiome of maize is jointly structured by soil substrate and root architectural traits. Soil texture mainly affected bacterial diversity and community composition in the rhizosphere compartment, while root architectural traits slightly gained importance with increasing spatial proximity to the root. Patterns in bacterial alpha and beta diversity along the root longitudinal axis were largely conserved across substrates, indicating the presence of universal mechanisms in microbial community assembly along the root. However, the sequential patterns detected for root types that were associated with their time of emergence varied in their extent between substrates, having a much larger impact on community composition in sandy substrates than in loam. This indicates that soil properties like soil texture can modulate root-associated microbial colonization processes, even if they do not alter the root system architecture directly. To shed more light on the origin of conserved patterns of root section and the sequential patterns of root type, rhizodeposition as a central process for microbiome assembly should be investigated in a high spatial resolution and in association with root system architecture.

Acknowledgements

This work was conducted within the framework of the priority program 2089, funded by the Deutsche Forschungsgemeinschaft (DFG, German Research Foundation) – P18 (Project ID 403637614). We would like to thank Merle Noschinski-Rees and Juliane Zaunick (Molecular Biology of the Rhizosphere, University of Bonn) for their help with DNA extractions. Furthermore, we thank Esther Breuer (Enabling Technologies, IBG2, Forschungszentrum Jülich) for her valuable support during the imaging trials at Forschungszentrum Jülich. Caroline Marcon and Frank Hochholdinger (Crop Functional Genomics, University of Bonn) are acknowledged for providing maize seeds for this study.

Supplementary material

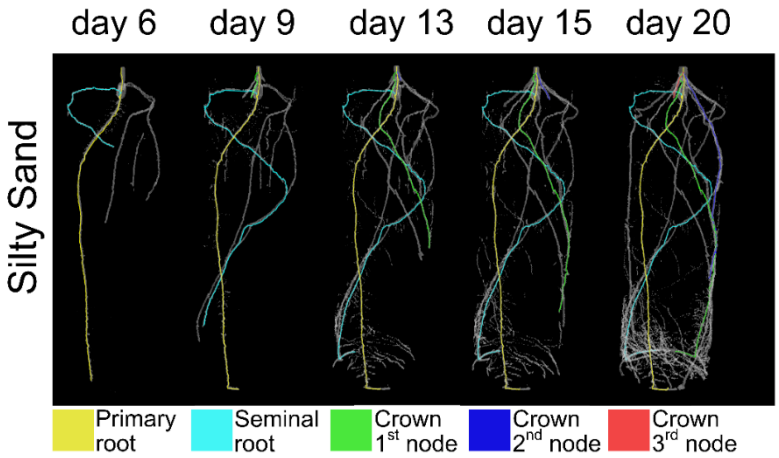

Fig. S1 The axial roots selected for sampling of the rhizosphere and root tissue as highlighted in the program NMRooting (exemplary plant).

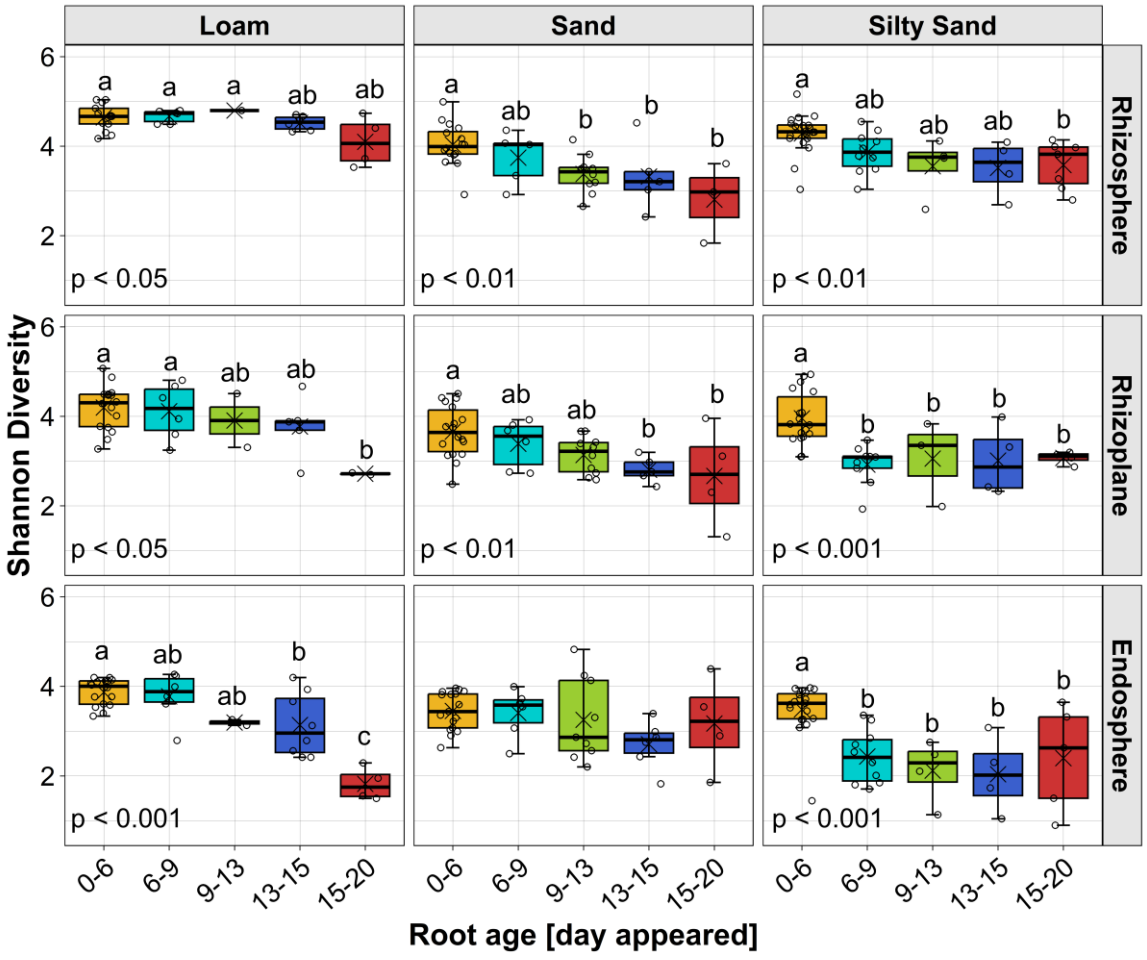

Fig. S2 Variation in bacterial alpha diversity associated with root age, displayed as Shannon diversity index. The *p*-values and distinct lowercase letters indicate significant differences within each substrate-compartment subset, as determined by ANOVA and Tukey HSD post-hoc tests.

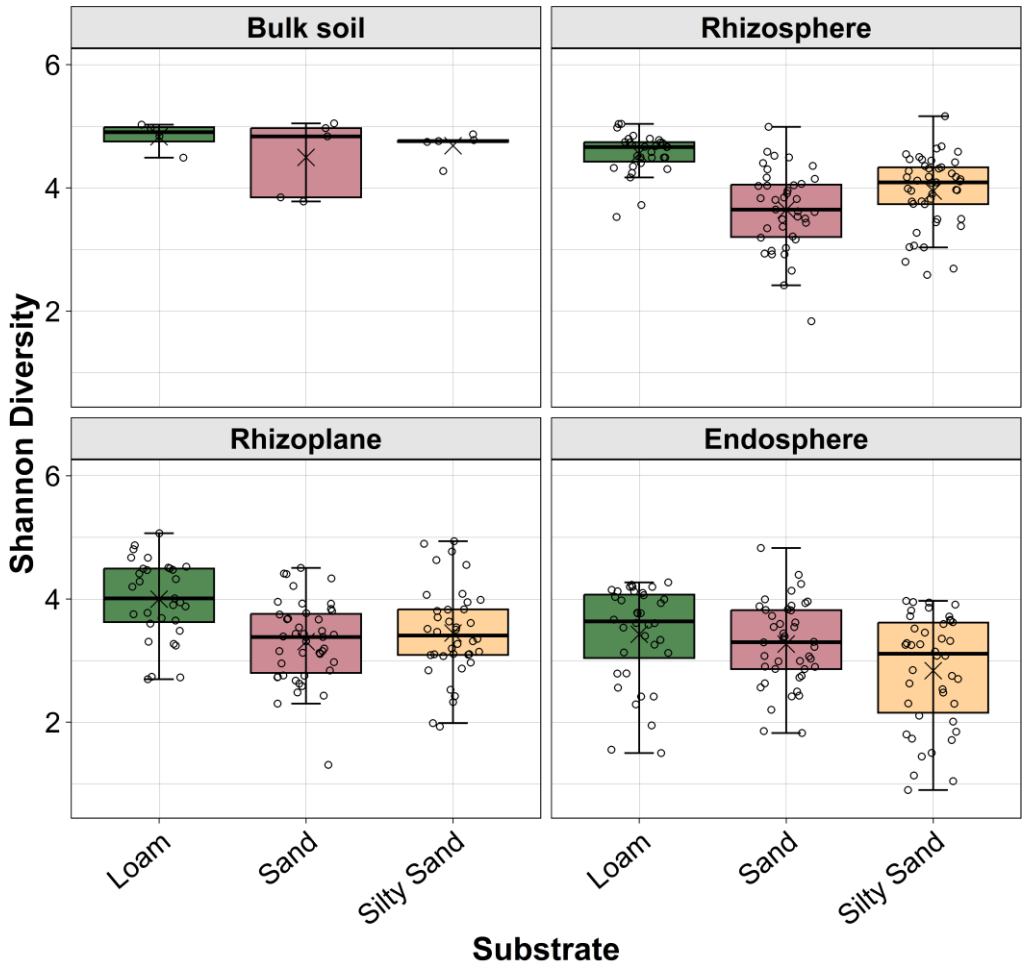

Fig. S3 Variation in bacterial alpha diversity in the bulk soil and the three root-associated compartments, evaluated based on the Shannon diversity index.

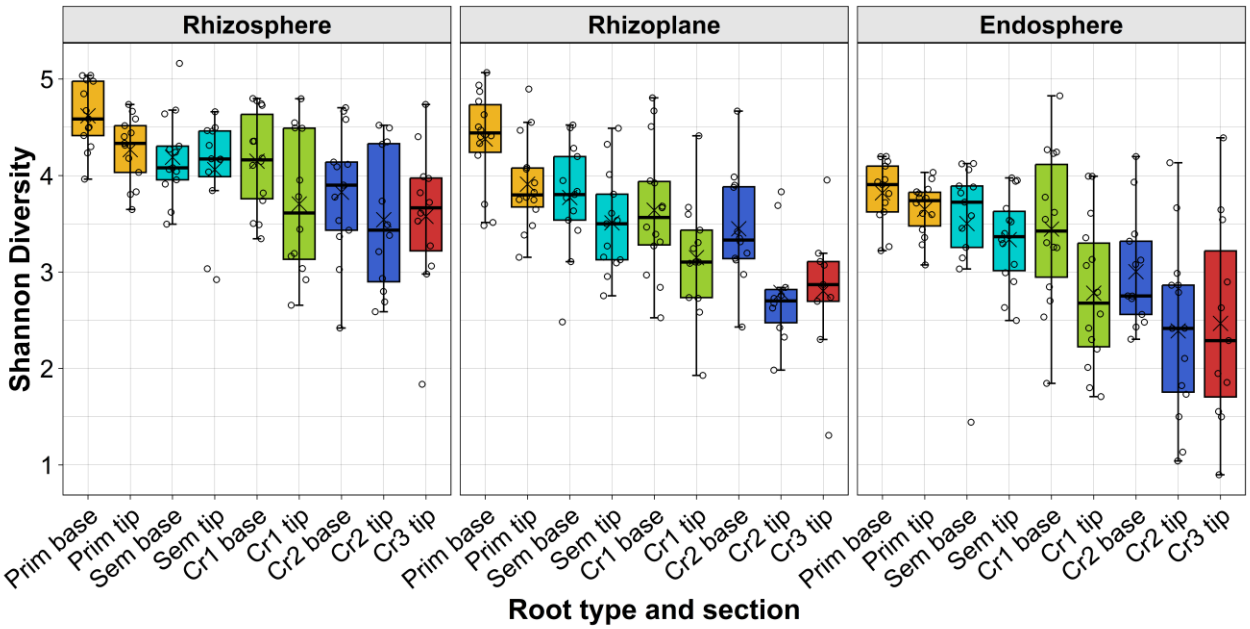

Fig. S4 Variation in bacterial alpha diversity across different root types and their respective sections, analyzed within three root-associated compartments rhizosphere, rhizoplane, and endosphere. Alpha diversity was assessed using the Shannon diversity index, averaged across the three soil substrates.

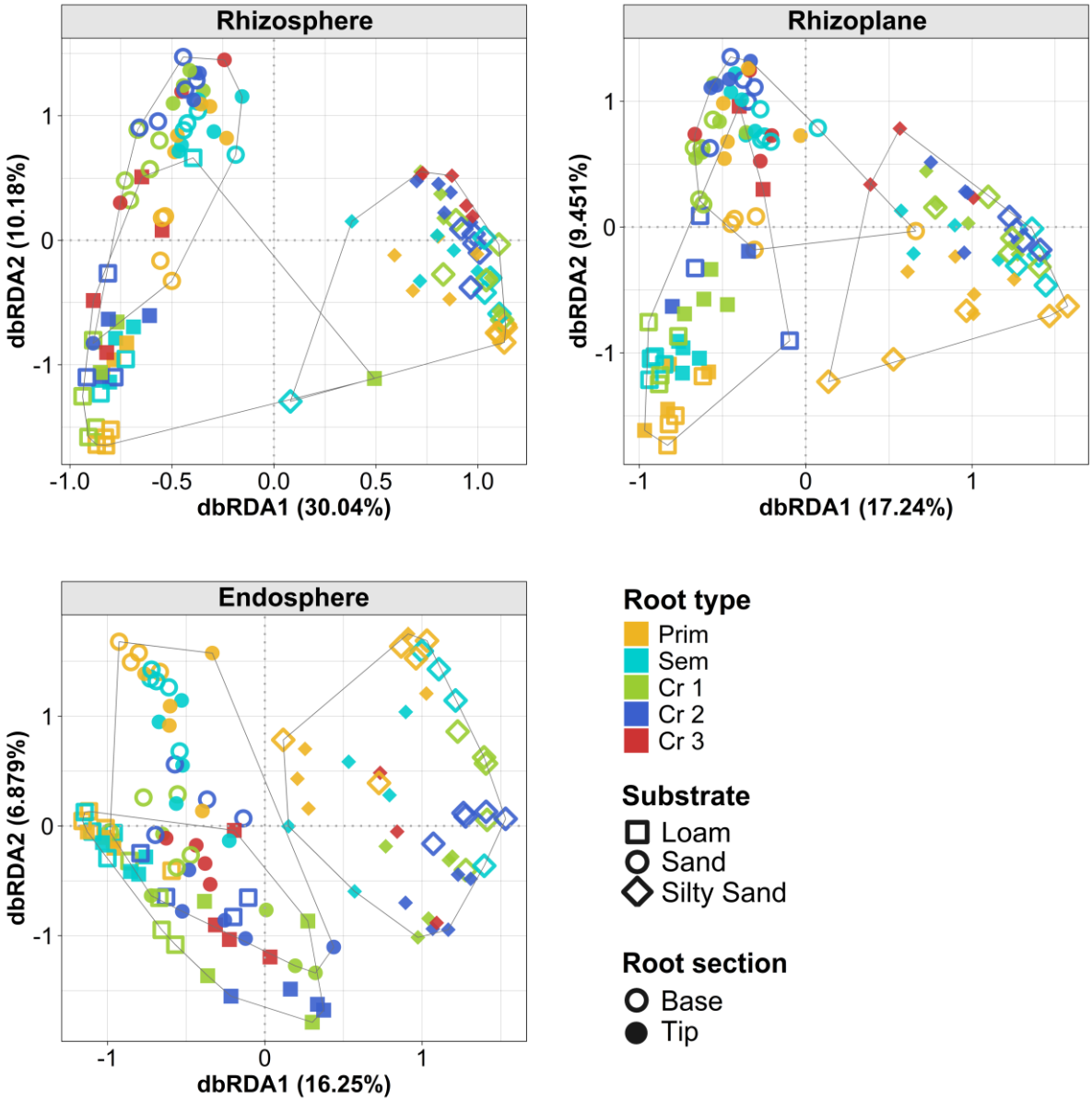

Fig. S5 Constrained ordination visualized by db-RDA plots based on Bray-Curtis dissimilarities. Information on the db-RDA models and the corresponding variation partitioning analysis can be found in Table S9 and S10.

Table S1 Substrate characteristics, as derived from Vetterlein, Lippold et al. (2021) for sand and loam, and from agricultural institution LUFA Speyer (Germany) for silty sand. Ct = total carbon, Nt = total nitrogen, Nmin = mineral nitrogen (plant-available), Corg = organic carbon.

Substrate property	Loam	Sand	Silty sand
Origin	Haplic Phaeozem	83.3% Sand 16.7% Loam	Speyer 2.1 standard soil
Texture (sand/silt/clay) [%]	33/48/19	92/5/3	87/10/3
Bulk density in pot [g cm^{-3}]	1.26	1.47	1.47
Initial microbiome	original	Loam	original
pH ($CaCl_2$)	6.4	6.3	4.6
Ct [g kg^{-1}]	8.5	1.5	-
Nt [g kg^{-1}]	0.8	0.2	-
Nmin [mg kg^{-1}]	1.4	0.3	-
P available [mg kg^{-1}]	32.7	8.3	-
K available [mg kg^{-1}]	28.5	7.8	-
Corg [%]	0.84	0.14	0.55

Table S2 Composition of PCR assays.

Chemical	PCR round 1 (10 µl)	PCR round 2 (30 µl)
5 x Herculase II Fusion buffer	1x	1x
dNTPs	0.25 mM each	0.25 mM each
primer 63f mod	0.4 µM	-
primer 1492r mod	0.4 µM	-
primer LNA-Mit 63	0.6 µM	-
primer LNA-Mit 1492	0.6 µM	-
primer LNA-Pla 63b	0.6 µM	-
primer LNA-Pla 1492b	0.6 µM	-
primer 515f (barcoded)	-	0.25 µM
primer 806r	-	0.25 µM
$MgCl_2$	1 mM	1 mM
BSA	0.8 mg/ml	0.8 mg/ml
Herculase II Fusion Polymerase	0.5 U	1.5 U
DNA template	1 µl	1 µl

Table S3 PCR cycling conditions for LNA primer assisted 16S amplicon sequencing.

	Cycler protocol	
	Round 1	
Initial denaturation	2:00 min at 95°C	
Denaturation	25x	0:20 min at 95°C
Annealing LNA		0:20 min at 70°C
Annealing 16S		0:20 min at 56°C
Elongation		0:45 min at 72°C
Final elongation	3:00 min at 72°C	
	Round 2	
Initial denaturation	2:00 min at 95°C	
Denaturation	10x	0:20 min at 95°C
Annealing 16S		0:20 min at 52°C
Elongation		0:20 min at 72°C
Final elongation	3:00 min at 72°C	

Table S4 Information on back-fitted linear mixed effects models.

	Model information
Rhizosphere model	lmer(Shannon ~ (1|plant) + Substrate + Root type + Root section + Growth rate + Substrate:Growth rate, REML = FALSE, data = df)
	Observations: 114 AIC = 141.91, BIC = 177.48
	Pseudo-R^2 (fixed effects) = 0.61
	Pseudo-R^2 (total) = 0.64
Rhizoplane model	lmer(Shannon ~ (1|plant) + Substrate + Root type + Root section + Substrate:Root type, REML = FALSE, data = df)
	Observations: 112 AIC = 171.90, BIC = 220.84
	Pseudo-R^2 (fixed effects) = 0.62
	Pseudo-R^2 (total) = 0.63
Endosphere model	lmer(Shannon ~ (1|plant) + Substrate + Root type + Root section + Substrate:Root type, REML = FALSE, data = df)
	Observations: 120 AIC = 233.38, BIC = 283.55
	Pseudo-R^2 (fixed effects) = 0.55
	Pseudo-R^2 (total) = 0.58

Table S5 Pairwise comparison of marginal means estimated by the **rhizosphere** linear mixed effect model. Degrees-of-freedom method: Satterthwaite. Significant *p*-values are printed in bold.

Variable	Contrast	Estimate	SE	df	*p* adj (Bonferroni)
Substrate	Loam – Sand	0.963	0.121	13.8	**<0.0001**
	Loam – Silty Sand	0.620	0.118	12.6	**0.0005**
	Sand – Silty Sand	-0.343	0.109	11.7	**0.0260**
Root section	Base – Tip	0.300	0.078	99.4	**0.0002**
Root type	Prim – Sem	0.287	0.112	99.3	0.1176
	Prim – Cr 1	-0.223	0.162	109.7	1.0000
	Prim – Cr 2	-0.237	0.248	112.4	1.0000
	Prim – Cr 3	-0.640	0.153	102.8	**0.0006**
	Sem – Cr 1	0.064	0.151	108.1	1.0000
	Sem – Cr 2	0.049	0.233	112.2	1.0000
	Sem – Cr 3	-0.353	0.150	100.7	0.2067
	Cr 1 – Cr 2	0.015	0.150	108.0	1.0000
	Cr 1 – Cr 3	0.417	0.159	102.4	0.1023
	Cr 2 – Cr 3	0.402	0.224	109.6	0.7565

Table S6 Pairwise comparison of marginal means estimated by the **rhizoplane** linear mixed effect model. Degrees-of-freedom method: Satterthwaite. Significant p-values are printed in bold.

Variable	Contrast	Estimate	SE	df	*p* adj (Bonferroni)
Substrate	Loam – Sand	0.561	0.177	112	**<0.0001**
	Loam – Silty Sand	0.416	0.121	112	**0.0025**
	Sand – Silty Sand	-0.145	0.107	112	**0.5357**
Root section	Base – tip	0.467	0.088	112	**<0.0001**
Root type (Loam)	Prim – Sem	-0.007	0.222	112	1.0000
	Prim – Cr 1	-0.131	0.222	112	1.0000
	Prim – Cr 2	-0.466	0.253	112	0.6811
	Prim – Cr 3	-1.242	0.354	112	**0.0064**
	Sem – Cr 1	-0.138	0.222	112	1.0000
	Sem – Cr 2	-0.473	0.253	112	0.6420
	Sem – Cr 3	-1.249	0.354	112	**0.0060**
	Cr 1 – Cr 2	0.335	0.253	112	1.0000
	Cr 1 – Cr 3	1.111	0.354	112	**0.0216**
	Cr 2 – Cr 3	0.775	0.375	112	0.4099
Root type (Sand)	Prim – Sem	0.670	0.199	112	**0.0101**
	Prim – Cr 1	-0.643	0.199	112	**0.0158**
	Prim – Cr 2	-1.087	0.204	112	**<0.0001**
	Prim – Cr 3	-1.054	0.266	112	**0.0013**
	Sem – Cr 1	0.028	0.199	112	1.0000
	Sem – Cr 2	-0.417	0.204	112	0.4344
	Sem – Cr 3	-0.384	0.266	112	1.0000
	Cr 1 – Cr 2	0.444	0.204	112	0.3149
	Cr 1 – Cr 3	0.412	0.266	112	1.0000
	Cr 2 – Cr 3	-0.033	0.271	112	1.0000
Root type (Silty Sand)	Prim – Sem	0.768	0.211	112	**0.0040**
	Prim – Cr 1	-1.402	0.204	112	**<0.0001**
	Prim – Cr 2	-1.253	0.211	112	**<0.0001**
	Prim – Cr 3	-1.019	0.295	112	**0.0080**
	Sem – Cr 1	-0.634	0.216	112	**0.0401**
	Sem – Cr 2	-0.485	0.222	112	0.3084
	Sem – Cr 3	-0.251	0.304	112	1.0000
	Cr 1 – Cr 2	-0.147	0.216	112	1.0000
	Cr 1 – Cr 3	-0.383	0.300	112	1.0000
	Cr 2 – Cr 3	-0.234	0.304	112	1.0000

Table S7 Pairwise comparison of marginal means estimated by the **endosphere** linear mixed effect model. Degrees-of-freedom method: Satterthwaite. Significant p-values are printed in bold.

Variable	Contrast	Estimate	SE	Df	*p* adj (Bonferroni)
Substrate	Loam – Sand	0.009	0.158	15.4	1.0000
	Loam – Silty Sand	0.472	0.160	16.4	**0.0282**
	Sand – Silty Sand	0.462	0.155	17.8	**0.0239**
Root section	Base – tip	0.404	0.103	106	**0.0002**
Root type (Loam)	Prim – Sem	0.210	0.268	106	1.0000
	Prim – Cr 1	-0.345	0.268	106	1.0000
	Prim – Cr 2	-0.839	0.268	106	**0.0227**
	Prim – Cr 3	-1.952	0.333	106	**<0.0001**
	Sem – Cr 1	-0.135	0.268	106	1.0000
	Sem – Cr 2	-0.630	0.268	106	0.2080
	Sem – Cr 3	-1.743	0.333	106	**<0.0001**
	Cr 1 – Cr 2	0.494	0.268	106	0.6825
	Cr 1 – Cr 3	1.607	0.333	106	**<0.0001**
	Cr 2 – Cr 3	1.113	0.333	106	**0.0113**
Root type (Sand)	Prim – Sem	0.324	0.247	107	1.0000
	Prim – Cr 1	-0.212	0.247	107	1.0000
	Prim – Cr 2	-0.682	0.254	108	0.0826
	Prim – Cr 3	-0.245	0.326	107	1.0000
	Sem – Cr 1	0.112	0.240	106	1.0000
	Sem – Cr 2	-0.358	0.247	107	1.0000
	Sem – Cr 3	0.080	0.323	109	1.0000
	Cr 1 – Cr 2	0.470	0.247	107	0.5967
	Cr 1 – Cr 3	0.032	0.323	109	1.0000
	Cr 2 – Cr 3	-0.438	0.327	109	1.0000
Root type (Silty Sand)	Prim – Sem	0.377	0.247	107	1.0000
	Prim – Cr 1	-1.239	0.240	106	**<0.0001**
	Prim – Cr 2	-1.530	0.240	106	**<0.0001**
	Prim – Cr 3	-1.048	0.359	111	**0.0428**
	Sem – Cr 1	-0.863	0.247	107	**0.0069**
	Sem – Cr 2	-1.153	0.247	107	**0.0001**
	Sem – Cr 3	-0.671	0.364	112	0.6741
	Cr 1 – Cr 2	0.291	0.240	106	1.0000
	Cr 1 – Cr 3	-0.191	0.359	111	1.0000
	Cr 2 – Cr 3	-0.482	0.359	111	1.0000

Table S8 Information on soil-based db-RDA models corresponding to Fig. 6 (F values and significance for predictors and models).

Model	Predictor	df	Sum of Squares	F	*p*
Loam	Whole model	7	10.730	8.894	**0.001**
	Compartment	2	4.873	14.137	**0.001**
	Root type	4	4.148	6.018	**0.001**
	Root section	1	1.709	9.915	**0.001**
Sand	Whole model	7	10.694	8.087	**0.001**
	Compartment	2	2.222	5.881	**0.001**
	Root type	4	5.410	7.159	**0.001**
	Root section	1	3.062	16.208	**0.001**
Silty Sand	Whole model	7	10.773	8.626	**0.001**
	Compartment	2	3.531	9.895	**0.001**
	Root type	4	4.529	6.345	**0.001**
	Root section	1	2.713	15.207	**0.001**

Table S9 Information on compartment-based db-RDA models corresponding to Fig. S5 (F values and significance for predictors and total models).

Model	Predictor	df	Sum of Squares	F	*p*
Rhizosphere	Whole model	7	16.580	14.331	**0.001**
	Substrate	2	13.339	40.354	**0.001**
	Root type	4	2.148	3.249	**0.001**
	Root section	1	1.093	6.611	**0.001**
Rhizoplane	Whole model	7	13.220	8.946	**0.001**
	Substrate	2	8.968	21.239	**0.001**
	Root type	4	2.853	3.378	**0.001**
	Root section	1	1.400	6.630	**0.001**
Endosphere	Whole model	7	14.556	9.036	**0.001**
	Substrate	2	8.411	18.275	**0.001**
	Root type	4	4.370	4.748	**0.001**
	Root section	1	1.775	7.714	**0.001**

Table S10 Variation partitioning results corresponding to Fig. S5.

	Rhizosphere	Rhizoplane	Endosphere
Substrate	0.4107	0.2603	0.2150
Root type	0.0456	0.1603	0.0907
Root section	0.0297	0.0988	0.0422
Shared variation	0.0000	0.0004	0.0002
Residuals	0.5350	0.6534	0.6641

2.2. Photosynthate distribution determines spatial patterns in the rhizosphere microbiota of the maize root system

Sina R. Schultes[1], Lioba Rüger[2], Daniela Niedeggen[2], Jule Freudenthal[2], Katharina Frindte[1], Maximilian F. Becker[1], Ralf Metzner[3], Daniel Pflugfelder[3], Antonia Chlubek[3], Carsten Hinz[3], Dagmar van Dusschoten[3], Sara Bauke[4], Michael Bonkowski[2], Michelle Watt [3,5], Robert Koller[3], Claudia Knief[1]

[1]Institute for Crop Science and Resource Conservation (INRES), Molecular Biology of the Rhizosphere, University of Bonn, Bonn, Germany

[2]Institute of Zoology, Terrestrial Ecology, Cluster of Excellence on Plant Sciences (CEPLAS), University of Cologne, Cologne, Germany

[3]Institute of Bio- and Geosciences, IBG 2: Plant Sciences, Forschungszentrum Jülich GmbH, Jülich, Germany

[4]Institute for Crop Science and Resource Conservation (INRES), Soil Sciences, University of Bonn, Bonn, Germany

[5]Adrienne Clarke Chair of Botany, School of BioSciences, Faculty of Science, University of Melbourne, Melbourne, Australia (present)

https://doi.org/10.1038/s41467-025-62550-y

Abstract

The spatial variation and underlying mechanisms of pattern formation in the rhizosphere microbiota are not well understood. We hypothesized that specific patterns in the distribution of recently fixed carbon within plant root systems influence the spatial organization of the rhizosphere microbiota. We non-invasively analyzed the distribution of carbon in the maize root system at high spatiotemporal resolution using ^{11}C tracer-based positron emission tomography combined with magnetic resonance imaging. Image analysis showed a high spatial heterogeneity in carbon allocation, with highest accumulations at root tips and differences between root types. Image-guided sampling of rhizosphere soil from different root regions after additional $^{13}CO_2$ labeling showed strong correlations between root internal carbon allocation and rhizodeposition. Bacterial, fungal and protistan (cercozoan) community structure in these rhizosphere samples differed depending on root structure and related spatial heterogeneities in carbon allocation. Especially ^{13}C-labeled consumers of rhizodeposits, identified by DNA stable isotope probing, were responsive to photosynthate distribution, whereby specific taxa profited most from rhizodeposits in specific root regions. Thus, root photosynthate allocation is a key determinant of rhizosphere microbial food web development and causes niche differentiation, resulting in the formation of characteristic spatiotemporal patterns in the rhizosphere of the plant root system.

Introduction

The assembly of the rhizosphere microbiome is the result of complex interactions between the plant and microorganisms. It is further affected by abiotic and biotic factors such as soil properties and interactions between microorganisms in the rhizosphere. It is suggested that microbiome enrichment by the plant host is, for a large part, mediated by rhizodeposition of various compounds into the rhizosphere (Hu et al., 2018). Plants exude a substantial amount of carbon into the rhizosphere(Pausch & Kuzyakov, 2018), and different exudate compounds have been reported to attract specific microbial consumers (Schütz et al., 2021; Thoenen et al., 2024; Yu et al., 2021). These microbial consumers of rhizodeposits have been identified using $^{13}CO_2$ labeling followed by DNA-based stable isotope probing (DNA-SIP) (Hünninghaus et al., 2019).

The root system is mostly sampled as a whole, but no studies have yet systematically unraveled how spatially heterogeneous rhizodeposition affects microbiome assembly and creates spatial patterns within the root system. In particular cereal plants such as maize have a complex root system consisting of different root types with seed-borne (primary and seminal) roots and shoot-borne (crown) roots that develop sequentially over time from different nodes (Fig. S1) (Haichar et al., 2012; Hochholdinger, Park, et al., 2004). This likely results in the development of root-type specific microbiomes in the rhizosphere (Kawasaki et al., 2021). Further, variation is known to occur along the longitudinal root axis (Rüger et al., 2021). These heterogeneities in the microbiome suggest the presence of consistent, small-scale selection mechanisms in the rhizosphere. However, apart from the notion of exudation hotspots at root tips that a specific bacterial reporter strain profited from (Waller et al., 2020), photosynthate distribution within the root system remains largely unresolved at the small scale. It is thus unclear to what extent spatial variation in the rhizosphere microbiome is related to spatial patterns of carbon allocation within the root system and rhizodeposition.

We address this uncertainty by combining $^{11}CO_2$ pulse labeling of plants coupled with positron emission tomography (PET) and magnetic resonance imaging (MRI). The short-lived carbon radioisotope ^{11}C ($t_{1/2}$ = 20.4 min) allows for tracing recently fixed carbon in vivo and enables detailed time series of ^{11}C tracer allocation processes in the root system (Jahnke et al., 2009; Metzner et al., 2022; Yu et al., 2024). Using image-guided sampling for destructive sample collection, data on photosynthate allocation were integrated with microbial data from community compositional analysis (study I). In a second study, this approach was complemented by photosynthate labeling using $^{13}CO_2$ as stable isotopic tracer to track the transfer of carbon from the root into the rhizosphere and its microbiota, followed by DNA-based stable isotope probing (SIP) to identify key microbial consumers of rhizodeposits (Fig. 1). We analyzed the prokaryotic, fungal and cercozoan consumers,

the latter representing a major group of soil protists (Fiore-Donno et al., 2019). We hypothesize that (I) photosynthates are heterogeneously distributed in the root system and released into the rhizosphere, (II) the rhizosphere microbiota develops specific spatial patterns in the plant root system, and (III) in particular microbial consumers of rhizodeposits respond strongly to photosynthate patterns. This would make photosynthate distribution a central driver of microbial small-scale heterogeneity in the rhizosphere of a root system.

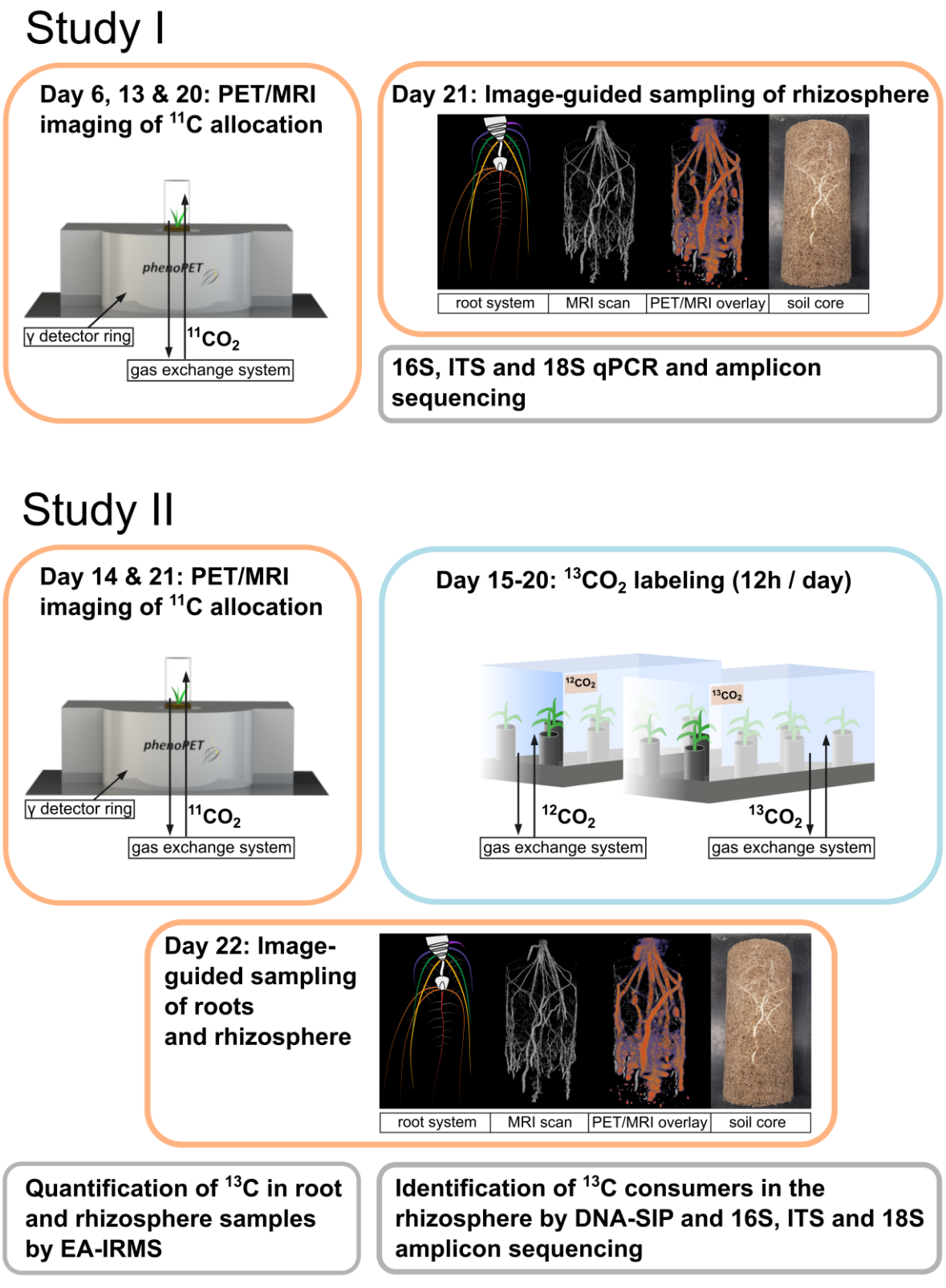

Fig. 1 Conceptual study design. In Study I we investigated temporal changes in photosynthate allocation and the effect of small-scale spatial heterogeneity in photosynthate allocation on the prokaryotic, fungal and cercozoan rhizosphere communities. PET-MRI imaging (orange boxes) enabled us to define root regions with distinct photosynthate levels (low, medium, high) and to consider root architecture at high spatial resolution for identifying root types and sections during sampling. Study II combines this approach with $^{13}CO_2$ labeling (blue box) to specifically identify

photosynthate consumers and investigate their response to spatially heterogeneous photosynthate distribution. Analyses upon destructive sampling (grey boxes) included elemental analysis coupled to isotope ratio mass spectrometry (EA-IRMS) to obtain quantitative data on photosynthate contents of root and rhizosphere samples and DNA-based microbial community compositional analyses.

Material and methods

Soil preparation and plant cultivation

Soil columns were established according to Vetterlein et al. (2021). Briefly, 16.7% loam soil derived from a Haplic Phaeozem (Schladebach, Germany) was mixed with 83.3% quartz sand (WF33, Quarzwerke GmbH, Frechen, Germany). This growth substrate was dried, sieved to <1 mm and fertilized (Vetterlein et al., 2021) before homogeneously filling PVC columns (20 cm height, 8 cm diameter) up to a bulk density of 1.47 g cm^{-3}. *Zea mays* seeds (line B73) were surface sterilized in 10% H_2O_2 for 10 min, primed in a saturated $CaSO_4$ solution for 3 h and sown at 1.5 cm depth. Plants were grown in a climate chamber for 22 days as described (Vetterlein et al., 2021), while upholding a volumetric soil water content of 18%.

$^{13}CO_2$ labeling of plants

Stable isotope labeling to trace photosynthates into the rhizosphere and its microbiota was conducted in two Perspex® chambers adapted from Hünninghaus et al. (2019) (Fig. 1). Eight plants were transferred into each labeling chamber at day 15 after sowing and either exposed to $^{13}CO_2$ or unlabeled CO_2, (referred to as $^{12}CO_2$). Plants were continuously labeled during the whole 12-hour light period for 6 days. Both chambers were initially scrubbed of ambient CO_2 by passing air through a soda lime cartridge at each labeling day before $^{12}CO_2$ or 99% $^{13}CO_2$ (Linde GmbH, Pullach, Germany) were pumped into the respective chambers and evenly dispersed by ventilators. In both chambers, constant gas concentrations of 407 ± 20 ppm were established using an automated system combining $^{12}CO_2$ and $^{13}CO_2$ gas analyzers ($^{12}CO_2$ = Li-820, LI-COR Biosciences – GmbH, Bad Homburg, Germany, $^{13}CO_2$ = S710, Sick AG, Waldkirch, Germany) (Fig. S14). Temperature within chambers was regulated to maintain 18 °C at night and 23 °C during the light period, ± 2°C. At the end of each labeling day, the labeling gases within the chambers were scrubbed by passing through a soda lime cartridge and the chambers were opened to allow for inflow of ambient CO_2.

2.2. Results

Radioactive $^{11}CO_2$ labeling and PET-MRI scanning

Plants were supplied with ^{11}C ($t_{1/2}$≈20 min) labeled CO_2 and scanned by PET (Fig. 1) to non-invasively visualize the short-term photosynthate distribution in the root system. Due to the short half-life of ^{11}C, it is produced on site with a dedicated cyclotron. The night before PET scanning, plants were transferred to the *pheno*PET facility (Hinz et al., 2024) and mounted in an environmentally controlled labeling cuvette connected to the gas exchange system with the roots in the field of view of the *pheno*PET. The shoot was subjected to labeling with ~200 MBq $^{11}CO_2$ for 6 min after the start of the 2.5 h PET measurement. Data processing and image reconstruction is based on Hinz et al. (2024) except for the coincidence sorting, which had already been updated to the multi-window coincidence sorter with takeAllGood handling of multiple coincidences. The image reconstruction was done in 5-minute frames. Scatter and attenuation corrections were not applied. PET measurements were complemented by transferring the plant to MRI to non-invasively monitor root system architecture. We used a 4.7-T vertical bore magnet (Magnex Scientific, Oxford, United Kingdom) equipped with a 21-cm gradient system up to 400 mT/M (MR Solutions, Guildford, United Kingdom) and a 10-cm RF coil (Varian, Palo Alto, CA) as previously described by van Dusschoten et al. (2016). To counter imaging artifacts observed in this soil, the imaging parameters were set to: Spin-Echo Multi-Slice (SEMS) sequence, Bandwidth = 400 kHz, 4 averages, Field of view = 96 mm, 0.5 mm resolution, 1 mm slice thickness, echo time TE = 9 ms, repetition time TR = 2.8 s. MRI data were analyzed using the program NMRooting (van Dusschoten et al., 2016). We restricted root tree analysis to the axial roots, i.e. the primary root, seminal roots and crown roots, thus excluding all lateral roots and quantified root length (Fig. S15). For further analysis and to enable image-guided sampling, overlays of the PET and MRI 3D-scans were constructed in the MeVisLab environment (MeVis Medical Solutions AG, Bremen, Germany).

Image-guided root and rhizosphere soil sampling

Before sampling, the soil was brought to the targeted volumetric water content to ensure comparable extension of the rhizosphere. Soil cores were pushed out of the pots and MRI images were used for orientation and identification of root and rhizosphere samples. We took root tip samples of about 2 cm length and root base samples of about 10 cm length (Fig. S1) from every root, while distinguishing between the primary root, seminal roots, and crown roots from the first to the third or fourth underground node. PET scans enabled to roughly categorize root samples according to three ^{11}C tracer signal intensity levels. We distinguished root tips with high signal intensity, root tips with medium signal intensity and basal root sections with low signal intensity. Lateral roots were cut off to avoid mixed root type signals. As the youngest crown roots were very small on the day of

sampling, only root tip samples were taken from this root type. Rhizosphere samples were taken by dipping the root pieces in 0.3% sterile NaCl solution. To sediment the rhizosphere soil, the suspension was centrifuged at 5000 x g and 4 °C for 30 min. Root tissue samples were further cleaned upon dipping by vortexing the root pieces in 0.3% sterile NaCl for 15 seconds. The pelleted rhizosphere soil samples and the washed root pieces were stored at -80 °C.

Analyses were done in study I for individual roots from a total of three plants, whereas the same type of root sample, i.e. roots of each root type and section, from two plant replicates were pooled in study II to obtain enough material for all analyses (Fig. S1). The previously obtained PET-MRI scans ensured that the photosynthate allocation and development of sampled roots were comparable (Fig. S3). Using 16 plants in total, this resulted in four replicate ^{13}C-labeled sample sets and four corresponding ^{12}C-control sets covering all root types, root sections and photosynthate allocation categories in study II (Table S4).

Determination of ^{13}C isotopic abundances in root and rhizosphere samples

A subsample of each rhizosphere and root sample was dried for 4 days at 50 °C and ground to a fine powder by hand. Approximately 70 mg of rhizosphere soil and 0.5 mg of root material was used for $^{13}C/^{12}C$ isotope analysis with an elemental analyzer (Flash EA 1112; Thermo Fisher GmbH, Bremen, Germany) coupled to an isotope ratio mass spectrometer (Delta V Advantage; Thermo Fisher Scientific, Waltham, MA, USA). We calibrated results against the reference materials calcite (IAEA 603; $\delta^{13}C$ = 2.46‰) and corn starch (Schimmelmann Research, Indiana University; $\delta^{13}C$ = -11.01‰).

DNA extraction

DNA was extracted from ~500 mg of wet rhizosphere sample using the FastDNA™ SPIN Kit For Soil (MP Biomedicals™, Santa Ana, Canada) following the protocol of Tournier et al. (2015) with minor alterations (2 x 45 s cell disruption, 100 µl elution volume). The DNA was quantified using the QuantiFluor dsDNA System on a Quantus™ Fluorometer (Promega, Madison, WI, USA).

DNA stable isotope probing

DNA-SIP was performed for 36 ^{13}C-labeled samples and 36 corresponding ^{12}C-control samples following the protocol of Lueders (2010) with minor alterations. Per sample, ~1500 ng of DNA was loaded onto CsCl (≥99.999% p.a., Carl Roth, Karlsruhe, Germany) suspensions with a starting density

of 1.721 g ml^{-1}. Samples were randomly assigned to different ultracentrifuge runs to compensate for possible run-related variation. Gradients were spun at 20°C and 177.000 x g for 38 h in an Optima™ XPN-80 ultracentrifuge with VTi 65.2 rotor (Beckman Coulter, Brea, CA, USA). Gradients were fractionated from bottom (heavy) to top (light) into 12 fractions (~400 µl) by displacement of the gradient solution with bromophenol blue stained DEPC-water. The buoyant density of each fraction was determined by measuring the temperature-corrected refractive index (nDTC) of a small sample aliquot on an AR200 refractometer (Reichert, Depew, NY, USA). Depending on sample origin (root type, root section), we observed that light, unlabeled DNA peaked at densities around 1.705 - 1.710 g ml^{-1} and heavy, ^{13}C-labeled DNA peaked at buoyant densities of around 1.720 – 1.728 g ml^{-1} (Fig. S16). The DNA in each fraction was precipitated by adding 2 Vol of 30% PEG 6.000 in 1.6 M NaCl and 1 µl of glycogen (20 µg; Roche, Basel, Switzerland) before incubating the samples at room temperature for 2 h. This was followed by 40 min of centrifugation at 4 °C and 21.000 x g, a washing step in 70% EtOH and a second centrifugation step of 25 min before the pellet was eluted in 25 µl of 10 mM Tris-HCl and stored at -80 °C. After centrifugation, one heavy and one light fraction of each sample was selected for amplicon sequencing. The selection was done individually for bacteria, fungi and Cercozoa based on quantitative PCR (qPCR) data generated for all fractions. Plotting the 16S rRNA, ITS1 and 18S rRNA copy numbers against the buoyant density revealed the fractions that contained peaks of ^{13}C- and ^{12}C-DNA, respectively (Fig. S16).

Quantitative PCR and amplicon sequencing

Quantitative PCR assays were performed as previously described (Frindte et al., 2020) using 10-fold diluted DNA solutions with slightly adapted thermal cycling protocols (Table S5) and the same primers as for amplicon sequencing (Table S6).

Prokaryotic 16S rRNA gene amplicons, fungal ITS1 amplicons and cercozoan SSU/18S rRNA gene amplicons were generated following group-specific two-step PCR protocols (Table S6, S7, S8). As ITS1 amplification products showed several unspecific bands on a 1.5% agarose gel, correct bands were excised after the first round of PCR and purified using the NucleoSpin® Gel and PCR Clean-up Kit (Macherey-Nagel, Düren, Germany) Prokaryotic and fungal amplification products were quantified using the QuantiFluor dsDNA System on a Quantus™ Fluorometer and pooled at equimolar concentrations. 18S rRNA gene amplicons were processed using the SequalPrep Normalisation Plate Kit (Invitrogen GmbH, Karlsruhe, Germany). Pooled PCR products were purified with the CleanNA magnetic bead system (GC-Biotech, Waddinxveen, the Netherlands). Library preparation and sequencing of the amplicons was performed by the West German Genome Center (WGGC) and the

Cologne Center for Genomics (Cologne, Germany), on MiSeq instruments (Illumina, San Diego, Canada) generating 2x300 bp paired-end reads.

Sequence data analysis

The raw sequence reads were preprocessed using a customized bash script with Cutadapt version 4.2 to demultiplex the samples (Martin, 2011). Primer trimming was performed using QIIME 2, version 2022.11 (Bolyen et al., 2019) and denoised ASVs were created for bacteria and fungi using the DADA2 pipeline (Callahan et al., 2016). The denoising step also comprised forward and reverse read merging and chimera removal. Sequence alignment was performed using the MAFFT software (Katoh & Standley, 2013). The SILVA database (version 138) was used for prokaryotic taxonomy assignment (Quast et al., 2012) and the UNITE database (version 9) for fungal taxonomy assignment (Abarenkov et al., 2024). Data were exported into R (version 4.2.3) and analyzed with the packages *phyloseq* (McMurdie & Holmes, 2013), *vegan* (Dixon, 2003) and *microbiome* (Lahti & Shetty, 2018). Singletons and reads unclassified above class level were removed from the data sets (Table S9).

Cercozoan raw sequence reads were processed using the custom MOTHUR pipeline v.39.5 (Schloss et al., 2009). After demultiplexing and primer- and tag-sequence trimming, the remaining reads were clustered into OTUs using VSEARCH (Rognes et al., 2016) with an abundance-based greedy clustering algorithm (agc) at a similarity threshold of 97%. Clusters with fewer than 214 reads were removed to eliminate potential amplification or sequencing noise (Fiore-Donno et al., 2019). OTUs were assigned to taxa using BLAST+ (Camacho et al., 2009) with an e-value cutoff of 1e-50 and the PR2 database (Guillou et al., 2012), retaining only the best hit. Non-target sequences were excluded. Sequences were aligned using the provided template (Fiore-Donno et al., 2019) allowing gaps of up to five nucleotides, and cleaned for chimeras using UCHIME (Edgar et al., 2011).

Statistical evaluation

Alpha diversity was analyzed using rarefied datasets and differences were assessed by ANOVA and Tukey-HSD posthoc tests or Mann-Whitney U-tests with Benjamini-Hochberg correction. Beta diversity was assessed by NMDS plots based on Bray-Curtis dissimilarities calculated from rarefied datasets. Differences in community structure were evaluated by PERMANOVA using the function *adonis2()* of the *vegan* package.

To identify microbial consumers of ^{13}C-labeled recent photosynthates, we employed the *HRSIP()* function from the R package *HTSSIP* (Youngblut et al., 2018). To increase statistical power, we

grouped samples in two different ways. In one approach, samples were grouped into four categories based on their ^{13}C abundance in the rhizosphere as measured by EA-IRMS (Category 1: 1.5% - 6.5%; Category 2: 6.5% - 11.5%, Category 3: 11.5% - 16.5%; Category 4: 16.5% - 21.5%; Fig. S9). Alternatively, samples were classified into four categories based on their origin within the root system: seed-borne tip, seed-borne base, shoot-borne tip, and shoot-borne base. A separate *HRSIP* analysis was conducted for each category using non-rarefied sequence datasets. *HRSIP* utilizes the differential gene expression analysis from the R package *DESeq2* (Love et al., 2014) to identify ASVs that are significantly enriched in high buoyant density fractions (BD of 1.72 – 1.75 g ml^{-1}) of ^{13}C-labeled samples compared to the high buoyant density fractions of unlabeled control samples (Youngblut et al., 2018).

We conducted co-occurrence network analyses to explore associations between bacterial, fungal and cercozoan communities in the rhizosphere of the root tip and base sections for the ^{13}C-labeled plants. Prior to network calculation, sequence read counts were summarized at species level. Species that were present in less than 1/4 of all samples were summed into one pseudo taxon to reduce spurious edges (Röttjers & Faust, 2018). Additionally, the location of the sample within the root system and the abundance of ^{13}C in the rhizosphere (AT% ^{13}C) were included in the network calculation. To account for the compositionality of community data, the bacterial, fungal and cercozoan datasets were individually normalized by centered log-ratio transformation. Further, z-transformation was applied to the numeric metadata, while categorical metadata were hot-encoded. The networks were calculated using FlashWeave v.0.18.0 (Tackmann et al., 2019) with parameters for homogeneous data (sensitive = true and heterogeneous = false) and without normalization. The species networks were summarized in R to genus and order level and visualized in Cytoscape v.3.9.0 (Shannon et al., 2003). The node parameters were assessed with the NetworkAnalyzer (Assenov et al., 2008) implemented in Cytoscape.

Data availability

Amplicon sequencing data have been deposited in the Sequence Read Archive (SRA; bioproject number PRJNA1145186).

Results

PET-MRI imaging reveals highly heterogeneous distribution of recently fixed carbon

In the two experimental studies, the root systems of all plants were regularly imaged by PET-MRI to non-invasively collect data on photosynthate allocation and root growth. ^{11}C-PET in combination with MRI measurements revealed that recently fixed carbon was heterogeneously distributed in the plant root system over time (Fig. 2). Nevertheless, consistent patterns were observed among the $^{11}CO_2$ labeled plants in study I (Fig. S2) and study II (Fig. S3).

We evaluated the spatial patterns in ^{11}C-photosynthate allocation into the root system at three different time points in study I. After 6 days of plant development, no ^{11}C tracer was detected in the root system, indicating that recently fixed carbon was not yet allocated into the roots (Fig. 2a). In contrast, intensive and heterogeneous belowground allocation of carbon was observed in plants of 13 and 20 days of age, with primary, seminal and crown root tips exhibiting high levels of ^{11}C tracer signal. Tips of the most recently emerged crown roots held particularly strong accumulations of the tracer. On day 13, the tips of crown roots of the 2nd node were rapidly supplied with recently fixed carbon and showed the highest ^{11}C signal intensity. On day 20, the newly emerging crown roots of the 3rd and 4th node showed particularly high signal intensity, while intensity in crown roots of the 2nd node had declined as the roots matured. Lateral root tips also showed photosynthate accumulations, but this was more difficult to resolve due to their high number and overlapping tracer signals.

Belowground ^{11}C-photosynthate allocation into the root system occurred very rapidly (Fig. 2b, Vid. S1), with the first photosynthates being detected in the primary root at around 10-15 minutes after the start of the pulse labeling (Fig. 2b, white arrow). ^{11}C-photosynthate allocation into seminal and crown roots occurred at about 25-30 minutes after labeling started. This was observed in both, 13 and 20-day old plants (Fig. 2b). The first accumulations of labeled photosynthates at root tips were detected at about 25-30 minutes in 13-day old plants and at around 40-45 minutes in 20-day old plants (Fig. 2b, green arrow). Once established, these accumulations at root tips generally persisted over the total measurement time, whereas the tracer signal disappeared at the root bases of some roots over time including the primary root, which had received the tracer first.

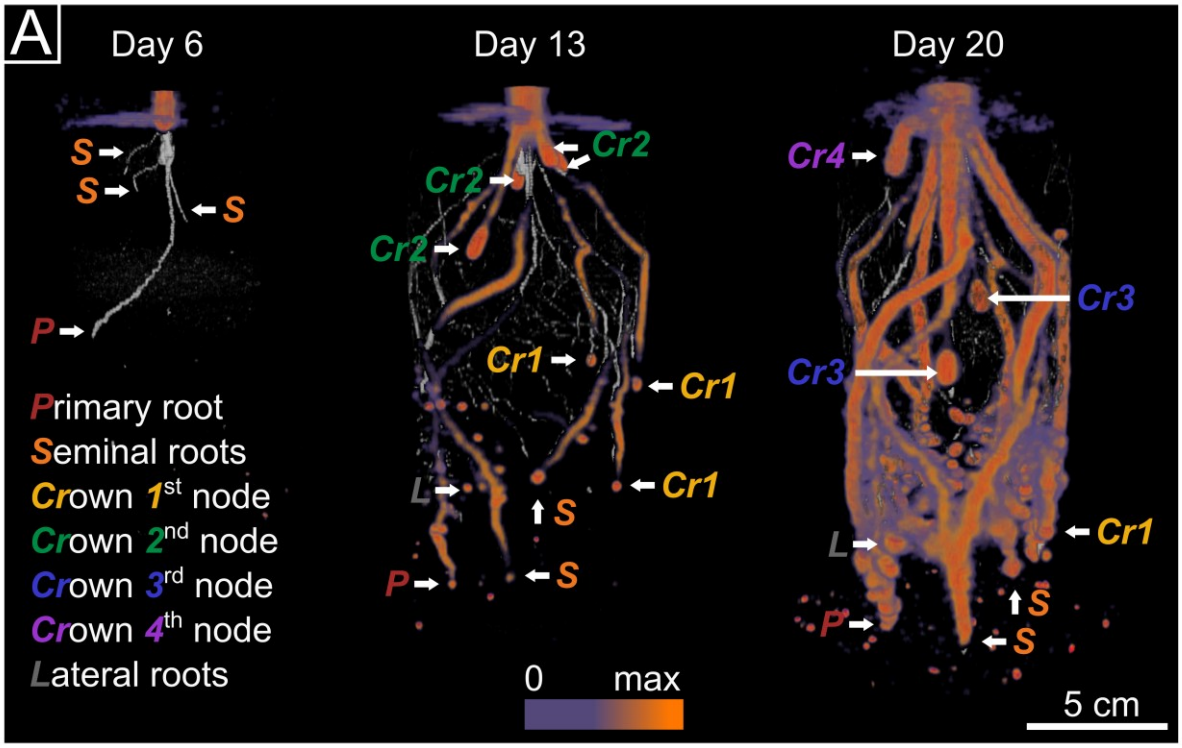
A
Day 6
Day 13
Day 20
S
S
S
P
Cr2
Cr2
Cr2
Cr1
Cr1
Cr1
L
S
P
S
Cr4
Cr3
Cr3
L
Cr1
S
P
S
Primary root
Seminal roots
Crown 1st node
Crown 2nd node
Crown 3rd node
Crown 4th node
Lateral roots
0
max
5 cm

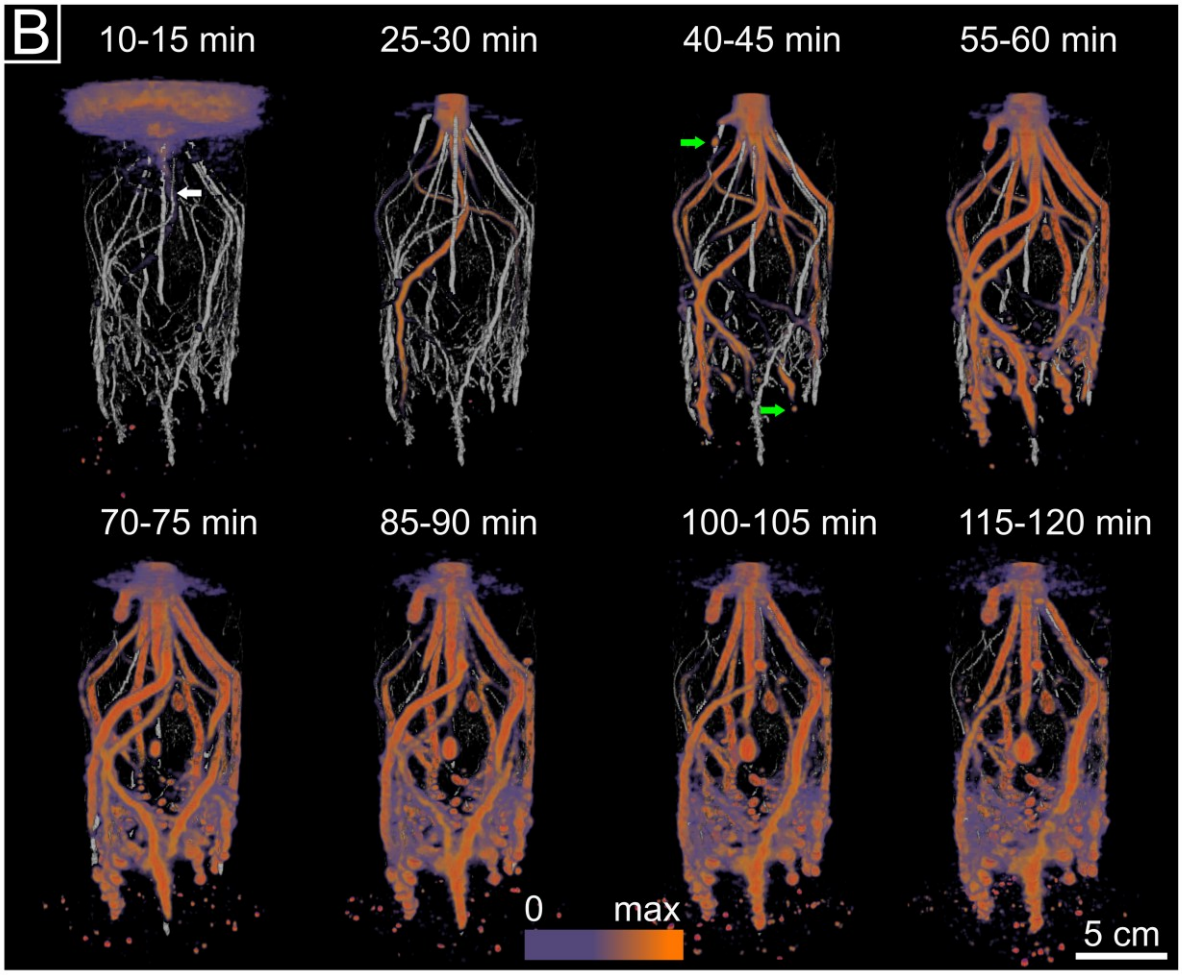
B
10-15 min
25-30 min
40-45 min
55-60 min
70-75 min
85-90 min
100-105 min
115-120 min
0
max
5 cm

Fig. 2 Allocation of recently fixed carbon in roots visualized by co-registered PET-MRI scans. The same maize plants were imaged in study I at three time points by PET (colored) and MRI (grey) over a period of 120 minutes. **(a)** Co-registered PET-MRI scans were obtained for 6-, 13-, and 20-day old plants at 85-90 minutes after labeling start. Prominently visible representatives of the different root types are marked with letters: P = primary root, S = seminal roots, Cr = crown roots of nodes 1-4, L = lateral roots. On day 6, the root system consisted of the primary root and three seminal roots. On day 20, around 10-12 crown roots from up to four different consecutive nodes had developed in all plants. **(b)** Belowground allocation of ^{11}C-labeled photosynthates in a 20-day old plant over the measurement period of 2 hours. Images are integrals calculated over 5 minutes of measurement. The white arrow indicates ^{11}C tracer arrival in the primary root and green arrows arrival at root tips. A time-lapse video showing ^{11}C-photosynthate allocation is available as supplementary material (Vid. S1).

Root photosynthate allocation as main driver of rhizodeposition

To relate carbon allocation inside of the roots to carbon allocation in the rhizosphere, the ^{11}C-PET analysis was complemented by stable isotope labeling of shoots with $^{13}CO_2$ and EA-IRMS measurements of root tissue and rhizosphere samples from root tips (2 cm length) and bases (upper 10 cm of a root) after destructive sampling in study II. The $^{11}CO_2$ labeling pulse was again 6 min long, whereas plants were exposed to 12-hour $^{13}CO_2$ pulses daily for the preceding 6 days to achieve good label incorporation into the microbiota for subsequent DNA-SIP.

As observed in ^{11}C-PET imaging, the ^{13}C abundance in the root tissue and rhizosphere soil was noticeably higher in most root tips compared to their bases, except for the root tissue from the youngest crown roots (Fig. 3a, b). Differences were also evident between different root types, whereby the root tissue and rhizosphere soil at the root bases showed a consistent increase in ^{13}C abundance from the primary root over the seminal roots to the different generations of crown roots. A specific comparison of the ^{13}C abundances between all root and corresponding rhizosphere samples revealed that ^{13}C abundances were consistently higher in the root tissue than in the rhizosphere soil samples with a significantly positive Pearson correlation ($R = 0.76$, $p < 0.001$) (Fig. 3c). When this was analyzed separately for root tips and bases, it became evident that this correlation was primarily driven by a very strong correlation in samples from the root bases ($R = 0.96$, $p < 0.001$; Fig. 3d), whereas correlation at the root tips was just not significant ($R = 0.44$, $p = 0.055$). For the tissue of the root tips, the ^{13}C abundance increased with decreasing root age, being highest for the first generation of crown roots, whereas ^{13}C abundances in the rhizosphere soil were less distinct and in case of the primary and seminal roots more heterogeneous. The decline in ^{13}C abundance in the root tips of the youngest crown roots compared to the preceding generation of crown roots and in contrast to the observed high ^{11}C signals in these youngest roots can be explained by the fastest

growth of these roots along with the lag period between the last $^{13}CO_2$ pulse and sample collection, which was needed for ^{11}C-PET and MRI imaging. The ^{13}C abundance in unlabeled controls matched closely the isotope's natural abundance of approximately 1.1% (Fig. S4).

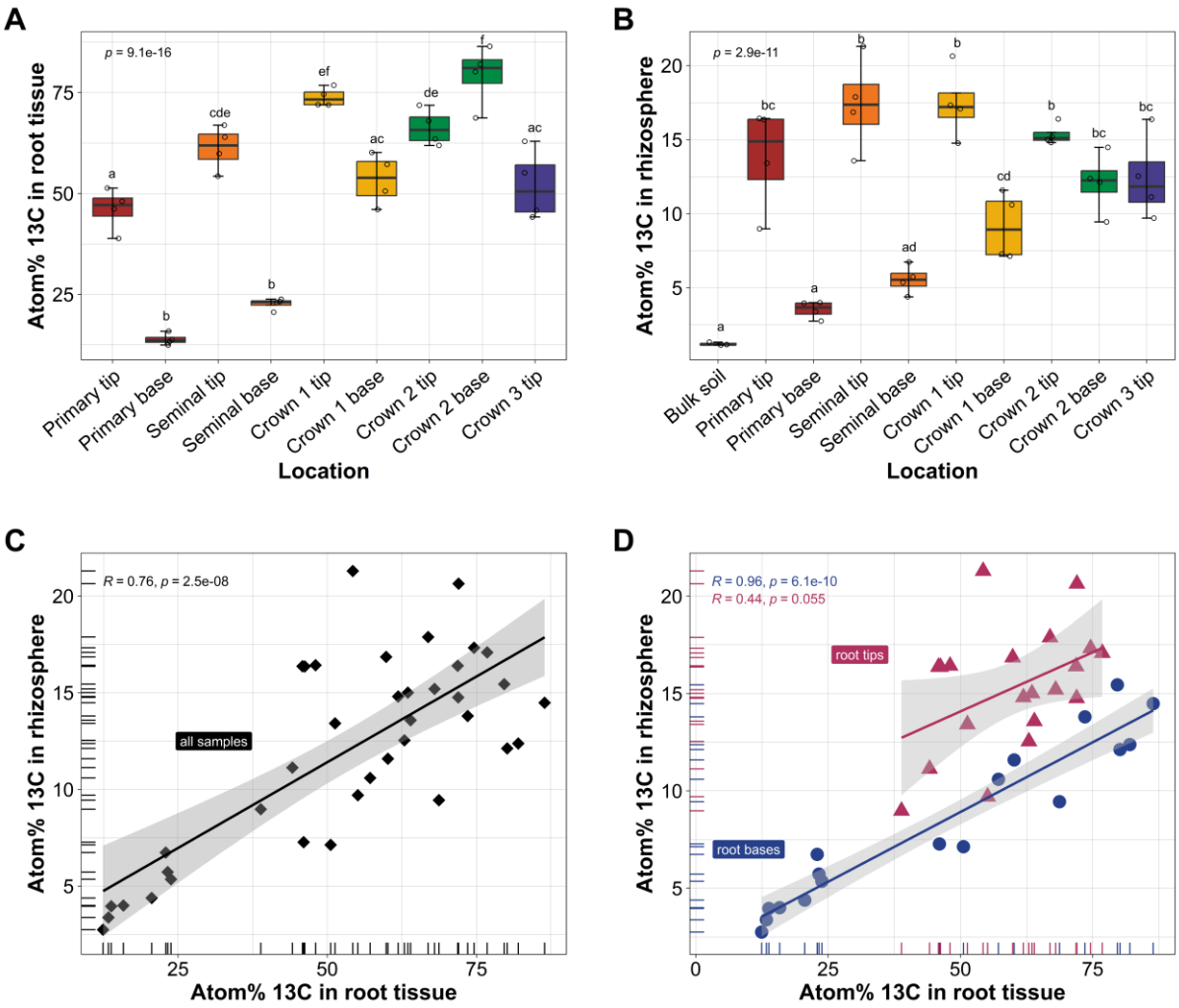

Fig. 3 ^{13}C tracer allocation in different root types and root sections and their associated rhizosphere soil samples. The ^{13}C abundance in **(a)** root tissue and **(b)** rhizosphere soil samples as measured by EA-IRMS and visualized in box plots across different locations in the root system. Significance of differences was tested by ANOVA, and distinct lowercase letters indicate significant differences between groups as tested by Tukey HSD post hoc tests. Scatter plots illustrate the relationship (Pearson correlation) between ^{13}C abundance in root tissue and the rhizosphere for **(c)** all samples and **(d)** for root tip and root base samples separately. Gray-shaded areas indicate the 95% confidence interval of the linear regression model fitted to the data.

Root architectural factors and photosynthate level determine microbial community composition

To investigate how photosynthate allocation, root type and root section affect the composition of the rhizosphere microbiota, we sampled root tips and bases from all root types and defined for these samples three levels of photosynthate allocation based on ^{11}C signal intensities (Fig. S1). We distinguished between root tips with high signal intensity, root tips with medium signal intensity and basal root sections with low signal intensity. The community compositional analysis targeted prokaryotes, fungi and Cercozoa. In study I, the communities were directly analyzed by amplicon sequencing, whereas the focus in study II was on the communities that incorporated ^{13}C-labeled photosynthates to more closely link carbon allocation patterns to the benefiting microbial taxa. ^{13}C-incorporating taxa were represented by ^{13}C-labeled DNA obtained from a heavy fraction upon density gradient centrifugation of the DNA. In both experimental studies, the composition of the prokaryotic, fungal and cercozoan communities differed in dependence on root type, root section and the ^{11}C signal categories, which was validated by permutational analysis of variance (PERMANOVA) (Table 1). The statistical model "root type * ^{11}C level" had the best explanatory power in study I. Thereby, root section could be excluded from the model, because the other two factors covered the variation by root section. When root section was introduced as first term in the model, significant variation was assigned to this factor and ^{11}C level could be eliminated.

The non-metric multidimensional scaling (NMDS) plots revealed a successive clustering according to root type, especially for bacteria (Fig. 4a, Fig. S5). This successive patterning became even more pronounced upon ^{13}C labeling in study II, especially for fungi. Clustering of Cercozoa according to root type remained less distinct, but a certain successiveness was also evident. These differences were well reflected in PERMANOVA results with R^2-values ranging in study I from 0.13 – 0.20 and in study II from 0.14 – 0.26 plus, in case of bacteria and fungi, an increased interaction term in study II (Table 1). Sample clustering by root type even reflected the chronology of root emergence in the NMDS plots, which was underlined by the analysis of differentially abundant taxa. It revealed a couple of abundant genera with consistently increasing relative abundance in the rhizosphere according to sequential root emergence, including the bacterial genera *Mizugakiibacter, Chujaibacter, Pseudolabrys, Hyphomicrobium, Porphyrobacter, Catenulispora* and *Massilia* as well as the fungal genus *Mortierella*. In contrast, a few taxa like *Methylotenera, Ralstonia* and *Dyella* showed the opposite pattern (Fig. S6). Clustering of samples according to root sections was also clearly noticeable in the NMDS plots.

Sample clustering according to ^{11}C-photosynthate allocation was rather weak in study I (R^2 between 0.07 and 0.10), but increased substantially in study II (R^2 between 0.34 and 0.47), where we focused on the analysis of DNA in the ^{13}C-heavy fraction, which represents predominantly the

consumers of rhizodeposits. This was reflected in the NMDS plots (Fig. 4a), where samples clustered according to ^{11}C tracer level as well as root section along the first axis and root type along the second axis. The explanatory power of recent photosynthate allocation in study II was also higher in the unlabeled control samples in this study, but values were not as high as for the ^{13}C-heavy fraction (mean R^2 of 0.28; Table S1). For reasons of direct comparability with study I, we applied the same PERMANOVA model in study II (Table 1), though the explanatory power of the model "^{11}C level * root type" was slightly better with even higher R^2 values for the factor ^{11}C level with R^2 values of 0.39 (fungi), 0.43 (bacteria) and 0.59 (Cercozoa).

Lastly, we were interested to see whether the ^{13}C abundance quantified in the rhizosphere was an even better explanatory factor for variation in microbial community composition than the ^{11}C tracer signals. The EA-IRMS-derived ^{13}C abundance data reflect C allocation into the rhizosphere over a longer labeling period than the ^{11}C signal in the root. The replacement of ^{11}C label categories by ^{13}C abundance data in the PERMANOVA model resulted in almost equal R^2 values of 0.31 to 0.37 for the ^{13}C abundance data (Table 1). In the NMDS plots, it became evident that sample clustering according to ^{13}C abundance coincided strongly with the clustering by root type and section, most clearly visible for bacteria (Fig. 4b). This demonstrates that recent photosynthate allocation in the root and rhizosphere is indeed strongly related to major spatial patterns in the microbiota according to root section and root type, over short periods of time, i.e. hours, as well as over days.

Study I included an analysis of alpha diversity and abundance. The Shannon diversity indices of the prokaryotic, fungal and cercozoan communities showed significant differences in dependence on photosynthate level, root type and root section, whereby the prokaryotes showed the strongest variation and Cercozoa the weakest (Fig. S7). A reduced diversity was observed with increasing ^{11}C allocation, decreasing age of root types, and at the root tips. For the prokaryotes and fungi, this was the consequence of a decrease in richness and evenness in response to the ^{11}C-photosynthate level and root region, whereas the differences related to root type were primarily driven by a decline in evenness. For Cercozoa, changes were primarily related to decreased evenness, but not richness. Concerning prokaryotic and fungal abundance, a strong increase in target gene copy numbers was seen in all rhizosphere samples compared to bulk soil, but strong patterns in dependence on ^{11}C allocation or root section were not evident (Fig. S8). However, a negative correlation between alpha diversity and abundance was seen for bacteria (Pearson correlation R = -0.23, p = 0.032) and fungi (Kendall correlation R = -0.22, p = 0.0025) (Fig. S9).

2.2. Results

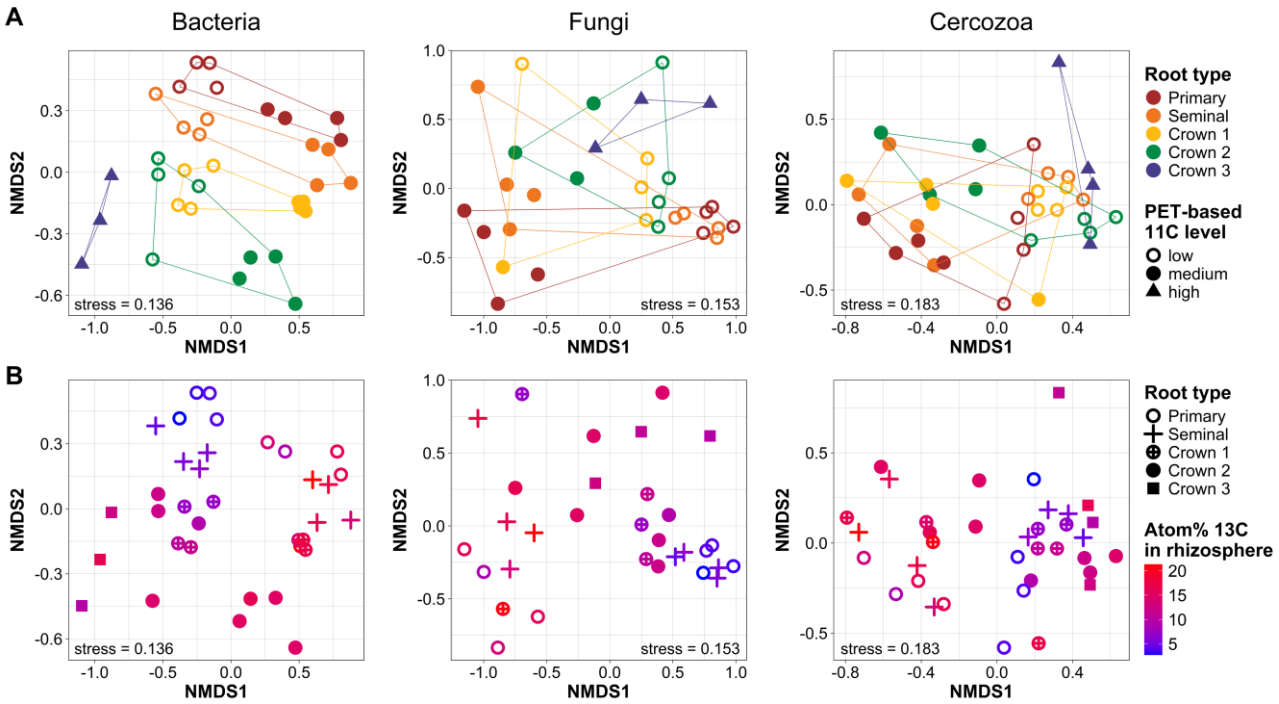

Fig. 4 Variation in microbial community composition in dependence on root type, root section and belowground photosynthate allocation (study II). Variation in community composition was assessed after $^{13}CO_2$ labeling in the DNA of the ^{13}C-heavy fraction, representing predominantly ^{13}C consumers. Variation is visualized by non-metric multidimensional scaling (NMDS) plots based on Bray-Curtis dissimilarities, highlighting the dependence on root type and **(a)** categorical photosynthate levels defined by ^{11}C-PET or **(b)** the ^{13}C abundance measured in the rhizosphere soil by EA-IRMS. Information on root sections can be inferred from the plots in **(a),** with root tip samples being represented by closed symbols, whereas root base samples are represented by open symbols.

Table 1 Influence of root type and photosynthate level on microbial community composition. Influence of both factors as well as their interaction on total community composition (study I) and photosynthate consumer community, reflected by the ^{13}C-heavy fraction of the DNA-SIP analysis (study II), was assessed by PERMANOVA (R^2 values given in table). Significance code: *** indicates *p*-values ≤ 0.001, ** *p*-values ≤ 0.01 and * *p*-values ≤ 0.05.

Study	PERMANOVA model	Factor	Bacteria	Fungi	Cercozoa
Study I: Total community	Root type * ^{11}C level	Root type	0.20***	0.13***	0.18***
		^{11}C level (categorical)	0.07***	0.08***	0.10***
		Interaction	0.07***	0.08***	0.04
		Residuals	0.65	0.71	0.68
Study II: ^{13}C-heavy fraction community	Root type * ^{11}C level	Root type	0.26***	0.14*	0.17**
		^{11}C level (categorical)	0.34***	0.35***	0.47***
		Interaction	0.13***	0.14**	0.05
		Residuals	0.27	0.37	0.31
	Root type * ^{13}C level	Root type	0.26***	0.14	0.17*
		^{13}C level (numeric)	0.31***	0.34***	0.37***
		Interaction	0.11**	0.10	0.05
		Residuals	0.32	0.42	0.41

Heterogeneity in photosynthate allocation impacts microbial consumers of ^{13}C-labeled photosynthates

To reliably identify specific taxa of microbial ^{13}C incorporators, we applied two alternative approaches to group samples for further statistical analysis with the DESeq2 algorithm. In one approach, samples were grouped into four categories based on the quantified ^{13}C abundances in the rhizosphere (Fig. S10). Alternatively, samples were grouped according to their origin in the root system. This enabled the identification of taxa that became labeled based on their location in dependence on root architecture or the amount of carbon transferred into the rhizosphere. Overall, the number of identified taxa ranged from 2 - 18 per kingdom and category (Table S2), which was rather low because of the conservative DESeq2 algorithm. More labeled taxa were detected in the groups of bacteria and Cercozoa than fungi. Most taxa identified as ^{13}C-labeled were identified by both approaches (Fig. 5, Fig. S11), underlining that their labeling was strongly related to both, the spatial location of the taxa in the root system and the amount of ^{13}C rhizodeposition. Several of the

^{13}C-labeled taxa had been identified as responsive to ^{11}C level and/or root type already in study I, confirming the strong responsiveness of these taxa to one or both of these factors. Among others, the bacterial genera *Paenibacillus*, *Massilia*, *Methylotenera* and *Rhodotorula* as well as the fungal genera *Fusarium, Trichoderma* or *Ustilago* were identified in both studies (Fig. 5, Fig. S6).

Several fungal amplicon sequencing variants (ASVs) were exceptionally strongly labeled in samples with the highest ^{13}C signature in the rhizosphere soil, while their labeling was significantly lower than that of bacteria and Cercozoa in samples with low ^{13}C abundance in the rhizosphere (i.e., label categories 1 and 2; Fig. 5a). The alternative approach, during which ^{13}C incorporators were identified upon sample grouping based on their origin in the root system, showed that this intensive fungal labeling occurred at root tips (Fig. 5b), and thus, taken together, at root tips with highest carbon allocation. Bacterial and cercozoan taxa showed less variation in label intensity between the four defined categories, regardless of the underlying sample grouping strategy (Fig. 5a and b).

Visualizing 13C consumer label intensity for each significantly labeled taxon revealed that several ASVs represented 13C consumers of the bacterial class Bacilli, especially the genus *Paenibacillus* was identified in samples with high ^{13}C content in rhizosphere soil, i.e. in ^{13}C-label category 3 and 4 (Fig. 5c). In contrast, almost all ^{13}C-labeled ASVs within the Gammaproteobacteria (e.g. *Pseudomonas, Methylotenera, Massilia* and unidentified Oxalobacteraceae) and Actinobacteria were detected in the weakly labeled category 1 samples. The Bacilli, especially *Paenibacillus,* showed the highest relative abundance in the labeled fraction of root tip samples (Fig. S12), whereas the Gammaproteobacteria with *Massilia* as well as unidentified Oxalobacteraceae and Comomonadaceae were particularly prominent in root base samples (Fig. S12). For some taxa, a further differentiation between seed- and shoot-borne root bases was seen, especially in the case of ASVs from the Rhizobium group, occurring preferentially as labeled at the seed-borne root bases.

Among the fungi, the most intensively labeled ASVs were represented by the class Sordariomycetes, especially the genus *Fusarium* (Fig. 5c), resulting in the high fold-change for fungi in ^{13}C-label category 4 (Fig. 5a). This category is represented by tips of seminal and crown roots of the first node (Fig. S10), but *Fusarium* occurred also in the ^{13}C-heavy fraction of other root tips (Fig. S12). Also striking was the ^{13}C labeling of some ASVs representing non-identified members of the Lobulomycetes (Chytridiomycota) (Fig. 5c) with high relative abundance in rhizosphere soil samples of ^{13}C-label category 1 to 3, i.e. at all root bases and tips of the crown roots (Fig. S12). Among the Cercozoa, most ^{13}C-labeled operational taxonomic units (OTUs) represented members of the Cercomonadida and Glissomonadida, but in contrast to the highlighted bacterial and fungal taxa, these did not show very particular enrichment or abundance patterns in dependence on the ^{13}C

abundance in the rhizosphere or related to the root system (Fig. 5). Their labeling and relative abundance were more balanced.

Lastly, we explored the role of ^{13}C-labeled taxa within the total microbial community by network analysis (Fig. 6). This was done separately for the root tip and root base microbiota, as major differences were observed between samples from these two root sections in the SIP amplicon dataset (Fig. 4). Networks were calculated at species level resolution and condensed at phylum (bacteria, fungi) / order (Cercozoa) level (Fig. 6) or at genus level (Fig. S13) for a better overview. Compared to the network constructed for the root tip (49 associations), the network for the root base showed more associations between bacteria and Cercozoa (63 associations), especially between bacteria and Glissomonadida (22 and 29 associations, respectively) (Fig. 6). In both networks, we found many associations between Actinobacteria and Proteobacteria. Many fungal taxa disappeared from the root base network. To assess the role of the ^{13}C-labeled taxa within these networks, we analyzed their connectivity and compared it to non-labeled taxa. While there were no significant differences observed in the root tip network, the labeled taxa showed a higher degree, radiality and centrality in the network of the microbiota associated to the root bases (Table S3), indicating that these had more prominent positions in the network.

2.2. Results

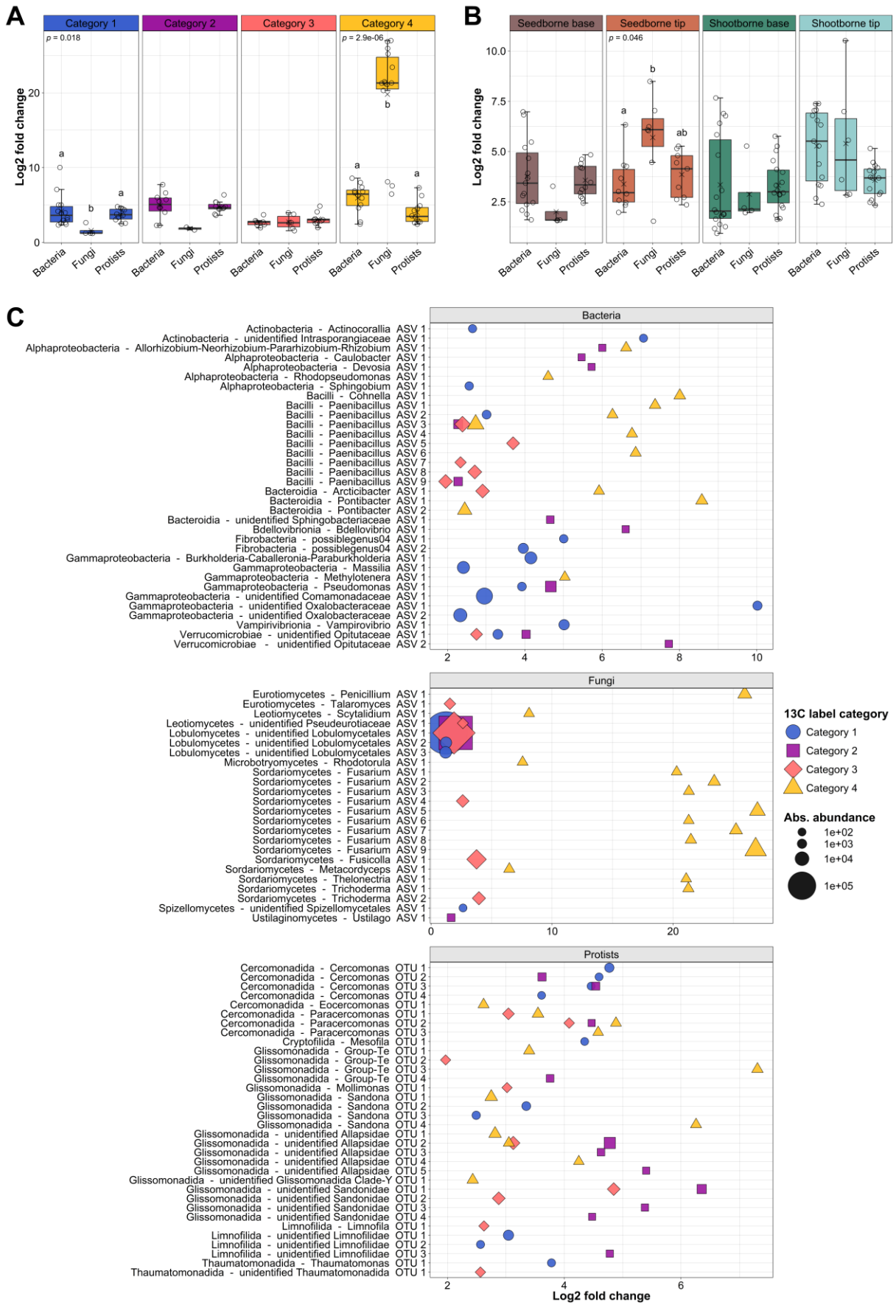
A
Category 1
Category 2
Category 3
Category 4
p = 0.018
p = 2.9e-06
Log2 fold change
Bacteria
Fungi
Protists
B
Seedborne base
Seedborne tip
Shootborne base
Shootborne tip
p = 0.046
C
Bacteria
Fungi
Protists
Log2 fold change
13C label category
Category 1
Category 2
Category 3
Category 4
Abs. abundance
1e+02
1e+03
1e+04
1e+05

Fig. 5 ^{13}C label intensity and identity of microbial taxa with significant label incorporation. Significantly labeled taxa were identified using the DESeq2 algorithm of the HTSSIP package. For this analysis, samples were grouped into four categories, either **(a)** and **(c)** in dependence on the ^{13}C isotopic abundance quantified in the rhizosphere soil (category 1: lowest ^{13}C abundance, category 4: highest ^{13}C abundance; Fig. S10) or **(b)** based on the sample origin within the root system. **(a)** and **(b)** show the label intensity of significantly labeled taxa according to the fold-change in sequence read abundance between the ^{13}C-heavy and ^{12}C-heavy fraction. Significance of differences within subsets was tested by Kruskal-Wallis rank sum test. Distinct lowercase letters indicate significant differences between groups as tested by Dunn's post hoc tests with Benjamini-Hochberg correction. **(c)** illustrates the identity of the labeled taxa along with the enrichment in the ^{13}C-heavy fraction over the ^{12}C-heavy fraction based on log2 fold changes and the summed abundance of the ^{13}C-labeled taxa in the ^{13}C-heavy fraction based on read counts. Absolute abundance equals the sum of all reads of a labeled ASV over all samples of a label category. Bacteria and fungi are labeled as Class_Genus_ASV and Cercozoa as Order_Genus_OTU.

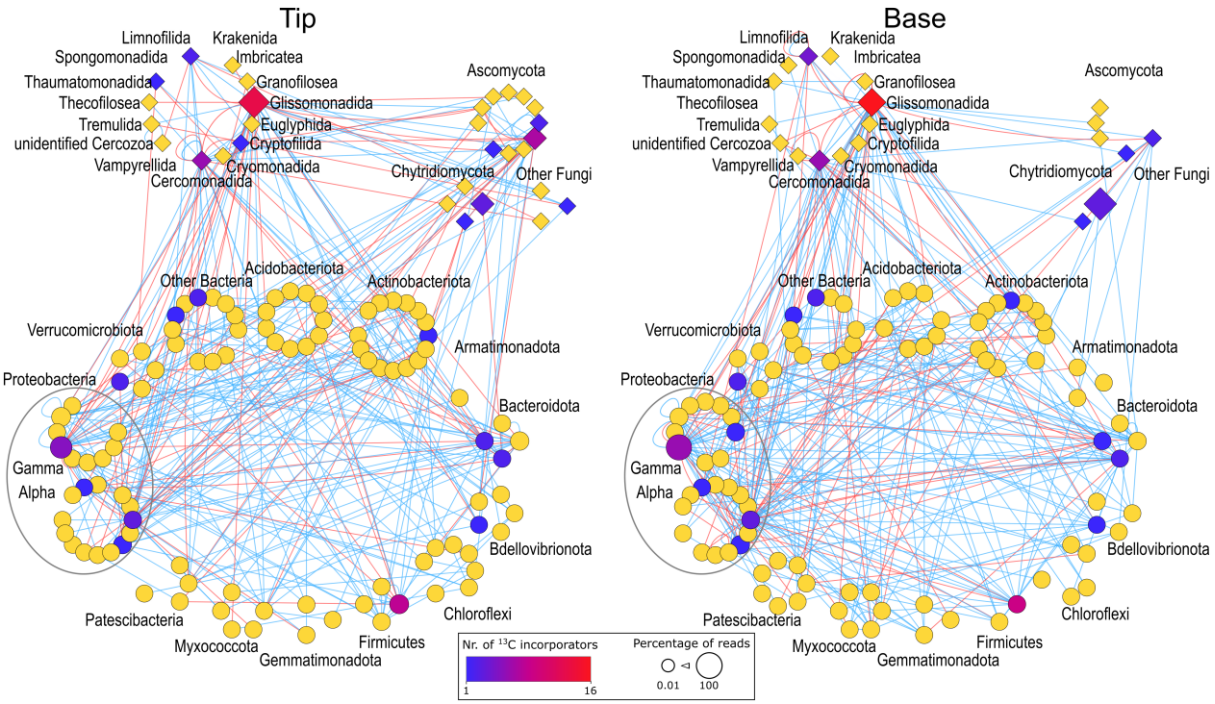

Fig. 6 Core networks illustrating the associations between bacterial, fungal and cercozoan taxa and the positioning of ^{13}C-labeled taxa. Networks were independently calculated for the root tip and root base microbiota based on ^{13}C amplicon sequence data of study II. Nodes are arranged at phylum (bacteria, fungi) and order level (Cercozoa). Positive associations are indicated by blue lines, negative associations by red lines. Network taxa are colored according to the number of ^{13}C incorporators (blue to red) or non-incorporators (yellow) as determined by DESeq2 analysis. The node size is proportional to the percentage of reads.

Discussion

$^{11}CO_2$ labeling in combination with PET and MRI allowed the integration of tomographic data on photosynthate distribution with root structural information at high spatial and temporal resolution (Jahnke et al., 2009). Applied to 6-day old maize plants, it revealed that recently assimilated photosynthates remained in the shoot and were not translocated into the roots, which is explained by the early developmental stage at which the root system is still supplied by seed reserves. In 13 and 20-day old plants, the recent photosynthates were rapidly transferred into the entire root system, detectable 10-15 minutes post-labeling (Vid. S1), which is faster than previously reported for some other crops (Rattray et al., 1995). The primary root received the recently fixed carbon most rapidly after the $^{11}CO_2$ pulse, indicating an efficient reorganization from seed- to shoot-derived carbon supply until day 13. It is assumed that the reorganization from heterotrophy to autotrophy occurs in maize around day 10 (Enns et al., 2006). The observed fast transition ensures the further development and functionality of the shoot-borne roots.

Within the individual roots, the allocation of recently fixed carbon varied strongly along the longitudinal root axis with most intensive accumulations at the root tips. This was seen in ^{11}C-PET images (Fig. 2a) and confirmed by ^{13}C abundance analysis of the root tips as well as for the associated rhizosphere soil (Fig. 3). The intensive photosynthate accumulations in and around root tips align with previous studies using ^{14}C (Dennis et al., 2010; Pausch & Kuzyakov, 2011) and ^{13}C approaches (Keel et al., 2012) and can be linked to the energy demanding processes occurring at root tips, including cell division in the apical meristem, mucilage synthesis at the root cap and membrane transport. The related high photosynthate accumulations in the rhizosphere are the consequence of different rhizodeposition processes with photosynthate loss at the root tips due to exudation, mucilage production and border cell shedding (Darwent et al., 2003; Dennis et al., 2010; Jones et al., 2009; Watt, Kirkegaard, et al., 2006).

We also detected clear differences in photosynthate allocation between root types, whereby the youngest crown roots showed particularly high ^{11}C signal intensity, especially at their tips. This indicates that these young roots are already well connected to leaves via the phloem and efficiently supplied by recent photosynthates, supporting their high elongation rates (Orman-Ligeza et al., 2013) and dominant role in soil exploration (Lynch, 2015). The $^{13}CO_2$ labeling confirmed that photosynthate accumulations at root tips decreased consistently for root types of increasing age (Fig. 3b). This can be explained by the development of lateral roots as additional local sinks, therewith reducing the initially very high accumulations at the main root tip. It is assumed that both, root elongation and the emergence of lateral roots contribute to the total photosynthate sink strength of

a root, and these processes are thought to be regulators of root photosynthate transport in the root system (Farrar et al., 2003; Poorter et al., 2012).

At the root bases, the recent photosynthates merely passed through according to ^{11}C-PET imaging (Vid. S1). Also, the $^{13}CO_2$ labeling over several photoperiods showed that root bases did not accumulate much of the ^{13}C tracer, especially not the primary and seminal roots (Fig. 3). These roots were already established with the full length that we sampled for the base section when the $^{13}CO_2$ labeling period began. In the younger roots, part of the sampled base section developed during the ^{13}C labeling period and incorporated ^{13}C-labeled photosynthates into the tissue, explaining the consistent increase in ^{13}C abundance of root samples with decreasing age. Further, the ^{13}C abundance within the root system was very closely correlated to the ^{13}C abundances in the rhizosphere at the root bases (Fig. 3d) pointing to tightly coupled processes for photosynthate allocation within the root and their release into the rhizosphere. This aligns with the knowledge about reduced rhizodeposition with increasing root maturity along the root axis, which comes with a stricter control of diffusion and increasing relevance of specific secretion mechanisms (Jones et al., 2009; Marschner et al., 2011). These obviously link root internal photosynthate allocation tightly with allocation in the rhizosphere. At the root tips, the root internal and external ^{13}C tracer accumulations were not well correlated (Fig. 3d), merely because the rhizosphere samples from different root types showed less distinct patterns and more variation than the root tissue samples did. Differences in microbial carbon mineralization might have contributed to this discrepancy, considering that we observed root type specific variation in the microbiota at the root tips (Fig. 4, Fig. S5).

As an asset of the temporal resolution of ^{11}C-PET imaging, we observed heterogeneity regarding the arrival of the short-lived ^{11}C tracer signal in the individual roots. This may indicate differences in flow velocity between individual roots. In combination with the variation in photosynthate accumulation at root tips, it indicates that regulatory mechanisms play a role in determining the distribution of recent photosynthates within the root system. Intensely debated in this context are functional differences between the roots (Keel et al., 2012), root length and size (Darwent et al., 2003; Keel et al., 2012), as well as root growth rates (Dupuy & Silk, 2016).

As rhizodeposits present a major energy source for microorganisms (Kuzyakov & Blagodatskaya, 2015), the observed variation in photosynthate allocation within the roots and into the rhizosphere should have consequences for the rhizosphere microbiota. We have multiple lines of evidence that the spatial patterns observed in the microbiota in dependence on root type and root section were closely related to photosynthate allocation. When evaluating the explanatory power of root section,

root type and the two isotopic tracer levels as a proxy for recent photosynthate allocation in the root system on microbial community composition by PERMANOVA, high complementarity in the explanatory power of these factors was observed. In agreement, the NMDS plots revealed that sample clustering occurred according to root section and root type, and in addition to the ^{11}C tracer level and the amount of ^{13}C quantified in the rhizosphere. The taxa that were identified as significantly labeled by the DESeq2 algorithm were largely the same, independent of the grouping of samples according to their origin in the root system or the ^{13}C tracer category. Further, PERMANOVA results of study II showed a comparable effect of the ^{11}C and the ^{13}C tracer on the microbiota, although $^{11}CO_2$ was only applied for 6 min, whereas $^{13}CO_2$ was applied at 6 days. This points to a temporally stable effect of recently fixed carbon allocation on the observed variation in the microbiota that profited from these photosynthates in the rhizosphere.

The most striking differences in photosynthate allocation were observed along the root axis with accumulations at the root tips (Fig. 2a). These patterns were reflected by differences in community composition of bacteria, fungi and Cercozoa between root tips and bases (Fig. 4, Fig. S5, Fig. S6) and a reduced alpha diversity of prokaryotes and fungi at root tips (Fig. S7). Differences in the microbiota between root tip and base reflect stages of a successive community developmental process along the axis, largely in dependence on rhizodeposition processes (Loo et al., 2024; Rüger et al., 2021). The population size of bacteria and fungi in the rhizosphere did not differ substantially between root base with low recent photosynthate accumulation and root tips with high accumulations, indicating a very rapid population build-up at root tips, supported by the high substrate availability at root tips (Van Bruggen et al., 2000; Van Diepeningen et al., 2005; Van Vuurde & Schippers, 1980). This comes along with a decline in alpha diversity, i.e. reduced richness and evenness, explained by a specific enrichment of selected fast-growing taxa (Bonkowski et al., 2021), such as *Paenibacillus* or *Fusarium*, as identified by DNA-SIP.

Root type was the second major factor that differed in recent photosynthate allocation and to which variation in microbial community structure was related (Table 1). Evidence for root type-dependent differences in microbial communities of cereals is recently accumulating (Kawasaki et al., 2021; Kawasaki et al., 2016; Sivasithamparam et al., 1979). For maize, differences in bacterial communities have been reported to exist between primary and crown roots (Cotton et al., 2019). Beyond these root type related differences, we demonstrate with our results a successive change in community composition from the oldest, primary root to the most recently emerged crown roots for bacteria, Cercozoa and, with more variability, for fungi (Fig. 4, Fig. S5). Similarly, a successive decrease in alpha diversity from the oldest to youngest roots was seen, especially for bacteria, primarily a decline in evenness (Fig. S7). These successive changes can also be explained by

population development, based on the observation that several taxa showed consistent increases in relative abundance across root types and related to the chronology of root emergence (Fig. S6). The development is likely driven by different processes, including root type specific exudation patterns, which have been reported to exist in maize (Cotton et al., 2019), and time-related deterministic processes as roots and rhizosphere mature. The sequential emergence of the roots gives more time for community assembly, competitive outcomes, plant-selection processes and top-down control by predators along the root axis towards the bases for older roots compared to younger roots.

However, root type related patterns were not only observed at the root bases but likewise seen at the root tips. While this can be seen for bacteria in study I, the results of study II show this even more clearly for the communities of bacteria, fungi and Cercozoa that profited from rhizodeposits (Fig. 4a). This demonstrates that root-type related differences in the microbiota develop already at a very early stage of rhizosphere establishment. This requires deterministic processes, which occur in addition to stochastic events during assembly. The latter have been reported to contribute to microbiome assembly especially at root tips due to the rich amount of rhizodeposits that are released (Bonkowski et al., 2021; Rüger et al., 2021). Considering that differences existed between all analyzed root types including the different generations of crown roots, the underlying mechanism leading to these differences is not necessarily only related to root type, but likewise driven by further processes, probably related to root length, root age or root growth rate (Watt, Silk, et al., 2006).

The focus on taxa with significant ^{13}C label incorporation revealed an exceptionally high labeling of fungi in rhizosphere regions that received highest levels of ^{13}C-labeled photosynthates, i.e. the root tips (Fig. 5, Fig. S11). While bacteria have traditionally been considered the prime consumers of rhizodeposits, recent studies reported that fast-growing “sugar” fungi can also profit from this plant-derived carbon (Hannula et al., 2017) (Hannula et al., 2020). Our data indicate that this occurs in particular in rhizosphere regions with highest rhizodeposition. Towards the root basis, competition between fungi and bacteria for the more limited rhizodeposits increases, giving an advantage to bacteria over fungi, demonstrated by higher log2 fold changes in this root region for bacteria than fungi (Fig. 5a) and the disappearance of fungal taxa from the co-occurrence network. A particular high ^{13}C labeling in samples with highest ^{13}C-photosynthate rhizodeposition was linked to *Fusarium* (Fig. 5c), which was apparently very efficient at obtaining organic carbon from rhizodeposition in these regions, i. e. root tips. Considering that the genus *Fusarium* includes different species of potential maize pathogens (Blacutt et al., 2018; Okello et al., 2019), it is tempting to speculate that such potentially pathogenic fungi establish in the rhizosphere preferentially in regions that provide ample amounts of organic carbon and that do not yet host a very competitive microbiome, conditions they encounter at root tips. Besides, root tips are known to represent a good entry point

for pathogens (Ye et al., 2013). Potentially beneficial fungi such as *Trichoderma* were also labeled, likewise as *Fusarium* in samples with high ^{13}C-photosynthate deposition (Modrzewska et al., 2022). In contrast, the very high relative abundance of unidentified Lobulomycetales within the labeled fungal community indicates that not all fungi follow the same pattern, because this not yet well-known taxon was prominently present and labeled at all root bases and the tips of shoot-borne roots (Fig. S12). The different colonization pattern of this taxon was reflected in the co-occurrence network, where it remained visible in the network of the root base with only positive associations to other taxa, whereas many other fungal taxa disappeared (Fig. S13). Members of the Chytridiomycota, to which the Lobulomycetales belong, have been reported to profit from rhizodeposits in grassland soil and is was speculated that these might be secondary consumers rather than primary consumers of rhizodeposits (Hannula et al., 2020). Our data for the unidentified Lobulomycetales support this assumption considering their rather weak labeling and their position in the co-occurrence network, suggesting that fungi may be more competitive as secondary consumers than as primary consumers at root bases. At later plant developmental stages, fungal taxa with potential benefits, i.e. mycorrhizal fungi, may establish behind the root tips, but these were not detected in the present study due to the young age of the plants and the well-fertilized soil.

Among the bacteria, the most intensive ^{13}C label incorporation was observed for *Paenibacillus* in rhizosphere samples with high ^{13}C content, which reflects the pattern of *Fusarium* and *Trichoderma* and is well in line with their copiotrophic lifestyle, allowing them rapid proliferation in root regions with high photosynthate supply (Afzal et al., 2024). Indeed, *Paenibacillus* was prominent at both, seed-borne and shoot-borne root tips (Fig. S11) and showed high ASV diversity, to which operon heterogeneity within strains possibly contributed to some extent (Bosshard et al., 2002; Hamasaki et al., 2005). The ^{13}C-labeled taxon with the highest relative abundance among the labeled taxa in the ^{13}C-heavy DNA fractions was *Massilia*, which became labeled in particular at the bases of shoot-borne roots (Fig. S11). Further taxa with this pattern included different rhizobia*,* some of the *Paenibacillus* ASVs and other Oxalobacteraceae. All these genera have previously been identified as carbon consumers in the rhizosphere by DNA-SIP studies (el Zahar Haichar et al., 2008; Hünninghaus et al., 2019). These genera are known to include beneficial taxa (Ahmad et al., 2023; Yu et al., 2021), which may be particularly supported in root regions more distant from the tip, where overall fewer photosynthates are released, but the secretion or diffusion of specific compounds gains relevance compared to root tips (Bag et al., 2022; Jaeger et al., 1999) and may more specifically support these taxa, as reported for Oxalobacteraceae, which benefit from flavonoids and can improve plant nutrient acquisition (Yu et al., 2021). The fact that labeled taxa had prominent positions within the

network at the root bases underlines that these became particularly well established at the root bases upon community succession along the root axis.

Among the bacteria, not only primary consumers became ^{13}C-labeled, but also the predatory bacterial genera *Vampirovibrio* and *Bdellovibrio* as secondary consumers. They were labeled at the root bases, where they were detected at rather low relative abundance (Fig. S11), but with an intermediate ^{13}C label enrichment compared to the other ^{13}C-labeled bacterial taxa (Fig. 5). This aligns with a report that these bacterial predators can be highly active (Hungate et al., 2021). They may thus represent relevant players in the microbial food webs of the rhizosphere besides eukaryotic predators. The latter, studied here with a focus on cercozoan predators, became significantly ^{13}C-labeled in all different root regions. Although Cercozoa integrate the ^{13}C label at a higher trophic level, their mean label log2 fold changes followed closely the patterns of the bacterial communities (Fig. 5a, b). This was also seen in the community compositional variation of the total ^{13}C-heavy DNA fraction, which reflected very well the pattern of their bacterial prey (Fig. 4a). Further, a tight association of protist grazers with potential bacterial prey was seen in the co-occurrence network (Fig. 6), where the main ^{13}C-lableled cercozoan consumers of labeled prokaryotic prey were small flagellates in the Glissomonadida and Cercomonadida. These have short generation times and specific grazing impacts on bacterial communities (Flues et al., 2017; Glücksman et al., 2010). These findings indicate significant top-down control of the maize microbiome by predatory bacteria, protists and likely also fungi, especially towards the root bases.

In summary, the combination of isotope-based approaches to document recent photosynthate allocation within the root system and into the rhizosphere along with image-guided destructive rhizosphere sampling allowed to link this allocation with microbiota assembly. The spatial patterning in photosynthate allocation within the maize root system is dominated by strong photosynthate allocation at root tips and a tight correlation between root internal and external allocation especially at the root bases. The rhizosphere microbiota responds to this distribution of recent photosynthates with notable changes in community structure along the root axis. Thus, photosynthate availability is an important factor driving niche differentiation within the maize root system and causing spatial variation in the rhizosphere microbiome. Fast-growing taxa, here in particular *Paenibacillus*, benefit strongly from photosynthates at the root tips, likewise as some fungal taxa, including potentially pathogenic fungi like *Fusarium* that exploit these root sections efficiently. Towards the root bases, the microbiota undergoes a succession, whereby other taxa are strongly supported by rhizodeposits, including bacterial taxa with potential benefits for the plant, whereas fungal taxa become less competitive under the more limited photosynthate availability. Our study also revealed that community compositional differences exist between root types, also at the root tips. Even beyond,

such differences in the microbiota existed for each generation of crown roots, likely related to root age or length. This variation overlaps with recent photosynthate allocation, but it requires further analyses to resolve the underlying mechanisms in more detail. Lastly, our data showed that a range of prokaryotic and eukaryotic secondary consumers thrive in the rhizosphere, known or predicted predators that exert top-down control on the community. Taken together, the existence of spatiotemporal patterns in photosynthate allocation and resulting differences in rhizosphere microbial food webs requires that processes in the rhizosphere need to be spatially and temporally resolved to understand microbiota assembly and precisely assess microbially driven processes within the root system. This is crucial for developing effective management strategies for root microbiomes.

Acknowledgments

We would like to thank Marius Röder (Molecular Biology of the Rhizosphere, University of Bonn) for excellent technical assistance. Esther Breuer, Marco Dautzenberg and Gregor Huber (Enabling Technologies, IBG-2, Forschungszentrum Jülich GmbH) are acknowledged for their valuable assistance during labeling experiments. We furthermore thank Kirsten Unger (Soil Sciences, University of Bonn) for performing the EA-IRMS analyses. Caroline Marcon and Frank Hochholdinger (Crop Functional Genomics, University of Bonn) are acknowledged for providing maize seeds for this study. The Next Generation Sequencing Core Facility of the Medical Faculty at the University of Bonn is acknowledged for providing the instrumentation for MiSeq sequencing. This work was conducted within the framework of the priority program 2089, funded by the Deutsche Forschungsgemeinschaft (DFG, German Research Foundation) – P18 (Project ID 403637614) and P14 (Project ID 403635931). Michelle Watt currently holds the Adrienne Clarke Chair of Botany, which is supported through the University of Melbourne Botany Foundation.

Supplementary material

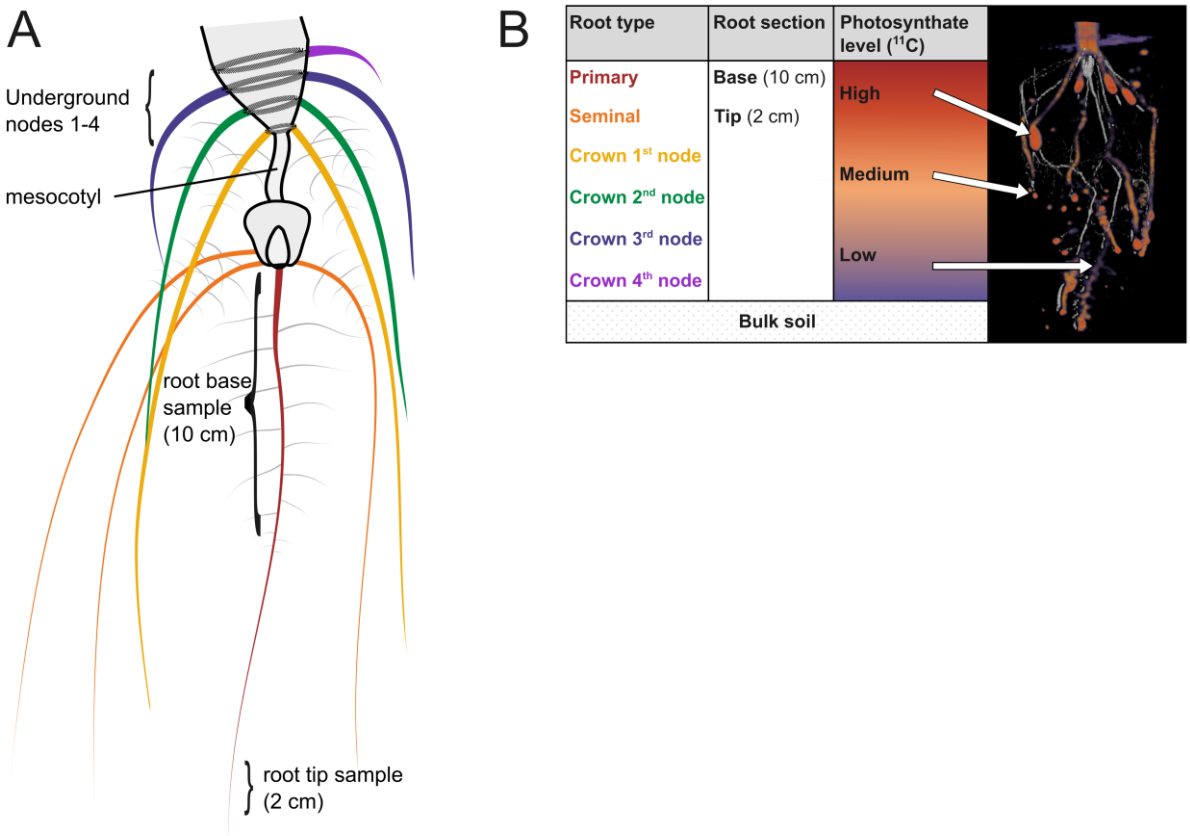

Fig. S1 Sampling concept in both studies. (a) Conceptual drawing of a maize root system on harvesting day. The seed-borne root system comprises the primary root and several seminal roots. The shoot-borne root system comprises crown roots originating from consecutive belowground nodes. The internodes between the first four underground nodes do not usually elongate, resulting in a 'triangle' of stacked nodes. The sampled root sections (tip and base) are exemplary illustrated on the primary root. **(b)** The sampling scheme: Root tips and bases of all root types including crown roots from consecutive nodes were collected. Photosynthate levels are explained based on an exemplary PET-MRI scan of day 13. We distinguished between root tips with high ^{11}C signal intensity, root tips with medium signal intensity and root basal regions with low signal intensity based on the acquired PET images in time frame 85-90 min after labeling.

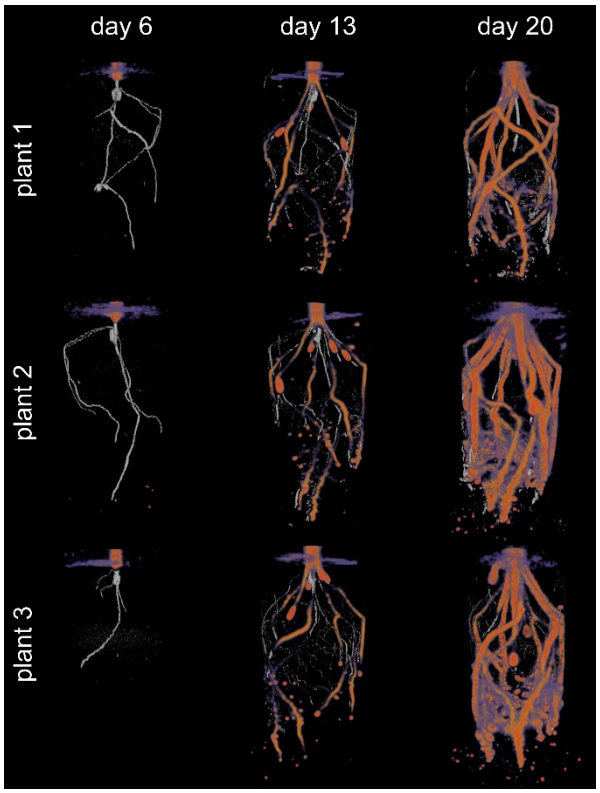

Fig. S2 The distribution of fresh, ^{11}C-labeled photosynthates in all plants of study I on day 6, day 13 and day 20 after sowing. Co-registrations of PET scans (colored) and MRI scans (grey) of the same maize plant for images taken 85-90 minutes after the start of labeling.

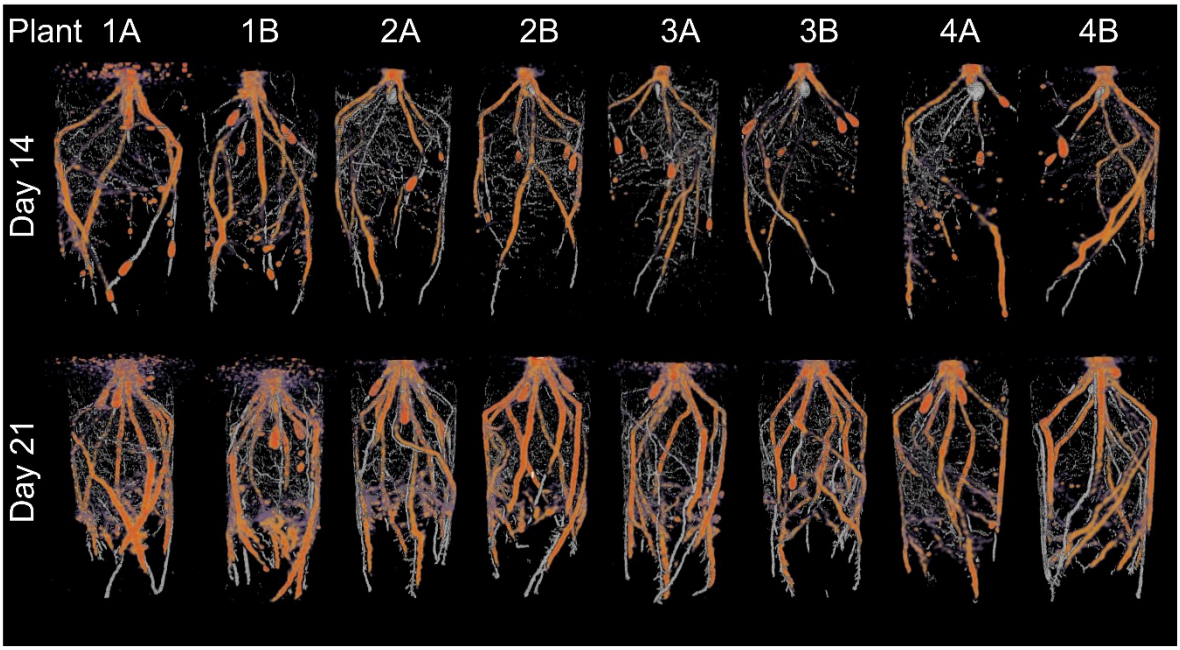

Fig. S3 The distribution of fresh, ^{11}C-labeled photosynthates in plants of study II on day 14 and day 21 after sowing. Co-registrations of PET scans (colored) and MRI scans (grey) of the same maize plant for images taken at 85-90 minutes after the start of labeling.

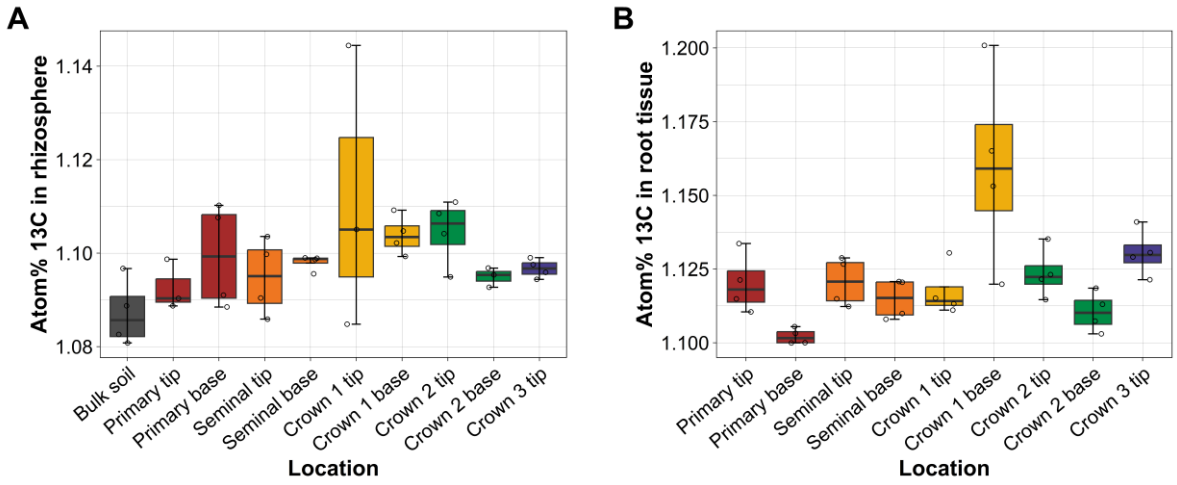

Fig. S4 ^{13}C abundance in the rhizosphere **(a)** and root tissue **(b)** of unlabeled control plants as measured by EA-IRMS.

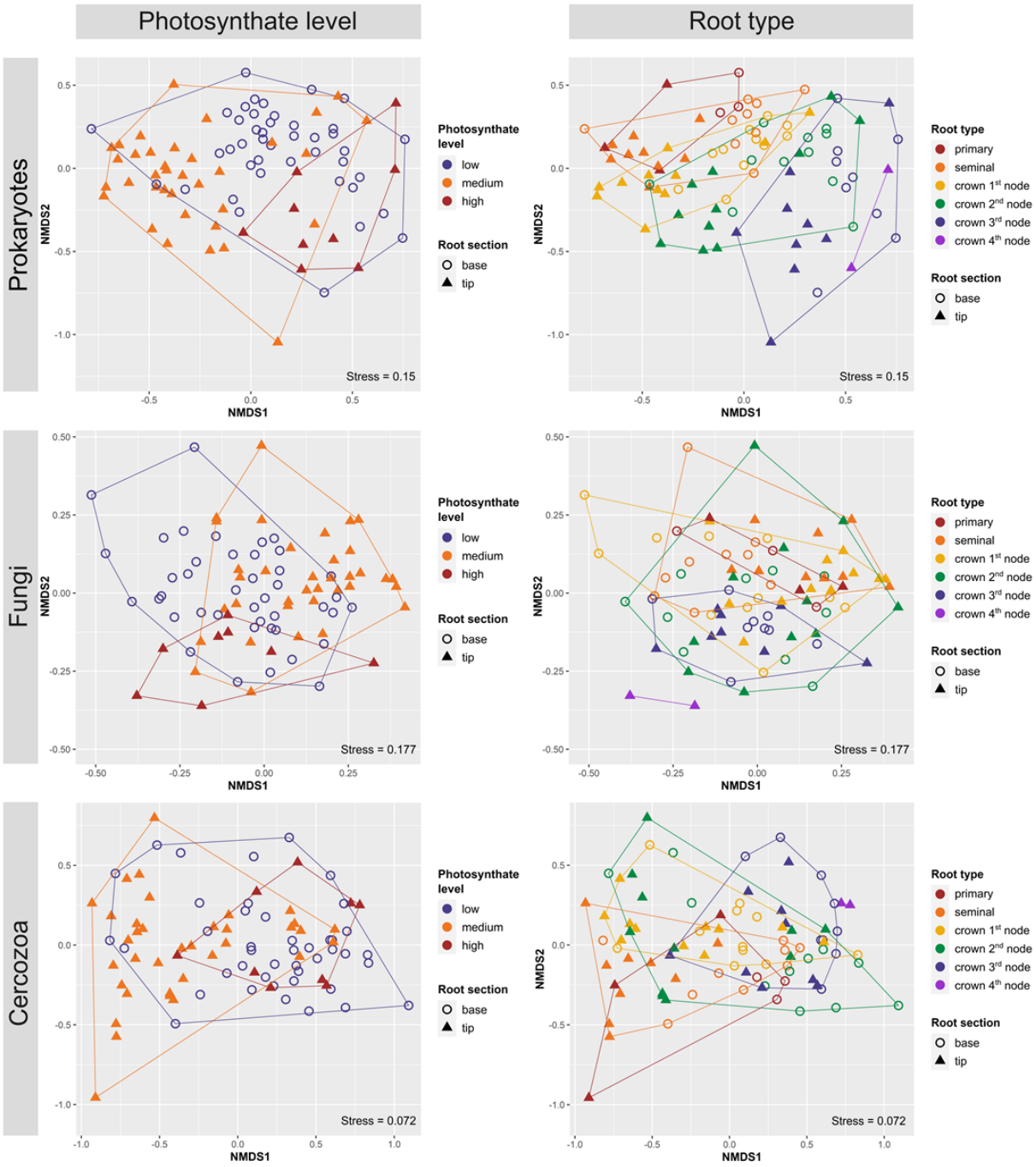

Fig. S5 Community composition of the maize rhizosphere microbiota (prokaryotes, fungi, Cercozoa) in study I, with sample coding in dependence on the factors root type, root section and categorical photosynthate levels as identified by ^{11}C-PET.

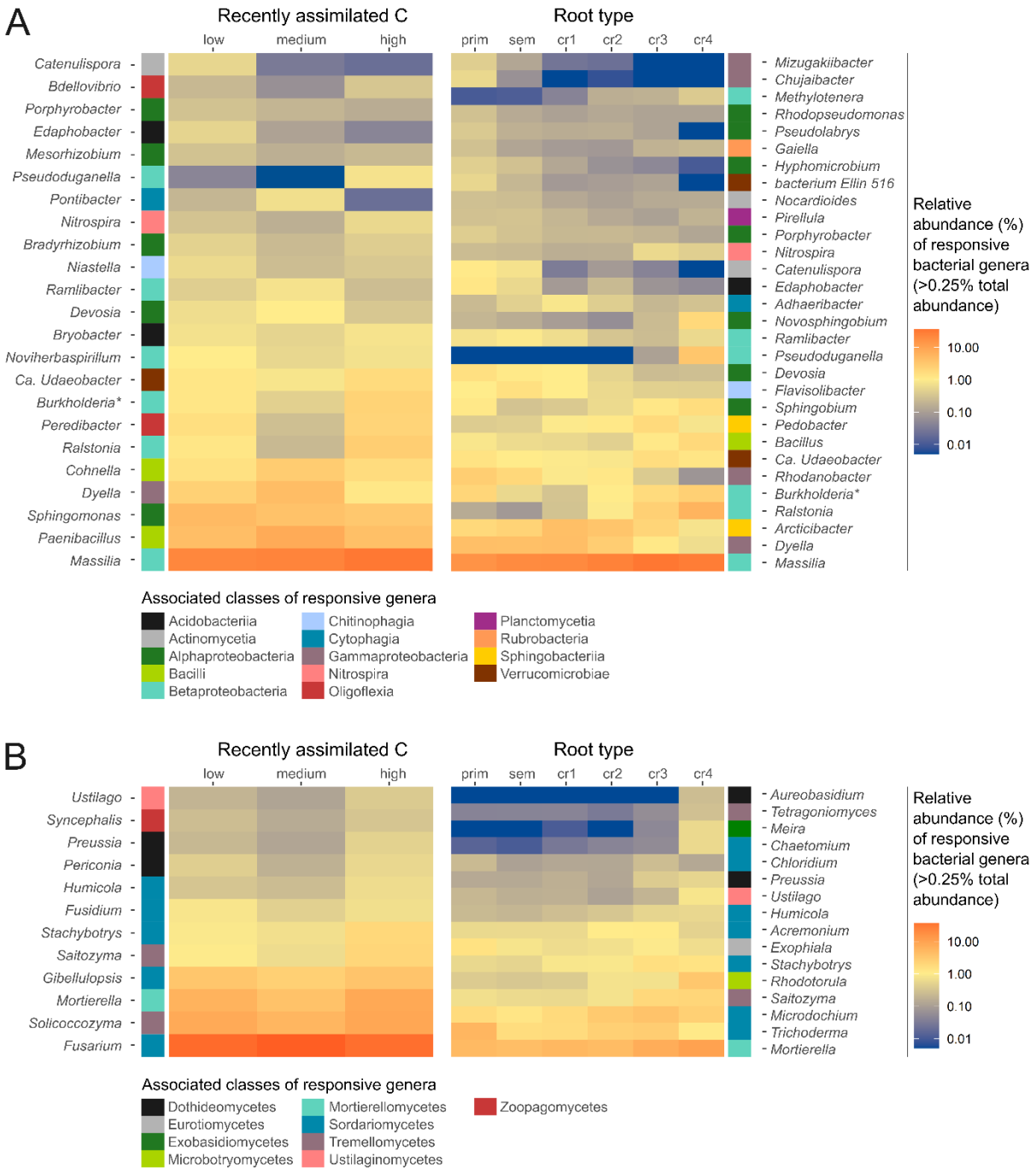

Fig. S6 Heatmaps displaying the relative abundance of dominant taxa (>0.25% relative abundance). **(a)** bacterial and **(b)** fungal genera that showed a significant response to photosynthate level or root type according to ANOVA with subsequent Tukey-Kramer post hoc tests and Benjamini-Hochberg correction for multiple comparisons. Bulk soil samples were excluded from this analysis. (*) Genus *Burkholderia* also encompasses members of *Paraburkholderia* and *Caballeronia*.

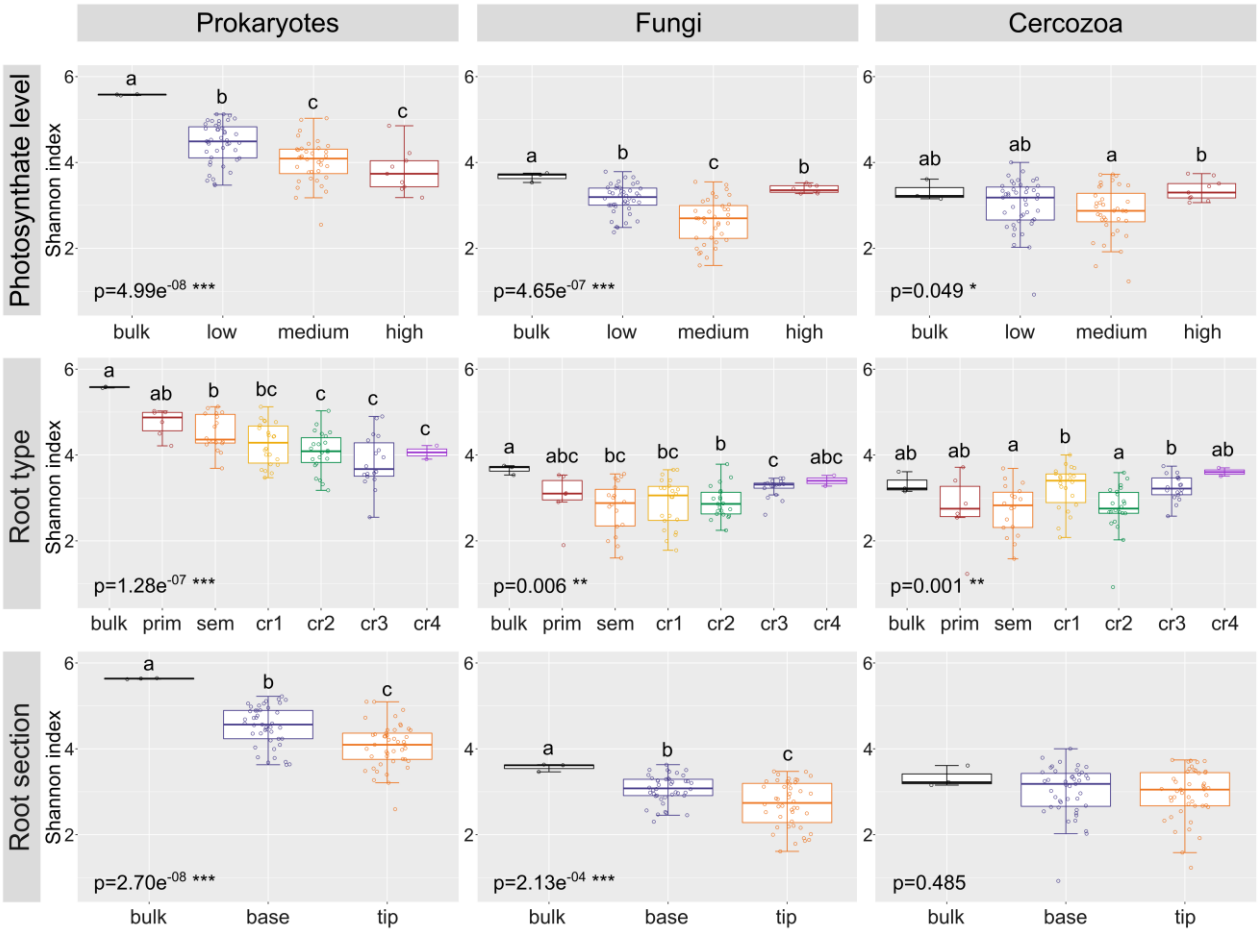

Fig. S7a The Shannon diversity index for prokaryotes, fungi and Cercozoa in dependence on root type, root section or categorical photosynthate levels according to ^{11}C-PET. Bulk = bulk soil, prim = primary root, sem = seminal roots, cr1 - cr4 = crown roots originating from nodes 1 - 4. Significance of differences was tested by ANOVA and Tukey-HSD post-hoc test for the prokaryotic dataset. A Kruskal-Wallis test with respective Mann-Whitney U-tests including Benjamini-Hochberg correction was conducted for fungi and Cercozoa, as Shapiro-Wilk test indicated non-normal data distribution. Distinct lowercase letters indicate significant differences between samples ($p < 0.05$).

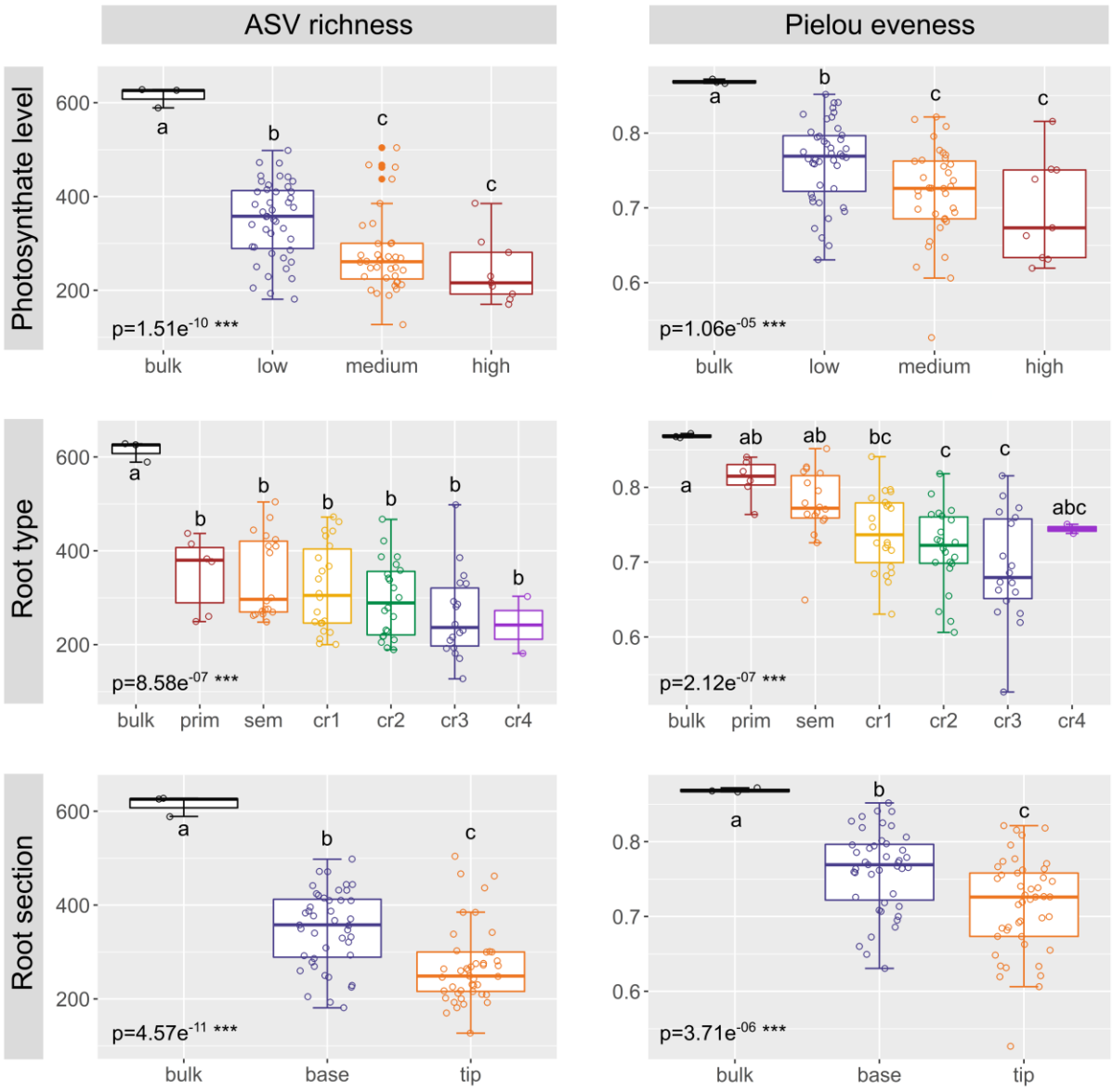

Fig. S7b The influence of photosynthate allocation, root type and root section on amplicon sequence variant richness and evenness (Pielou's index) of the prokaryotic community. Prim = primary root, sem = seminal roots, cr1 - cr4 = crown roots originating from leaf nodes 1 - 4. Significance of differences was tested by ANOVA and Tukey-HSD posthoc test.

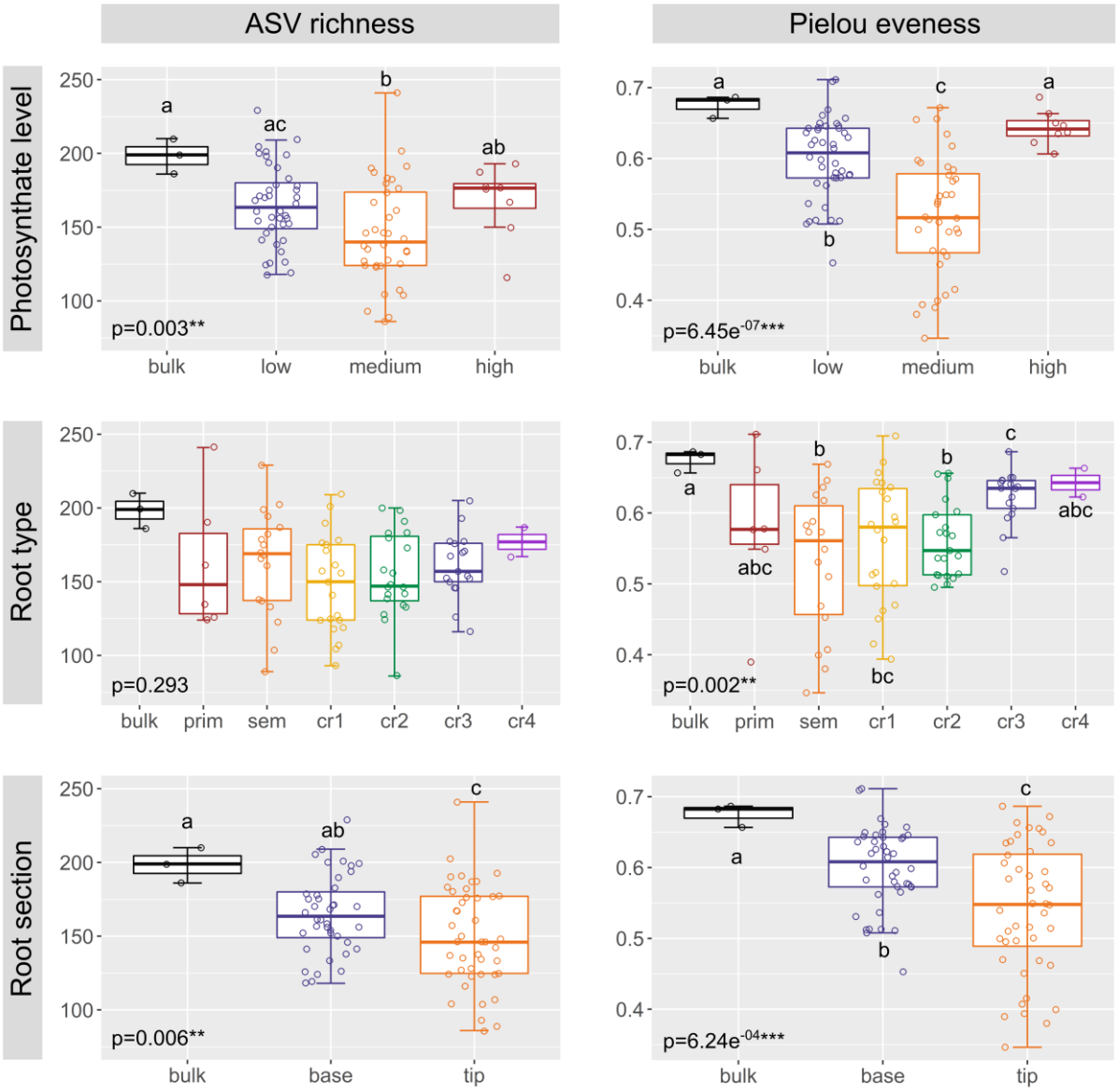

Fig. S7c The influence of photosynthate allocation, root type and root section on amplicon sequence variant richness and evenness (Pielou's index) of the fungal community. Prim = primary root, sem = seminal roots, cr1 - cr4 = crown roots originating from leaf nodes 1 - 4. Significance of differences was tested by Kruskal-Wallis test and respective Mann-Whitney U-test with Benjamini-Hochberg correction.

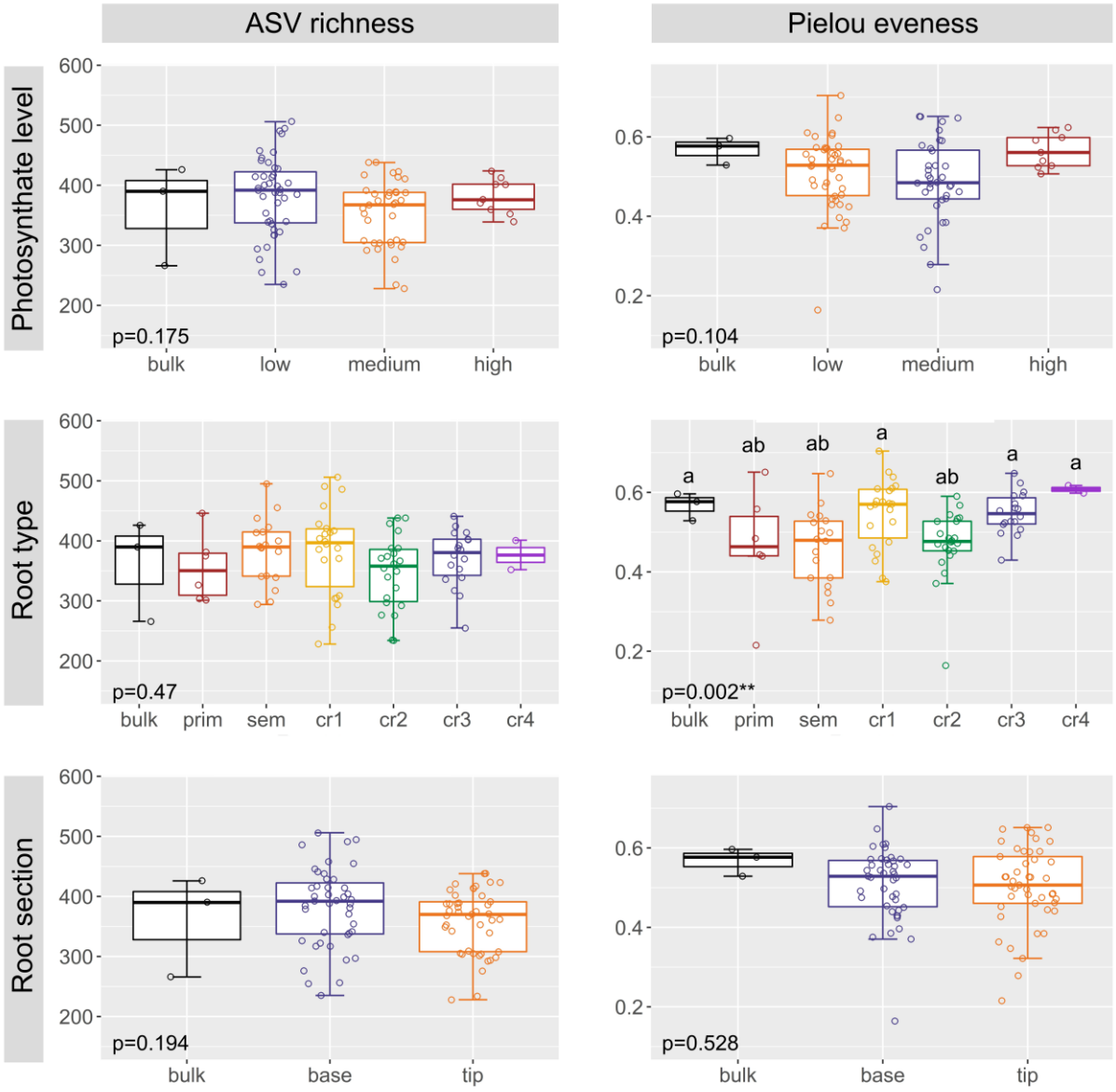

Fig. S7d The influence of photosynthate allocation, root type and root section on amplicon sequence variant richness and evenness (Pielou's index) of the cercozoan community. Prim = primary root, sem = seminal roots, cr1 - cr4 = crown roots originating from leaf nodes 1 - 4. Significance of differences was tested by Kruskal-Wallis test and respective Mann-Whitney U-test with Benjamini-Hochberg correction.

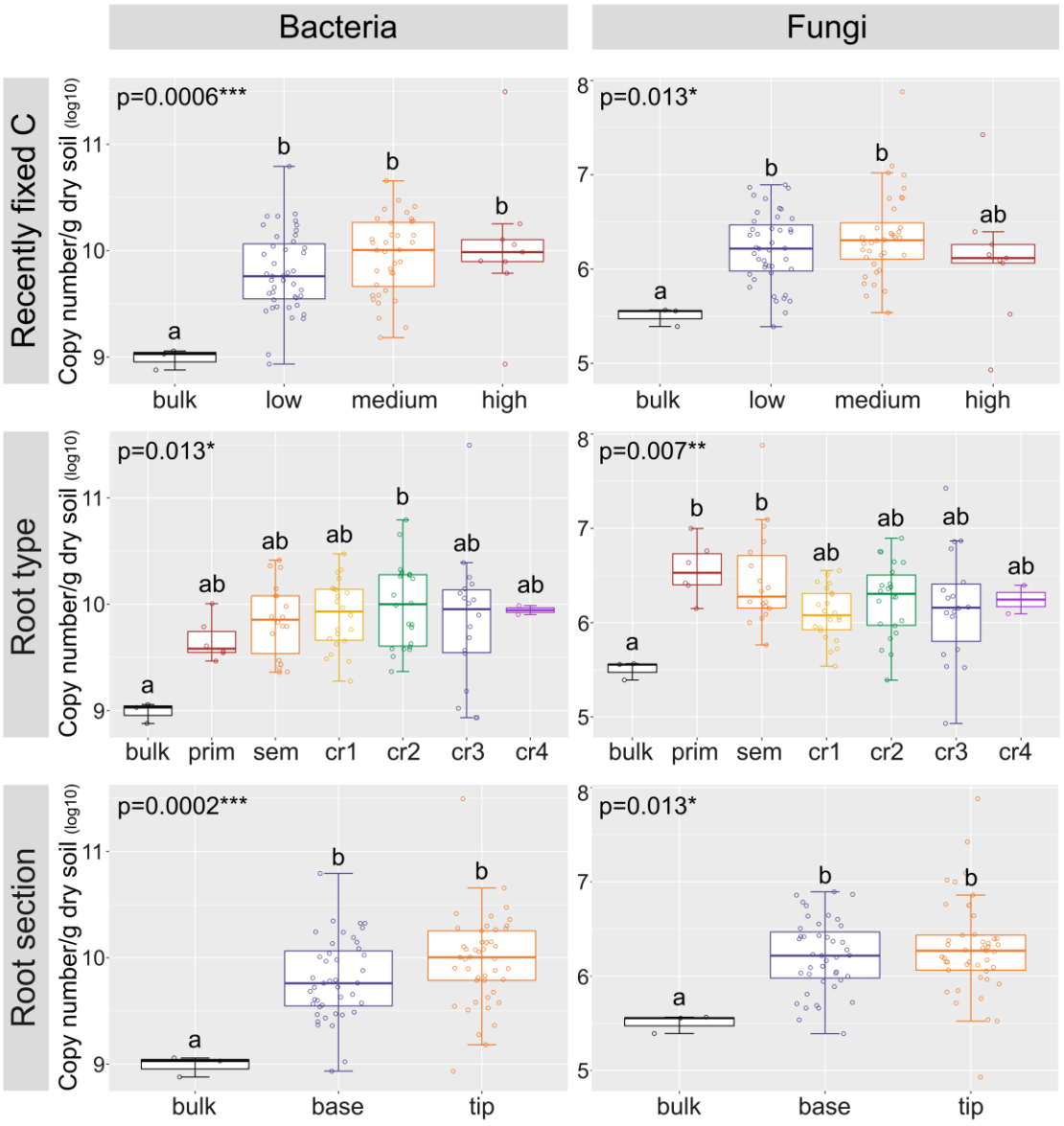

Fig. S8 Boxplots presenting the qPCR results for prokaryotic 16S rRNA gene and fungal ITS1 copy numbers and their variation in dependence on root type, root section or categorical photosynthate levels according to ^{11}C-PET. Prim = primary root, sem = seminal roots, cr1 - cr4 = crown root generations 1 - 4, originating from underground nodes 1 - 4. Significance of differences was tested by ANOVA and Tukey-HSD post hoc test for the normally distributed, log-transformed data. Distinct lowercase letters indicate significant differences between samples ($p < 0.05$).

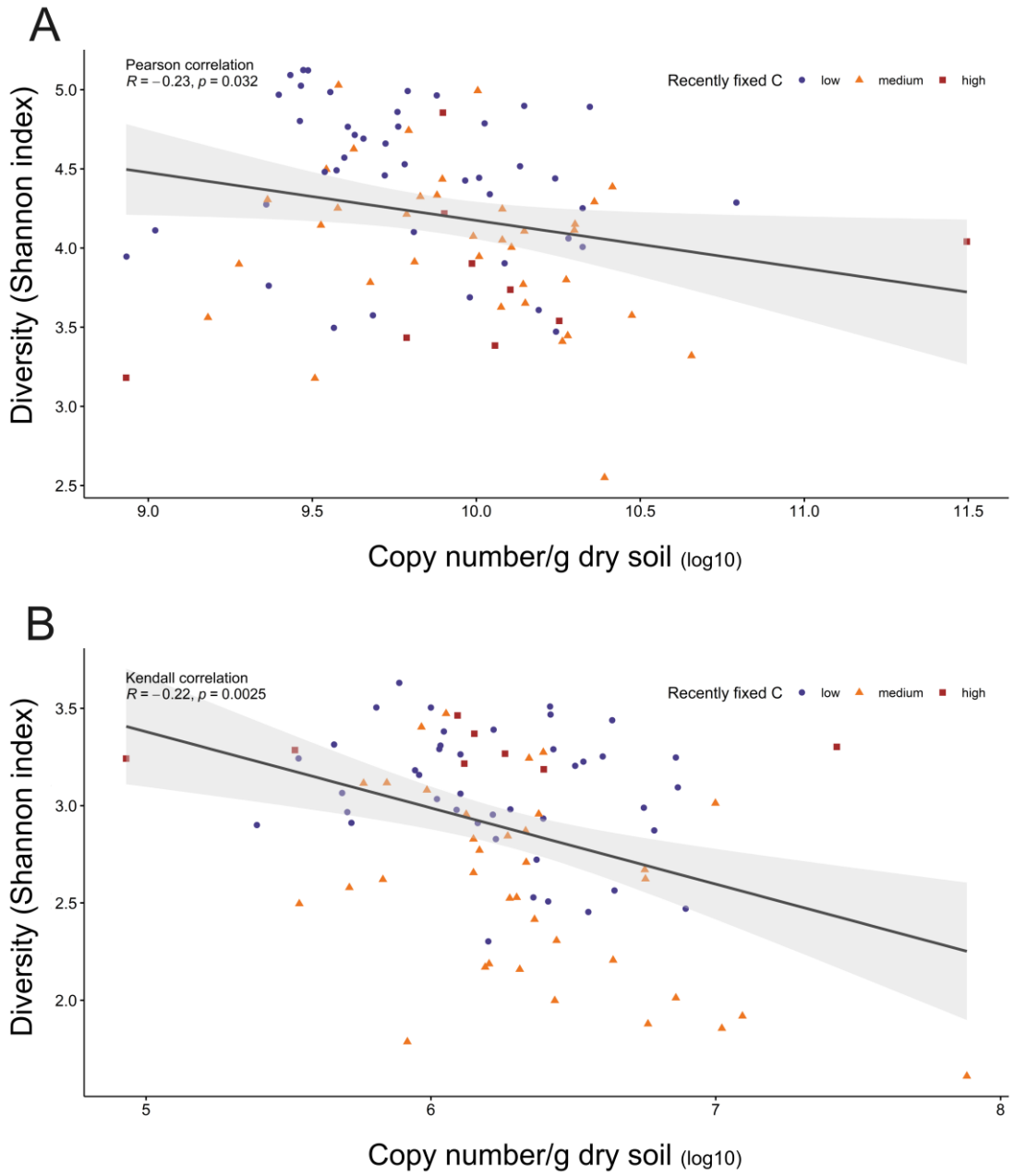

Fig. S9 Relationship between diversity and population size of **(a)** prokaryotes and **(b)** fungi as determined by qPCR targeting a 16S rRNA gene fragment (prokaryotes) or the ITS1 region (fungi). Color coding denotes samples with different categorical photosynthate levels according to ^{11}C-PET. Gray-shaded areas indicate the 95% confidence interval of the linear regression model fitted to the data. Correlations were verified using a Pearson correlation test for prokaryotes and a Kendall rank correlation test for the non-normally distributed fungal dataset.

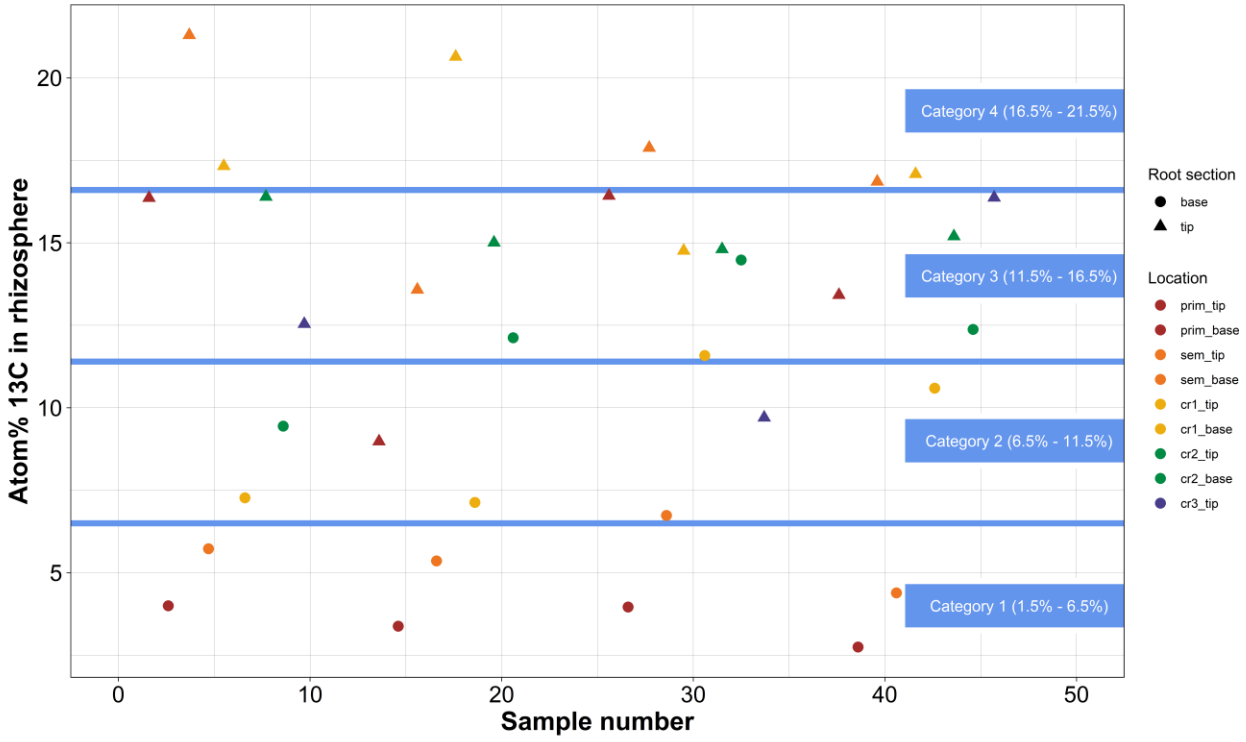

Fig. S10 Grouping of samples for HRSIP analyses into four categories based on their ^{13}C ratio in the rhizosphere soil as determined by EA-IRMS. Prim = primary root, sem = seminal roots, cr1 – cr3 = crown root generations 1 - 3, originating from underground nodes 1 – 3.

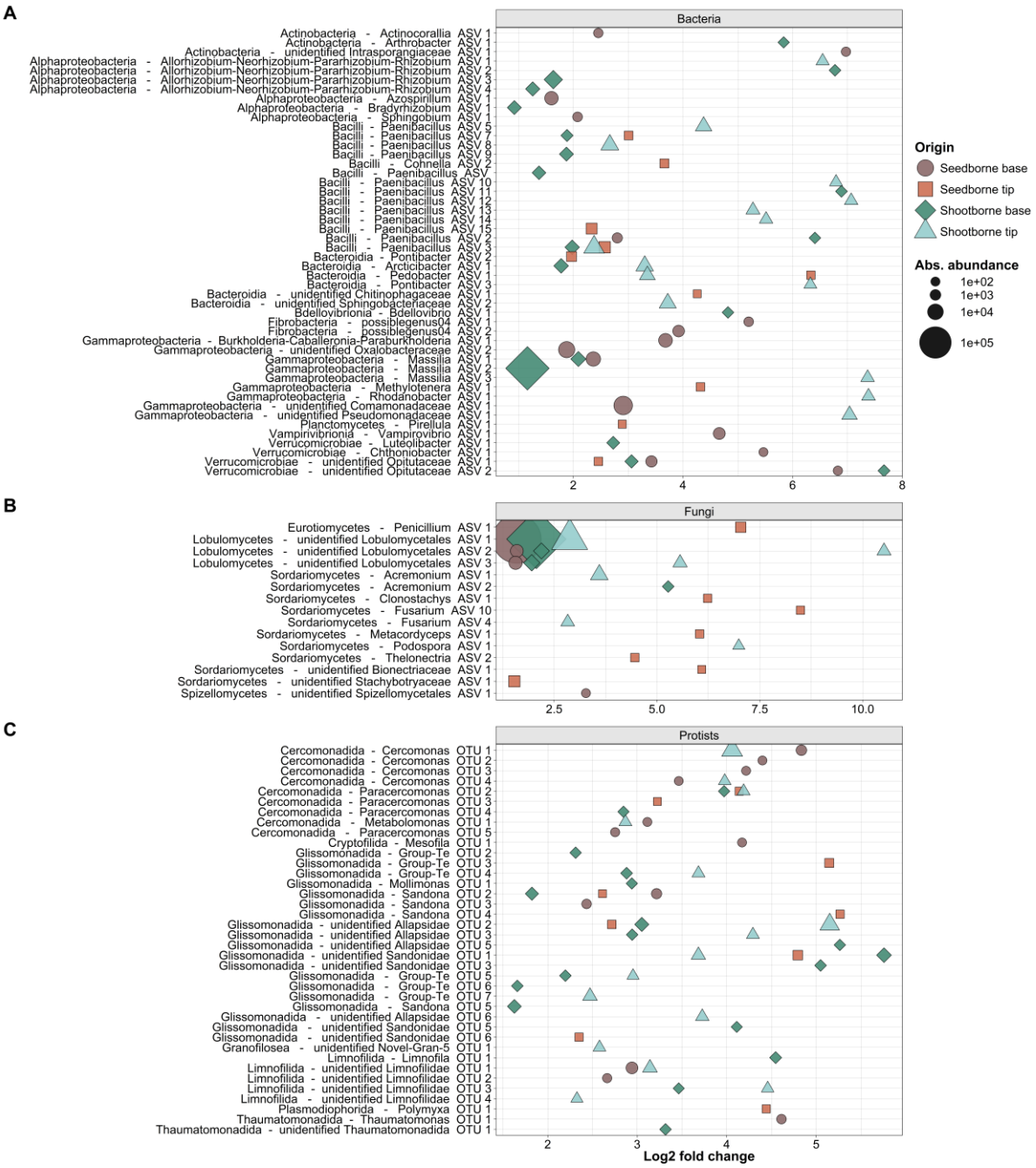

Fig. S11 ^{13}C label intensity and abundance of microbial taxa with significant label incorporation. Significantly labeled taxa were identified using the DESeq2 algorithm of the HTSSIP package. Samples were grouped into four categories in dependence on root origin in the root system. ^{13}C-labeling is presented as log2 fold change between the labeled-heavy and the labeled-light fraction. Absolute abundance equals the sum of all reads of a labeled ASV over all samples of a label category. Bacteria and fungi are labeled as Class_Genus_ASV and Cercozoa as Order_Genus_OTU.

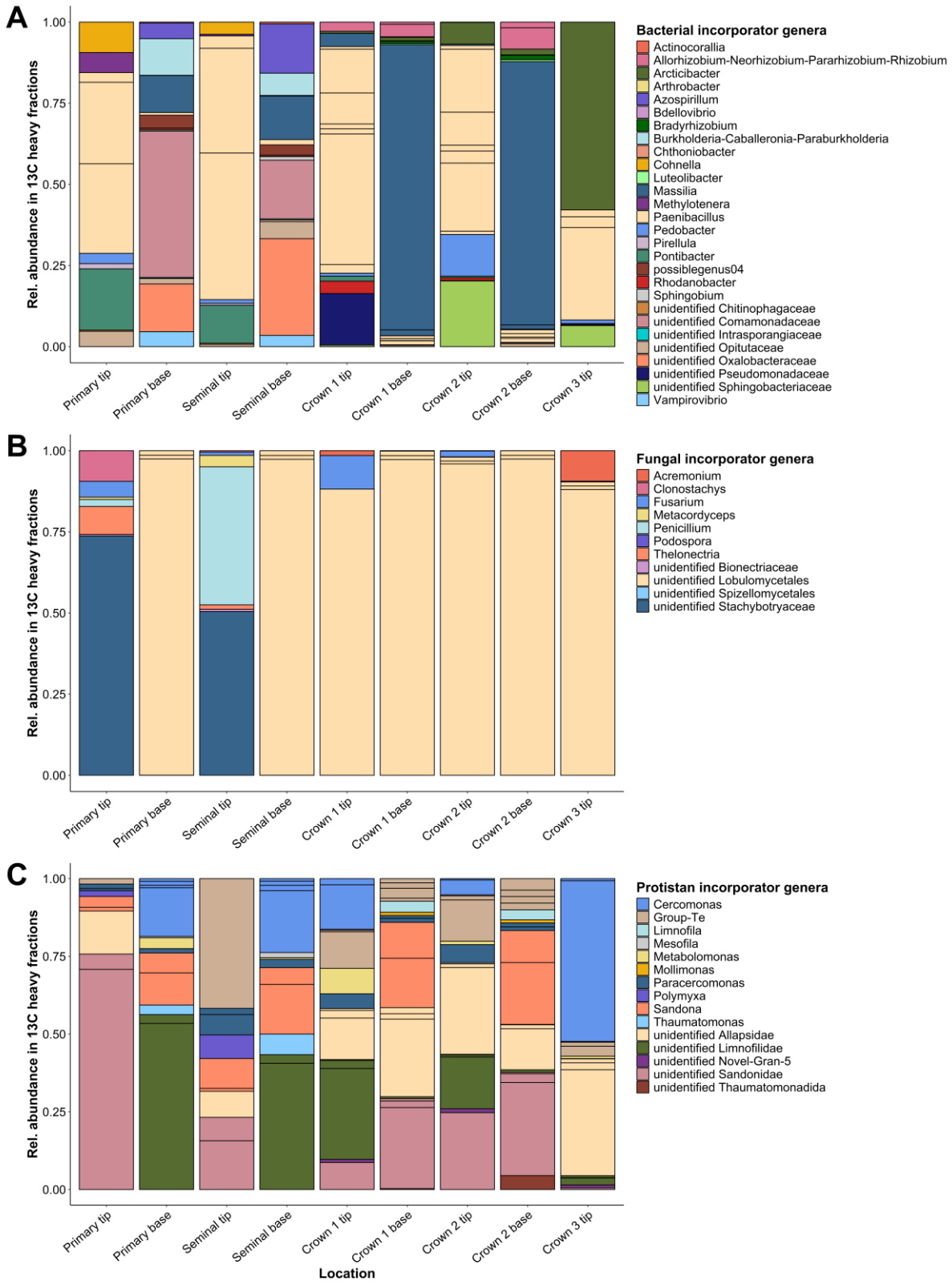

Fig. S12 Relative abundance of ^{13}C-labeled taxa at different locations in the root system. Taxa with significant ^{13}C label incorporation were identified by HR-SIP with replicate samples grouped based on their origin in the root system (seed-borne tip, seed-borne base, shoot-borne tip, shoot-borne base). Relative abundance was calculated based on sequence read counts in the ^{13}C-heavy fractions

of replicate samples per root type/section. Different ASVs within the same genus are shown in the same color.

Tip

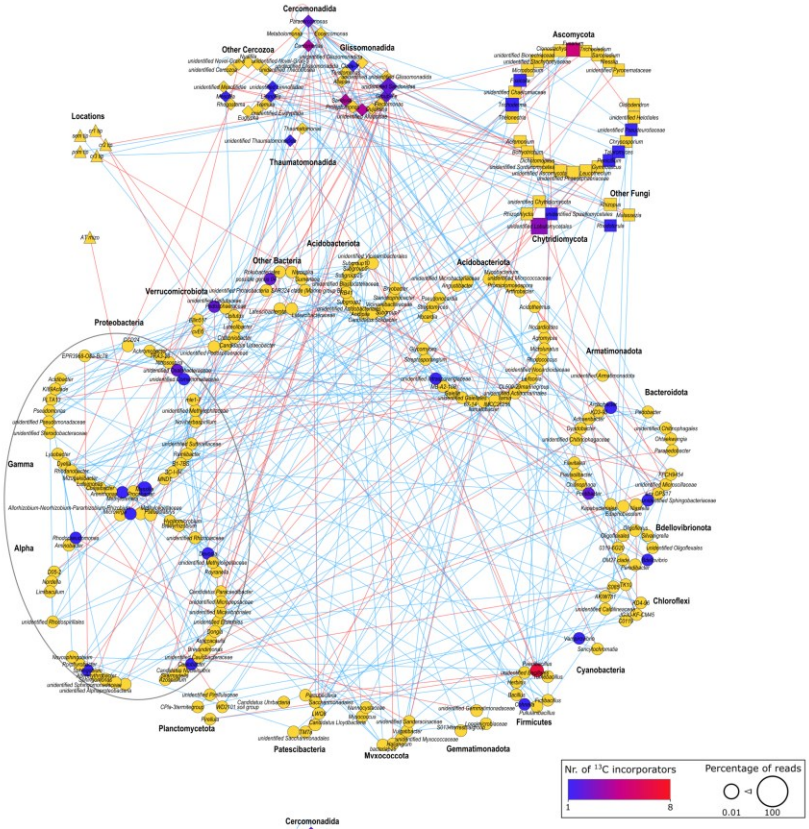

Base

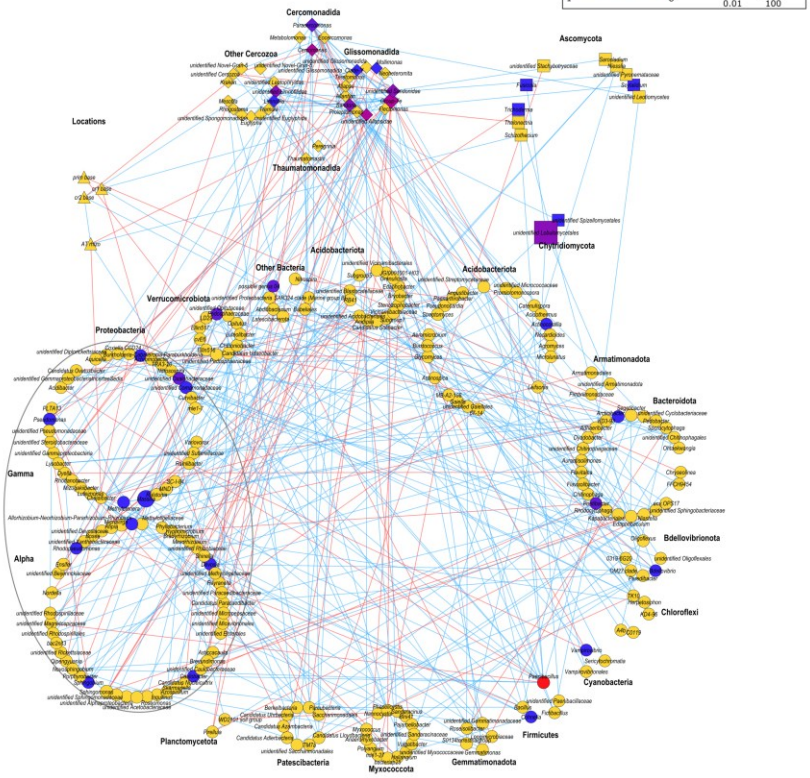

Fig. S13 Microbial co-occurrence networks resolved at genus level. The same networks for root tip and root base are shown here as in Fig. 6, but at higher taxonomic resolution. Positive associations are indicated as blue lines, negative associations as red lines. ^{13}C-incorporators are highlighted in a color range from blue to red depending on the number of labeled ASVs in the genus, non-incorporators are shown in yellow. The node size is proportional to the percentage of reads.

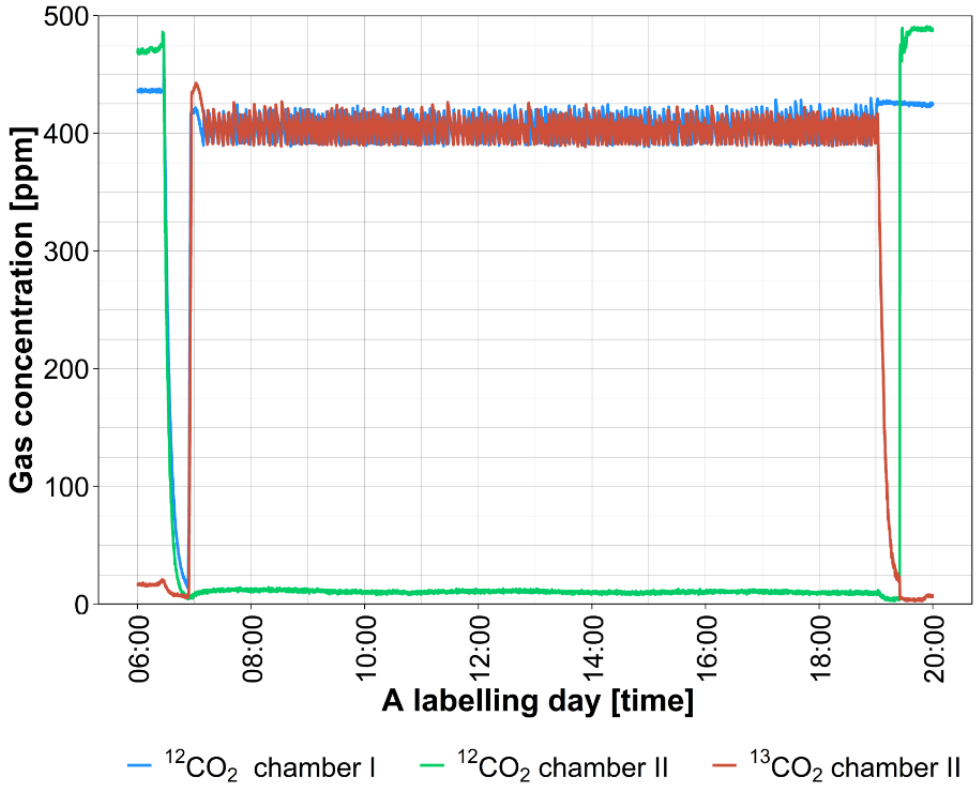

Fig. S14 Automatically regulated gas flow during a labeling day in the $^{13}CO_2$ labeling chamber (chamber II) and the $^{12}CO_2$ control chamber (chamber I). Gas concentrations were maintained at a constant level using a customized automatic valve regulation system, controlled based on measurements with the extractive gas analyzers LI-820 (LI-COR Biosciences, Lincoln, NE, USA) and S710 (SICK AG, Waldkirch, Germany). Gas exchange data were recorded in 10 second intervals. Temperature in both chambers was regulated using a DKRF400 sensor (Driesen+Kern GmbH, Bad Bramstedt, Germany) and a Julabo FN25-HE water cooling unit (Julabo GmbH, Seelbach, Germany).

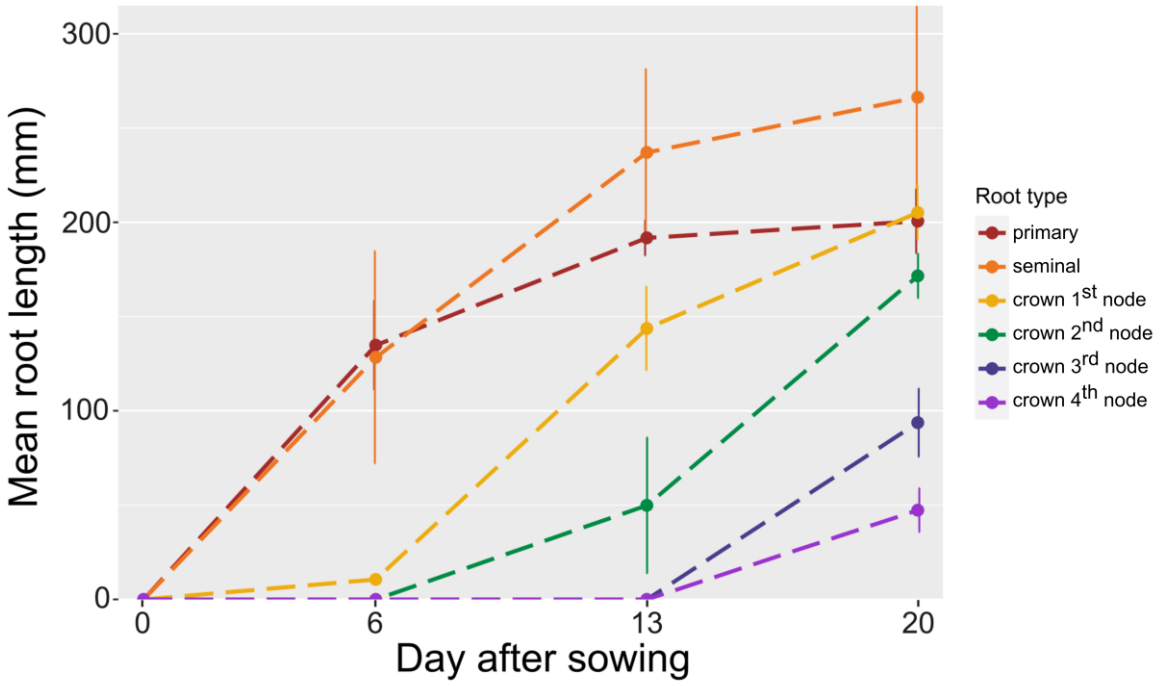

Fig. S15 Mean root length (mm) of the examined primary, seminal and crown root types from the four different leaf nodes, as determined by MRI measurements and NMRooting analysis at day 6, 13 and 20 after sowing (study I). Error bars denote the standard deviation.

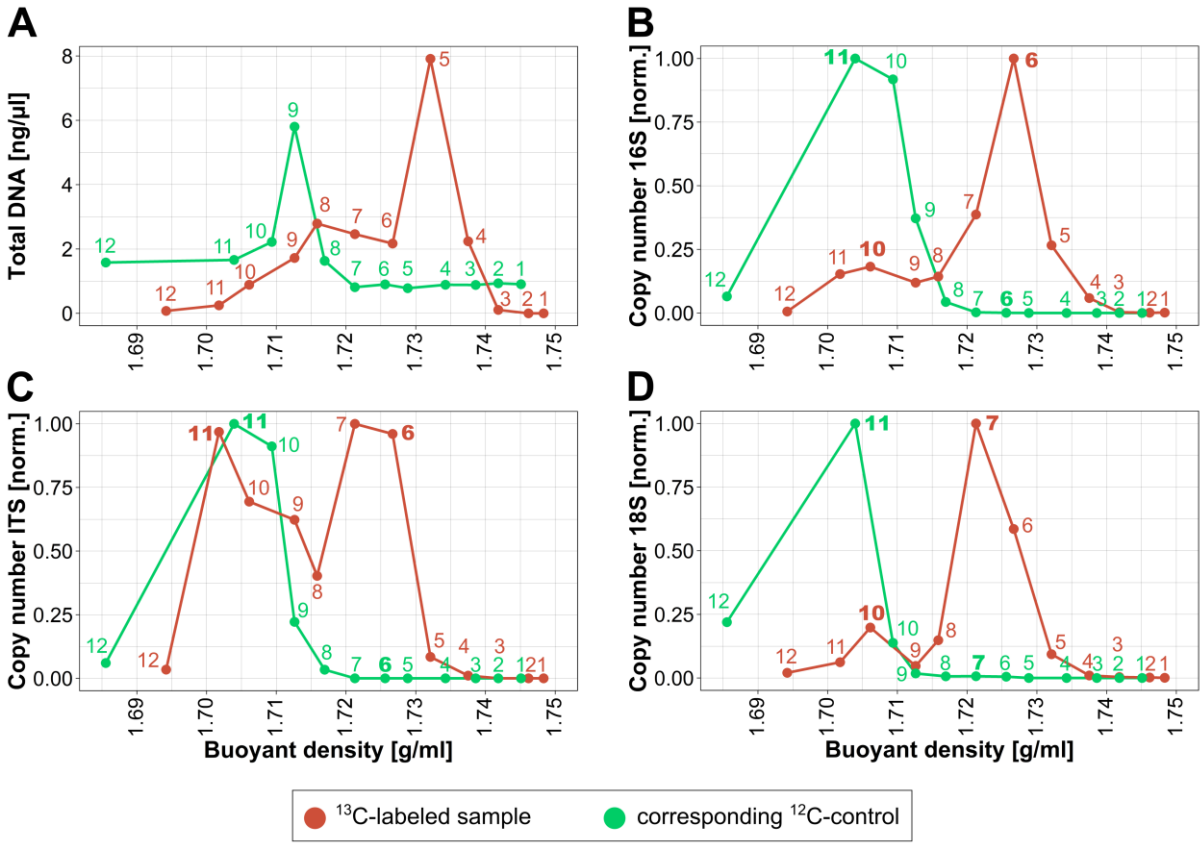

Fig. S16 A ^{13}C-labeled sample and its corresponding ^{12}C-control sample from the crown root 1 tip as an example for SIP fraction selection prior to amplicon sequencing. (a) The total DNA content and buoyant density of all fractions (numbered). **(b-d)** 16S rRNA gene, ITS1 region and 18S rRNA gen copy numbers of all fractions as determined by qPCR, normalized to 1.00. Fractions for amplicon sequencing were selected based on the qPCR results and corresponding numbers are printed in bold.

Table S1 Influence of photosynthate level and root type on microbial community composition of DNA fractions collected during DNA-SIP in study II. The influence of both factors as well as the interaction on community composition was assessed by PERMANOVA (R^2 values given in table). Factor root section was consistently eliminated in the PERMANOVA models. Significance code '***' indicates *p* values ≤0.001 and ** *p* values ≤0.01.

		Model: Root type * ^{11}C level				Model: Root type * ^{13}C level			
Group	**DNA Fraction**	**^{11}C-level (cat.)**	**Root type**	**Inter-action**	**Residuals**	**^{13}C level (num.)**	**Root type**	**Inter-action**	**Residuals**
Bacteria archaea	^{13}C light	0.28***	0.27***	0.09*	0.36	0.24***	0.27***	0.08	0.41
	^{12}C heavy	0.22***	0.36***	0.13*	0.29	NA	NA	NA	NA
	^{12}C light	0.20***	0.29***	0.10**	0.41	NA	NA	NA	NA
Fungi	^{13}C light	0.34***	0.12	0.10*	0.44	29***	0.12	0.17***	0.42
	^{12}C heavy	0.26***	0.22**	0.11	0.41	NA	NA	NA	NA
	^{12}C light	0.14*	0.32***	0.09	0.45	NA	NA	NA	NA
Cercozoa	^{13}C light	0.39***	0.17**	0.08*	0.36	0.32***	0.17**	0.09	0.42
	^{12}C heavy	0.25***	0.17**	0.09	0.49	NA	NA	NA	NA
	^{12}C light	0.41***	0.16**	0.06	0.37	NA	NA	NA	NA

Table S2 Number of different ASVs/OTUs detected as "labeled" by DESeq2 analysis within each taxon and per category. Categories were defined based on ^{13}C abundance in the rhizosphere soil or origin in root system as grouping factor.

Grouping factor	**Category**	**# bacterial ASVs**	**# fungal ASVs**	**# cercozoan OTUs**
^{13}C level	Category 1	14	4	10
	Category 2	10	2	11
	Category 3	7	6	9
	Category 4	12	14	12
Origin	Seed-borne tip	10	7	9
	Seed-borne base	15	4	12
	Shoot-borne tip	15	6	15
	Shoot-borne base	18	4	18

Table S3 Comparison of microbial co-occurrence network parameters between ^{13}C incorporators and non-incorporators. Significance of differences between groups was tested by Wilcoxon rank sum test.

Parameter	Base					Tip				
	Incorporators		No Incorporators		Wilcoxon Rank	Incorporators		No Incorporators		Wilcoxon Rank
	Mean	SD	Mean	SD		Mean	SD	Mean	SD	
Eccentricity	14.2	4.6	15.9	4.4	**<0.001**	15.2	6.5	17.0	5.2	0.109
Degree	2.6	1.3	2.2	1.3	**0.011**	2.1	1.1	2.2	1.3	0.890
Radiality	0.32	0.22	0.23	0.25	**0.013**	0.01	0.45	-0.10	0.38	0.059
Average Shortest Path Length	7.1	2.1	7.9	2.3	**0.013**	7.8	3.4	8.6	2.8	0.059
Closeness Centrality	0.20	0.22	0.17	0.20	**0.013**	0.23	0.27	0.17	0.21	0.059
Betweenness Centrality	0.06	0.19	0.02	0.06	**0.013**	0.06	0.17	0.03	0.10	0.905
Stress	4770	5850	3330	4705	**0.029**	3294	4416	3893	5720	0.604

Table S4 Number of roots per root type of each plant on days 14 and 21 after sowing as determined by MRI in study II. Plant pairs xA and xB were pooled for sampling on day 22.

Plant ID	^{13}C-labeled/ ^{12}C-control	Day after sowing	# of seminal roots	# of crown 1 roots	# of crown 2 roots	# of crown 3 roots
1A	^{13}C-labeled	14	3	3	3	0
		21	3	3	3	4
1B	^{13}C-labeled	14	3	3	3	0
		21	3	3	3	4
2A	^{13}C-labeled	14	4	4	2	0
		21	4	4	3	4
2B	^{13}C-labeled	14	3	4	1	0
		21	3	4	3	3
3A	^{13}C-labeled	14	3	4	0	0
		21	3	4	3	3
3B	^{13}C-labeled	14	3	5	0	0
		21	3	6	3	2
4A	^{13}C-labeled	14	3	3	2	0
		21	3	3	2	3
4B	^{13}C-labeled	14	3	3	0	0
		21	3	3	3	4
5A	^{12}C-control	14	3	3	3	0
		21	3	3	3	3
5B	^{12}C-control	14	3	4	2	0
		21	3	4	4	4
6A	^{12}C-control	14	3	4	0	0
		21	3	4	4	3
6B	^{12}C-control	14	4	3	2	0
		21	4	3	3	4
7A	^{12}C-control	14	3	3	0	0
		21	3	3	3	3
7B	^{12}C-control	14	3	3	2	0
		21	3	3	3	4
8A	^{12}C-control	14	3	4	0	0
		21	3	4	4	3
8B	^{12}C-control	14	3	3	1	0
		21	3	4	4	3

Table S5 Primers used to generate standards and cycling conditions for qPCR. Primer sequences available via reference list for bacteria/archaea(Heyer et al., 2002), fungi(Manter & Vivanco, 2007) and Cercozoa(Fiore-Donno et al., 2020).

		Bacteria/archaea		Fungi		Cercozoa	
Standard	Target region	16S rRNA		ITS1		18S rRNA (V4)	
	Primers	9f/1492r		ITS1f/ITS4		S615F_Cer/S947R_Cer	
Cycling	Initial denaturation	2:00 min, 95°C		2:00 min, 95°C		2:00 min at 95°C	
	Cycles including quantification steps	40x	0:10 min, 95°C 0:45 min, 60°C	40x	0:10 min, 95°C 0:45 min, 58°C	40x	0:10 min, 95°C 0:45 min, 57°C
	Optional read step		0:05 min, 84°C		-		0:05 min, 83.5°C

Table S6 Primers for amplicon sequencing and qPCR of prokaryotes (bacteria and archaea) (Caporaso et al., 2011), fungi (Gardes & Bruns, 1993; White et al., 1990) and protists (Cercozoa) (Fiore-Donno et al., 2020). BC indicates barcoded primers.

Organisms	Target region	Primer sets round 1	Primer sets round 2
Bacteria/ archaea	V4-V5 region of 16S SSU rRNA gene	**515f:** 5'-GTGCCAGCMGCCGCGGTAA-3' **806fr** 5'-GGACTACHVGGGTWTCTAAT-3'	**515f (BC)** **806r**
Fungi	ITS1 region of nuclear DNA	**ITS1F:** 5'-CTTGGTCATTTAGAGGAAGTAA-3' **ITS2:** 5'-GCTGCGTTCTTCATCGATGC-3'	**ITS1F (BC)** **ITS2**
Cercozoa	V4 region of 18S SSU rRNA gene	**S615F_Cerco:** 5'-GTTAAAAAGCTCGTAGTTG-3' **S615F_Phyt:** 5'-GTTAAAARGCTCGTAGTCG -3' **S963R_Phyt:** 5'-CAACTTTCGTTCTTGATTAAA-3'	**S615F_Cer (BC):** 5' GTTAAAARGCTCGTAGTYG-3' **S947R_Cer (BC):** 5'-AAGARGAYATCCTTGGTG-3'

Table S7 Two-step PCR conditions for amplicon sequencing of prokaryotes and fungi.

	Bacteria/archaea		Fungi		Cercozoa	
Round 1						
Initial denaturation	2:00 min, 95°C		1:00 min, 95°C		2:00 min, 95°C	
Denaturation		0:20 min, 95°C		0:20 min, 95°C		0:30 min, 95°C
Annealing	25x	0:20 min, 52°C	30x	0:20 min, 55°C	24x	0:30 min, 50°C
Elongation		0:20 min, 72°C		0:20 min, 72°C		0:30 min, 72°C
Final elongation	3:00 min, 72°C		3:00 min, 72°C		5:00 min, 72°C	
Round 2						
Initial denaturation	2:00 min, 95°C		1:00 min, 95°C		2:00 min, 95°C	
Denaturation		0:20 min, 95°C		0:20 min, 95°C		0:30 min, 95°C
Annealing	6x	0:20 min, 52°C	6x	0:20 min, 55°C	24x	0:30 min, 50°C
Elongation		0:20 min, 72°C		0:20 min, 72°C		0:30 min, 72°C
Final elongation	3:00 min, 72°C		3:00 min, 72°C		5:00 min, 72°C	

Table S8 PCR reaction composition for amplicon sequencing.

Chemical	PCR Round 1 (10 µl)	PCR Round 2 (30 µl)
5 x Herculase II Fusion buffer	1x	1x
dNTPs	0.25 mM each	0.25 mM each
primer A (barcoded in round 2)	0.25 µM	0.25 µM
primer B	0.25 µM	0.25 µM
$MgCl_2$	1 mM	1 mM
BSA	0.8 mg/ml	0.8 mg/ml
Herculase II Fusion Polymerase	0.5 U	1.5 U
DNA template	1 µl	1 µl round 1 product (16S) or 2 µl purified product (ITS)

Table S9 Total and mean read number per sample remaining for downstream analyses after initial quality filtering.

Target gene	Study I		Study II	
	Total reads	Mean / sample	Total reads	Mean / sample
16S rRNA gene	2241233	23346	3987467	31152
ITS1 region	4233112	46012	3200639	25605
18S rRNA gene	4794021	52682	3248382	21801

3. General discussion and conclusions

3.1. Résumé

The maize root system has the potential to facilitate plant-microbe interactions through the excretion of photosynthates. However, the spatial aspects of photosynthate distribution and excretion in this functionally complex root system are still largely unresolved. It is yet unknown how spatial heterogeneity in photosynthate distribution fuels microbiome assembly and impacts consumers of rhizodeposits at root system scale. We addressed this knowledge gap by investigating microbial colonization in relation to root structural traits, measuring the distribution of photosynthates in roots and rhizosphere, and evaluating its impact on the prokaryotic, fungal and cercozoan rhizosphere communities by tracing labeled photosynthates to their microbial consumers. For this, we conducted three experiments with maize grown in microcosms for about three weeks:

Experiment I (Chapter 2.1) focused on the assembly of the prokaryotic community at a small scale in relation to root system architectural traits. This was investigated in the compartments rhizosphere, rhizoplane, and endosphere and across three soil textures. In experiment II (Chapter 2.2) we continued with the sampling scheme from experiment I but added a measure for root-internal photosynthate level ($^{11}CO_2$ labeling and PET-MRI) to explore its effect on the variation in the prokaryotic, fungal and protistan (cercozoan) rhizosphere communities. Experiment III (Chapter 2.2) aimed to relate spatial variation in the prokaryotic, fungal and cercozoan rhizosphere communities to both, root-internal and rhizosphere photosynthate distribution. This was achieved by complementing the approach from experiment II with stable $^{13}CO_2$ labeling to quantify labeled photosynthates in the root tissue and rhizosphere and identify prokaryotic, fungal and cercozoan ^{13}C consumers using DNA-SIP. These experiments enabled us to explore the research questions outlined in the introduction, with the findings being discussed in the following chapters.

Firstly, the spatial patterns in the microbiota depending on root structural traits are discussed (Chapter 3.2). Secondly, we elaborate on the spatial distribution of photosynthates in the root and rhizosphere (Chapter 3.3) and thirdly, evaluate to what extent photosynthate allocation determines spatial patterns in the rhizosphere microbiota (Chapter 3.4). The collected findings then lead to the definition of four exemplary microhabitats that illustrate the predominant mechanisms of microbiota assembly in the maize rhizosphere (Chapter 3.5). Finally, the discovered mechanisms are placed into the context of additional factors contributing to rhizosphere spatial organization (Chapter 3.6) and the practical relevance of the findings is discussed (Chapter 3.7).

3.2. Root type and longitudinal section induce conserved spatial patterns in the rhizosphere microbiota

Our research contributed to the understanding of spatial relationships between plant roots and their associated microbiome. We show that, in addition to the already established concept of community establishment along the radial axis of roots (Bulgarelli et al., 2013; Edwards et al., 2015), the root longitudinal section and root types play a central role in shaping the prokaryotic, fungal and cercozoan community structure.

3.2.1. The root longitudinal section

Our findings in both studies revealed that the root longitudinal section played a pivotal role in driving microbial community variation. While it is commonly accepted that microbial alpha diversity declines in the rhizosphere as compared to the bulk soil (Chapter 2.1 Fig. S3, Ling et al. (2022)), we found that this selective enrichment is amplified at root tips. At root tips, the prokaryotic alpha diversity (Shannon diversity index) declined significantly as compared to root bases across all compartments investigated in Chapter 2.1 (Fig. 3c). The same effect could be observed for fungi and, as a trend, for Cercozoa in the rhizosphere of maize plants grown in sandy soil (Chapter 2.2 Fig. S7a). In line, bacterial and fungal evenness declined significantly at root tips (Chapter 2.2 Fig. S7b and c) while bacterial and fungal population size slightly increased (Chapter 2.2 Fig. S8); indicating that specific taxa are enriched at root tips. The reduced diversity and evenness can be considered a direct result of increased photosynthate resources at root tips, leading to the enrichment of copiotrophic colonizers that favour easily degradable carbon. These opportunistic root tip colonizers have been reported to prefer monosugars, organic acids and other low molecular weight compounds (Liljeroth et al., 1991), which are readily available from the fresh photosynthates. This is supported by root section associated patterns in prokaryotic community composition that showed a clear separation according to root tip and root base across compartments (Chapter 2.1 Fig. 5). A similar pattern was observed for fungal and cercozoan community composition in the rhizosphere (Chapter 2.2 Fig. S5). A previous study by DeAngelis et al. (2009) observed that taxa reacted very differently to the arrival of the root tip and behaved differently as roots matured. Specifically, they found that Acidobacteria, TM7 and Bacteroidetes showed a progressively increasing 16S copy number with aging root zones. In line, a recent study provided evidence of microbial community succession occurring along the root's longitudinal axis (Rüger et al., 2021). Although we did not investigate fungi and Cercozoa in the rhizoplane and endosphere compartments in Chapter 2.2, we expect that the patterns in alpha

diversity would be largely comparable, as many rhizoplane and endosphere microorganisms are recruited from the rhizosphere (Bulgarelli et al., 2013). Qian et al. (2019) observed that the root endosphere fungal community shared a high number of taxa with the rhizosphere community, while connectedness and centrality of networks was lower in the endosphere than in the rhizosphere. He et al. (2024) found that the protistan community in the *Sorghum* root endosphere was dominated by Endomyxa and Cercozoa and that it significantly differed from the leaf endosphere community. However, to the best of our knowledge, no studies have yet investigated the spatial variation of the cercozoan communities in the maize root endosphere, a point that should be addressed in future research.

To ensure a good comparability of the results, a similar sampling scheme of the maize root system was used throughout all experiments, which, however, does come with certain limitations. Firstly, the sampling of the root tip region has room for improvement, as we sampled a relatively large region of ~2 cm of the root tip which encompassed the root cap, the elongation zone as well as the beginning of the root hair zone. Recent studies showed that the microbiome can vary considerably between the root cap, tip and the root hair zone (Rüger et al., 2021; Rüger et al., 2023), which would require a more careful dissection of the root tip region into finer sections during sampling. Secondly, our sampling of the root base was limited to always sampling the top 10 cm of the root, leading to the sampling of root regions in different developmental stages. In the older seed-borne roots, lateral roots had already developed at the sampling timepoint, while the younger crown roots did not yet have any lateral roots. In future studies that aim to focus on community assembly along the root longitudinal axis, we would suggest to only sample roots that already have developed lateral roots as proposed by Yu et al. (2018). The distinct colonization of root types in different developmental stages are discussed in the following section.

3.2.2. Root types, their function, succession state and growth rate

Root type significantly affected the diversity and composition of the prokaryotic, fungal and cercozoan microbial communities (Chapter 2.2). In parallel with our research, other authors also found root type-dependent differences in microbial colonization. Kawasaki et al. (2021) found root type-dependent differences in wheat and rice that compared in order of magnitude with differences between plant species, while Yu et al. (2018) detected differences in fungal endosphere community composition between lateral and axial maize roots. Other authors found that the rhizosphere and endosphere bacterial communities shifted gradually with root diameter, indicating variation in the colonization of functionally diverse root types like fine roots versus larger structural roots (Becker et al., 2022; Zai et al., 2021). In our study, prokaryotic diversity consistently declined from primary roots

to seminal roots and then to crown roots, following their consecutive nodes of origin. This pattern was observed across soil types and compartments (Chapter 2.1 Fig. 3b) and across experiments (Chapter 2.2 Fig. S7a). Similarly, a shift in microbiome composition was observed in the clustering of samples by root type, which mirrored the chronology of root emergence in the ordination plots (Chapter 2.1 Fig. 5, S5 and Chapter 2.2 Fig. S5).

We argue that the observed root type-dependent microbial patterns arise from a combination of **I.** root physiological and functional characteristics, **II.** microbiota succession as roots age, and **III.** the influence of varying root growth rates.

I. Differences in microbial diversity and community composition between seed-borne and shoot-borne roots may be partially attributed to their physiological and functional differences (Chapter 1.1). While seed-borne roots primarily support the maize plant during the embryonic stage, shoot-borne roots form the backbone of the mature maize root system, being central for anchorage and responsible for the majority of water/nutrient acquisition (Hochholdinger, Woll, et al., 2004). These fundamental differences are highlighted by several mutants of maize that affect root development in a root type specific way, such as *slr1* and *slr2* that restrict lateral root elongation in seed-borne roots but not in shoot-borne roots (Hochholdinger, Park, et al., 2004). Primary, seminal and crown roots of maize do not only differ in diameter and growth rate (Chapter 2.1 Fig. 2), but also in their gene expression profiles (Tai et al., 2016). Apart from physiological traits such as root diameter, host-driven selection might lead to differences in the microbial colonization of seed-borne and shoot-borne roots, as plants likely recruit microorganisms tailored to their needs at earlier versus later developmental stages.

II. However, root functional characteristics cannot account for the successive patterns observed within the crown root functional group. These patterns suggest that a significant portion of the root type-dependent variation in microbial colonization may be attributed to microbial population succession as roots age. Microbial population succession in aging root systems (Micallef et al., 2009; Wagner et al., 2016) and along the root longitudinal axis (Rüger et al., 2021) has previously been demonstrated, but not yet resolved by root types. We found that root type-dependent patterns in prokaryotic diversity shown in Chapter 2.1 (Fig. 3b) and Chapter 2.2 (Fig. S7a) closely resembled root age-dependent patterns observed with MRI (Chapter 2.1, Fig. S2). These patterns corresponded well with differences in prokaryotic richness and evenness (Chapter 2.2 Fig. S7b), suggesting an enrichment of certain taxa in young roots, that are later complemented by other taxa. Especially for prokaryotes, community composition seemed to overlap more between samples of older root types, while samples from younger roots clustered separately (Chapter 2.1 Fig. 5 and Chapter 2.2 Fig. S5). Moreover, we found that the relative abundance of several prokaryotic but also fungal taxa was

related to the chronology of root emergence (Chapter 2.2 Fig. S6). Sampling of the rhizosphere at one timepoint only provides a snapshot of the colonization/succession state that the microbiome of specific root types and developmental stages are in. Nonetheless, our data suggests that older roots might host more established microbial communities, while communities are still establishing in younger roots.

III. Functional differences and root age do, however, not yet explain the differences in diversity and community composition between root tips of different root types that was observed across studies and microbial communities (Chapter 2.1 Fig. 5, 6, S4 and Chapter 2.2 Fig. S5). The continuously growing tissue at root tips is young and thus supposedly not as influenced by root age and functional differences as root bases. For root tips, differences in root growth rates might partially explain the observed patterns in microbial colonization. The growth rate of single roots is a factor that has often been neglected in past microbiome studies. This is mainly due to limitations in technology, which did not allow the non-destructive measurement of root parameters like age and growth rate and sampling of the same roots for microbiome sequencing. Here, non-invasive imaging methods like MRI are a helpful advancement. In Chapter 2.1, we were able to use MRI to get first insights on the effects of root growth rate and root age on the prokaryotic community. Young crown roots of the 2nd whorl had the highest growth rate of 3 to 4 cm d^{-1}, which is in line with the elongation rates frequently used in modeling approaches for maize crown roots (De Moraes et al., 2019). However, crown roots of the 3rd whorl had slightly lower growth rates, contrary to our expectations. This might be due to a gross underestimation of crown 3 growth rates due to the large last MRI scanning interval of 15-20 DAS, during which the crown 3 roots emerged. For future studies aiming to unravel the effect of root growth rate on microbiome assembly, we would recommend increasing the MRI measurement and sampling intervals, as daily measurement would achieve root architectural data at higher resolution, which would allow to confirm and better resolve microbial assembly processes. Prokaryotic diversity generally decreased with increasing root growth rate (Chapter 2.1 Fig. 4). This supports the concept that only a few fast-growing taxa are adapted to the high growth speed of young crown roots and are consequently enriched at root tips. However, while root growth rate might partially cause the observed root type related differences in microbial colonization at root tips (Chapter 2.1 Fig. 5, 6, S4), it did not stand out as an influential factor on community composition and was excluded from the db-RDA models. This might be because the model comprised samples from all root sections, while growth rate affects the tips more than the bases. Alternatively, root growth rate was masked by the other factors that explained community variation better, possibly due to underlying mechanisms not yet investigated in Chapter 2.1.

3.2.3. Conserved spatial patterns point at robust mechanisms of rhizosphere organization

Remarkably, both root type and root section patterns in alpha diversity were largely conserved between soil textures (Chapter 2.1 Fig. 3), even though the microbial community composition differed between soil textures. This finding supports one of the core hypotheses related to the concept of the rhizosphere as a self-organized system, namely that underlying mechanisms of spatiotemporal organization in the rhizosphere (i.e. interactions between roots and the microbiome) follow similar general patterns and that external drivers, like soil texture, only moderately change those patterns (Vetterlein et al., 2020). Indeed, while root type and root section associated microbial patterns varied in their extent between soil textures and microbial communities, the general patterns prevailed. This provides an intriguing perspective on the ongoing debate regarding whether root-associated microbiota assembly is primarily fueled by stochastic or deterministic processes. While some studies stress the important role of deterministic factors such as root exudate blend (Wen et al., 2022), predation (Yue et al., 2023) or plant genotype (Guo et al., 2021) in shaping the rhizosphere microbiome, others propose that stochastic processes like priority effects (Bonkowski et al., 2021) or dispersal (Munoz-Ucros et al., 2021) play a larger role than previously anticipated. We suggest that the answer to this is highly dependent on the spatial scale that is investigated. On a large scale, the recruitment of the overall core microbiome of the maize root system might have a considerable stochastic part, i.e. the community composition highly depends on which taxa are present in the plant's vicinity in the bulk soil. This is supported by our own data (Chapter 2.1 Fig. S5, Table S10) but also by other authors who found that soil type was a central influence factor on maize prokaryotic beta diversity (Gebauer et al., 2021) and maize prokaryotic, fungal and cercozoan beta diversity (Yim et al., 2022). On the other hand, many small-scale spatial variation patterns in microbial colonization seem to be rather deterministically influenced, as becomes apparent by the largely conserved colonization patterns observed across soil types (Chapter 2.1) and microbial communities (Chapter 2.2). This is supported by the observation that the effect of soil texture on community composition decreased, while the impact of root type and section increased in the rhizoplane as compared to the rhizosphere, implying a deterministic selection mechanism that increases with proximity to the root and that then varies by root architectural parameters (Chapter 2.1 Table 2 and S10).

Altogether, these findings allowed us to **answer research question 1**: *How does the complex root system architecture of maize affect the spatial variation of the rhizosphere, rhizoplane and endosphere microbiota and are these effects altered in response to soil texture?* → Our findings highlight that spatial variation in the microbiome of the maize root system is more heterogeneous than anticipated and influenced by a multitude of interacting factors. Root longitudinal section and

root type stand out as the most influential factors, with root type-related differences being present even at the root tips. Microbial patterns associated with root type can be partially attributed to root functional characteristics, root age, the microbiome's succession state, and root growth rate. Notably, microbial patterns linked to root type and root sections were largely conserved across soil types, and only slightly varied in their extent depending on soil properties (e.g. growth rate differences in loam) and microbial communities (e.g. fungi being less responsive than bacteria). This suggests robust mechanisms that underly rhizosphere organization. As rhizosphere microbiome assembly is, for a large part, mediated by rhizodeposition (Hu et al., 2018), we hypothesized that spatial heterogeneity of photosynthates in the root system might be a major underlying mechanisms accounting for the spatial variation observed in the microbiota. While hotspots of rhizodeposition at root tips are well-recognized, the partitioning of photosynthates in the root system and rhizosphere has not yet been systematically examined on a small scale, particularly with respect to functionally distinct root types. We thus proceeded to investigate photosynthate distribution in the maize root system and rhizosphere using isotopic labeling techniques.

3.3. Photosynthates are heterogeneously distributed and released in the maize root system

In this research, two methods were used to investigate photosynthate partitioning in the maize root system: radioactive $^{11}CO_2$ labeling coupled with PET-MRI for visualizing root internal photosynthate levels and stable $^{13}CO_2$ labeling coupled with EA-IRMS to measure photosynthates in root tissue and the rhizosphere simultaneously.

While measuring ^{13}C-labeled photosynthates in root tissue and the rhizosphere of the same samples, we encountered higher photosynthate levels in root tissue than in the rhizosphere. This is consistent with the results of a meta study by Pausch and Kuzyakov (2018), who found that photosynthate allocation to roots continuously exceeded net rhizodeposition in 80% of their reviewed data. Additionally, we observed a strong positive correlation (R^2 = 0.76) between root-internal photosynthate level and photosynthate level in the rhizosphere (Chapter 2.2 Fig. 3c), which was also detected by Remus et al. (R^2 = 0.75) in their ^{14}C labeling study of spring rye (Remus & Augustin, 2016). These observations support the hypothesis that root exudation is mostly dependent on passive diffusion and thus on the concentration gradient between root tissue and the surrounding rhizosphere (Canarini et al., 2019). This would make root internal photosynthate level a central determinant of rhizodeposition, which is only partially modified by active transport processes.

Photosynthate partitioning in the maize root system was spatially heterogeneous, especially among different root sections and types. PET imaging showed that root tips had in general high photosynthate levels, with the youngest crown roots exhibiting the largest accumulations (Chapter 2.2 Fig. 2). Additional stable isotope labeling with $^{13}CO_2$ confirmed consistently higher photosynthate levels in root tips as compared to bases for both the root tissue and the rhizosphere (Chapter 2.2 Fig. 3). This aligns well with pre-existing 2D (^{14}C) imaging studies that found root tips to be hotspots of photosynthate allocation and exudation (Dennis et al., 2010; Doan et al., 2017; Holz et al., 2019; Pausch & Kuzyakov, 2011). Moreover, our findings revealed a degree of variability across root types and root ages, indicating that the assumption of uniform photosynthate hotspots across all root tips requires reconsideration. The observation that ^{13}C abundance at root bases in both root tissue and rhizosphere generally increased with decreasing root age (Chapter 2.2 Fig. 3) indicates a more nuanced partitioning pattern than previously expected. It suggests that fine-scale structural and functional characteristics drive highly specific carbon allocation within the root system that might additionally vary with the developmental stage of individual roots, adding a new dimension to photosynthate partitioning concepts. Indeed, variation observed across root types mirrors studies demonstrating that maize root types vary in structure and function (Tai et al., 2016) and that the transcriptome of maize roots varies between root types (Yu et al., 2018). Tai et al. not only found a higher number of xylem vessels in crown roots as compared to seminal roots of maize, but also a significantly higher proportion of stele area relative to total root area (Tai et al., 2016). A larger stele area might offer more room for phloem vessels and thus increase the capacity of photosynthate transport in crown roots. Root system architecture and the plant's developmental stage are both reported to influence exudation dynamics (Pausch & Kuzyakov, 2018). We found rhizodeposit accumulations particularly around young, fast growing crown roots (Chapter 2.2), which is in line with the positive correlation between root growth and rhizodeposition detected by Remus et al. Remus and Augustin (2016). A high dependence of rhizodeposition on root growth rate would support the “optimal partitioning theory,” which suggests that plants allocate assimilated carbon preferentially to zones with the highest functional need (Li et al., 2024), such as fast-growing root tips. The contrasting “residual C” hypothesis states that excess photosynthates are the main drivers of partitioning patterns, leading to an increased rhizodeposition from root areas with elevated photosynthate concentrations (Li et al., 2024).

However, more research will be necessary to clarify the differences in photosynthate partitioning and rhizodeposition under various conditions, as we only conducted the $^{11}C/^{13}C$ labeling experiment in sandy soil and with 3-week-old maize plants. As a next step, we propose introducing zones of soil compaction to investigate the response of carbon partitioning and rhizodeposition to

compacted layers in soil. Previous research suggests that rhizodeposition generally increases in response to compacted soil layers (Somasundaram et al., 2009), although without differentiating between different root types. Another easy to manipulate soil parameter is nutrient availability through NPK fertilization, which has already been shown to increase rhizodeposition in maize and soybean as compared to non-fertilized soil (Qiao et al., 2017). Various biotic factors can also influence carbon partitioning and rhizodeposition. A continuously discussed question related to rhizosphere microbiome assembly is to what extent plants can modify their carbon partitioning blend or increase net rhizodeposition to purposefully attract beneficial microorganisms (Hartmann et al., 2009). Mechanisms for attracting beneficials are already well documented for symbionts like N-fixing rhizobia (Cooper, 2004) or AMF (Steinkellner et al., 2007). In a recent study, Metzner et al. (2022) employed ^{11}C labeling combined with PET-MRI to explore photosynthate partitioning in the root system and nodules of rhizobia-associated pea plants. Their findings revealed that nitrate fertilization reduced photosynthate allocation to nodules by nearly 50%, indicating that nodules continue to function as significant carbon sinks even when their nitrogen-fixing activity is temporarily redundant (Metzner et al., 2022). However, photosynthate partitioning in response free-living beneficials is still largely unresolved. To shed some light on this, we propose to artificially enrich sandy soil with members of potentially beneficial groups of photosynthate consumers identified in Chapter 2.2. In comparison to soil without purposefully enriched beneficials, ^{11}C labeling and PET-MRI could be performed to investigate differences in photosynthate partitioning. EA-IRMS could be used to comparatively quantify rhizodeposition. ^{13}C labeling and DNA-SIP could then verify photosynthate consumption of beneficial groups and even quantify label incorporation of specific taxa using quantitative SIP (Hungate et al., 2015). Although this approach might be complicated by the correct establishment of the beneficial synthetic community in the sandy soil, it still offers insights into plant-driven selection of rhizosphere microorganisms by rhizodeposition, knowledge which could advance microbiome engineering.

Improvements to the timing and intervals of ^{11}C and ^{13}C labeling might further increase the reliability and resolution of our labeling approach. Particularly, the 2-day lag time between the end of ^{13}C labeling and sampling due to PET measurement complicated the interpretation of the ^{13}C content for young crown roots. We assume that the ^{13}C content of young crown roots might have been higher if sampling occurred on the last day of labeling. It might be possible to improve root-internal vs. rhizodeposition measurement results by concurrent labeling of ^{11}C and ^{13}C to get rid of the lag time between PET measurement and ^{13}C and sampling. This might however be technologically ambitious as it would require a combinatory labeling chamber, in which the $^{11}CO_2$ cylinder for PET is mounted in a ^{13}C chamber and can be automatically opened as soon as the 6 min $^{11}CO_2$ labeling

period is over. This would guarantee a continuous supply with $^{13}CO_2$, even during PET measurements of several hours or multiple daily PET measurements.

Overall, the above findings allowed us to **answer research question 2**: *Where are photosynthates allocated within a complex root system and where are they released into the rhizosphere?* → $^{13}CO_2$ labeling showed strong correlations between root internal photosynthate allocation and rhizodeposition. The allocation of photosynthates varied significantly along the longitudinal root axis, with the highest accumulations observed at the root tips while at the root bases, recent photosynthates merely passed through. In addition, photosynthate allocation clearly differed between root types, with the youngest crown roots exhibiting particularly strong ^{11}C signal intensity. Photosynthate accumulations at root tips consistently decreased with increasing root age, suggesting a key role of photosynthate partitioning in explaining root type-dependent sequential patterns in microbial colonization. We thus proceeded to investigate to what extent spatial variation in the rhizosphere microbiome is related to spatially heterogeneous photosynthate allocation in the root system.

3.4. Heterogeneous photosynthate distribution drives spatial patterns in the rhizosphere microbiota

To investigate to what extent spatial variation in the rhizosphere microbiome is related to spatially heterogeneous photosynthate partitioning, microbial community variation was related to two measures of photosynthate allocation. Firstly, we defined three semi-quantitative levels of root-internal photosynthate distribution by $^{11}CO_2$ labeling and PET-MRI and related these levels to the variation in the total community and, more specifically, to the ^{13}C-consumers (Chapter 2.2). Secondly, we related the ^{13}C quantity as measured by EA-IRMS to the composition of the ^{13}C-labeled community (Chapter 2.2). Both analyses confirmed that spatial heterogeneities in photosynthate distribution indeed had a central role in structuring the rhizosphere microbial communities of prokaryotes, fungi and Cercozoa. While the total community composition (Chapter 2.2 Table 1, Fig. S5) rather depended on root type, both ^{11}C and ^{13}C photosynthate levels exceeded the influence of root type on community composition when only ^{13}C consumers were analyzed (Chapter 2.2 Table 1). This suggests that the patterns in microbial community composition based on root type and root section observed throughout all experiments (Chapter 3.2) can be partly explained by heterogeneities in photosynthate allocation. Indeed, differences between root types and sections were more pronounced in the ^{13}C-consuming community than in the total community (Chapter 2.2

Fig. 4, S5, Table 1), hinting at a central role of photosynthate distribution in shaping the consumer communities. The large overlap between DESeq2 results of root type and photosynthate level analyses (Chapter 2.2 Fig. 5, S11) supports this idea, as well as the opposing patterns in ^{13}C distribution (Chapter 2.2 Fig. 3b) and alpha diversity (Chapter 2.1 Fig. S4). Not many previous studies have attempted to investigate spatial patterns in photosynthate distribution associated with microbial colonization in the rhizosphere. Zhang et al. (2023) used ^{14}C labeling and phosphor imaging to visualize the spatial distribution of photosynthates in the maize root system an rhizosphere, and combined it with zymography to visualize β-glucosidase activity in the rhizosphere. β-glucosidase activity is a proxy for overall microbial activity and positively correlates with the presence of active consumers of plant-derived carbon. They found that spatial patterns and particularly hotspots of ^{14}C overlapped strongly with hotspots of ß-glucosidase activity (Zhang et al., 2023). This aligns well with our observations that microbial diversity patterns closely correspond to photosynthate patterns.

3.5. Microbial microhabitats created by root morphology and photosynthate distribution

Our results indicate that the spatial heterogeneity in photosynthate allocation supports the formation of microhabitats and thus enables niche differentiation in the complex root system of maize, as well as facilitating the development of the microbial food web. For simplicity, we here attempt to define **four microhabitats** (Chapter 3.5 Fig. 1) of the maize root system and discuss their microbial colonization in the following:

1. The root tips of fast-growing, young, shoot-borne roots with a high photosynthate level,
2. Root tips of older roots that are stagnating in growth, with a medium photosynthate level,
3. Root bases that have not yet developed lateral roots, with a lower photosynthate level,
4. Older root bases that have developed lateral roots, with the lowest photosynthate level.

We propose that microhabitats 1 and 2 are primarily colonized by microbial taxa with a metabolic preference for labile rhizodeposits that are fast-growing (Folman et al., 2001; Ho et al., 2017; Zelenev et al., 2005), and/or have the capabilities to attach to the growing root tip (Dupuy & Silk, 2016). This selection mechanism is demonstrated in our data by the reduced alpha diversity of prokaryotes and fungi and slightly increased bacterial and fungal copy numbers at photosynthate rich root tips as compared to root bases (Chapter 2.2 Fig. S7 b and c, S8), similar as seen in other research studies (DeAngelis et al., 2009; Rüger et al., 2023; Watt, Hugenholtz, et al., 2006). DNA-SIP analysis indeed demonstrated that specific taxa like *Paenibacillus*, *Fusarium* and *Trichoderma*

became particularly enriched and labeled at root tips with high photosynthate levels (Chapter 2.2 Fig. 5). At root tips, stochastic processes are thought to have a significant influence on community composition, as the root tip is initiating contact with the bulk soil, where chance determines which copiotrophic fast-growing colonizers are encountered and take advantage of readily available labile carbon. This leads to a higher degree of composition variation between individual root tips than between the root bases for the communities of prokaryotes, fungi and Cercozoa (Chapter 2.2 Fig. S5), (Rüger et al., 2021; Rüger et al., 2023), an observation that was even more pronounced for photosynthate consumers (Chapter 2.2 Fig. 4, Table 1).

In contrast, microhabitats 3 and 4 are characterized by a decline in fresh, labile rhizodeposits (Chapter 2.2 Fig. 3). The exudate profile at maize root tips has been reported to vary considerably from that at maize root bases (Tiziani et al., 2022). At the root base, a more complex mixture of carbon sources is encountered as shed root hairs degrade and older root areas undergo cell wall turnover for structural remodeling. This may attract more specialized consumers and cause a diversification in resource use. DNA-SIP analysis indeed demonstrated that most labeled Gammaproteobacteria (*Massilia*, *Burkholderia*) and Actinobacteria were enriched at root bases with a low photosynthate level (Chapter 2.2 Fig. 5). Dos Santos et al. found that maize lateral root emergence sites were hotspots of bacterial colonization (Figueiredo dos Santos et al., 2021), and metabolites released upon lateral root emergence have been reported to change local microbiome composition (Cotton et al., 2019; Park et al., 2004). In addition to a diversification of the rhizodeposit blend at root bases, biotic interactions like competition and predation also gain importance in microhabitats 3 and 4. Competition for labile carbon increases. Evidence for increased competition is demonstrated by the disappearance of fungal taxa from the co-occurrence network at root bases as compared to root tips (Chapter 2.2 Fig. 6). Also, prokaryotic and fungal population size slightly declined at root bases (Chapter 2.2 Fig. S8). Increased predation is illustrated by increased associations between bacteria and Glissomonadida at root bases, as seen in the network analysis (Chapter 2.2 Fig. 6) and by the presence of labeled bacterivore prokaryotic genera *Bdellovibrio* and *Vampirovibrio* in microhabitats 3 and 4 (Chapter 2.2 Fig. 5c, S11). The root base zone has already previously been reported to harbor more amoebae than the root tip (Bonkowski & Brandt, 2002), suggesting that it may be a prime region of nutrient remineralization by predators. Microbial succession from root tips to root bases is also a central process influencing community structure in microhabitats 3 and 4, as demonstrated in chapter 3.2. In agreement, Rüger et al. (2023) found that the absence of the root cap had a strong effect on the prokaryotic and cercozoan community composition, even on older root parts, which would also indicate priority effects and the influence of root tip colonizers on the establishment of the root base community.

Differences in the colonization between younger (microhabitat 1 and 3) and older roots (microhabitats 2 and 4) as well as different root types have been attributed to three potential mechanisms previously discussed in chapter 3.2.2. Heterogeneous photosynthate partitioning may account for a large part of the observed microbial patterns, by complementing, explaining and reinforcing these mechanisms. Microbiota succession between older and younger roots might be partially fueled by the reaction of the microbiome to a changing photosynthate supply as roots age. Our PET-MRI measurements showed that older root tips were supplied with less photosynthates than younger root tips (Chapter 2.2 Fig. 2, 3), which might influence the microbial community at tips as well as at more distal parts of the root (Rüger et al., 2023). Ho et al. (2017) suggests that copiotrophs are succeeded by oligotrophs as labile carbon substrates are depleted, which would mean that copiotrophs are slowly replaced by oligotrophs at older roots where carbon supply decreases. In our data, that might become apparent for some bacterial taxa like *Paenibacillus* that dominate the community at carbon rich root tips but not at root bases. However, other taxa like fungi belonging to the Lobulomycetales show less pronounced patterns (Chapter 2.2 Fig. S11, S12), suggesting an overlap of microhabitats, neutral processes such as dispersion or additional mechanisms influencing spatial colonization are at play (Chapter 3.6). Additionally, while the classification in copiotrophs and oligotrophs might be helpful to gain a rough overview of ecological processes, it certainly comes with limitations. The metabolic flexibility of many microorganisms (Nuccio et al., 2019) and their adaptation capacity to changing environments, which sometimes even occurs within their life cycle, complicates the assignment of lifestyles and thus the interpretation of substrate-based succession processes.

Functional differences between root types also entail differences in exudate blend (Cotton et al., 2019) that may have contributed to variation observed between microhabitats 1+3 and 2+4. These differences may already affect microbial community composition at the root tip (Chapter 2.2 Fig. 4, S5). Roots of different ages also differ in their lateral root status. All axial root types have the ability to form lateral roots (Yu et al., 2016), but in very young crown roots in our study (Cr3, Cr4), lateral roots had not yet formed at the time of destructive sampling. Although we removed the lateral roots before sampling, the emergence site of lateral roots is known as a site of root exudation and a microbial entrance point (Park et al., 2004; Ye et al., 2013), which is bound to affect the ambient microbial community before sampling.

Although we could define several taxa that did actively incorporate photosynthates and respond to photosynthate patterns (Chapter 2.2 Fig. 5); other taxa that were not identified as labeled showed corresponding colonization patterns in the rhizosphere (Chapter 2.2 Fig. S5, S6). On the one hand, this might be due to taxa that consumed and reacted to photosynthates prior to our $^{13}CO_2$ labeling

period. On the other hand, labeled taxa might exert indirect influences on the rest of the community, e.g. by competition for resources other than photosynthates like attachment sites on the root surface or water. This is supported by the central position of labeled taxa in the community networks (Chapter 2.2 Fig. 6). Labeled bacteria are prey to secondary consumers like protists, thereby affecting their community structure. Although labeled protist taxa were not confined to specific root regions (Chapter 2.2 Fig. 5c), their community composition and label intensity patterns roughly followed that of their bacterial prey (Chapter 2.2 Fig. 4, 5a, b).

All in all, the results discussed in sections 3.4 and 3.5 enabled us to **answer research question 3**: *To what extent do heterogeneous patterns in photosynthate distribution affect spatial variation in the rhizosphere microbiota and its photosynthate consumers?* → Our observations demonstrate that photosynthate heterogeneities play a key role in shaping the rhizosphere microbiome, driving the previously noted differences in colonization across root types and sections. Using DNA stable isotope probing, we identified prokaryotic, fungal, and cercozoan consumers of ^{13}C-labeled photosynthates, revealing that specific consumer taxa thrived in distinct regions based on localized photosynthate allocation. These findings indicate that photosynthate heterogeneities, along with root architectural traits, contribute to the formation of specialized microhabitats. Variability at root tips was linked to heterogeneous photosynthate allocation, coupled with stochastic colonization processes and the priority effects favoring copiotrophic taxa. In contrast, the microbial patterns observed at root bases of different root types and roots of varying ages turned out to be the result of successive developments of the microbiota as roots matured, also in response to changes in photosynthate distribution. These findings provide a conceptual framework for understanding spatiotemporal rhizosphere organization, suggesting a self-organizing system shaped by multiple interconnected factors.

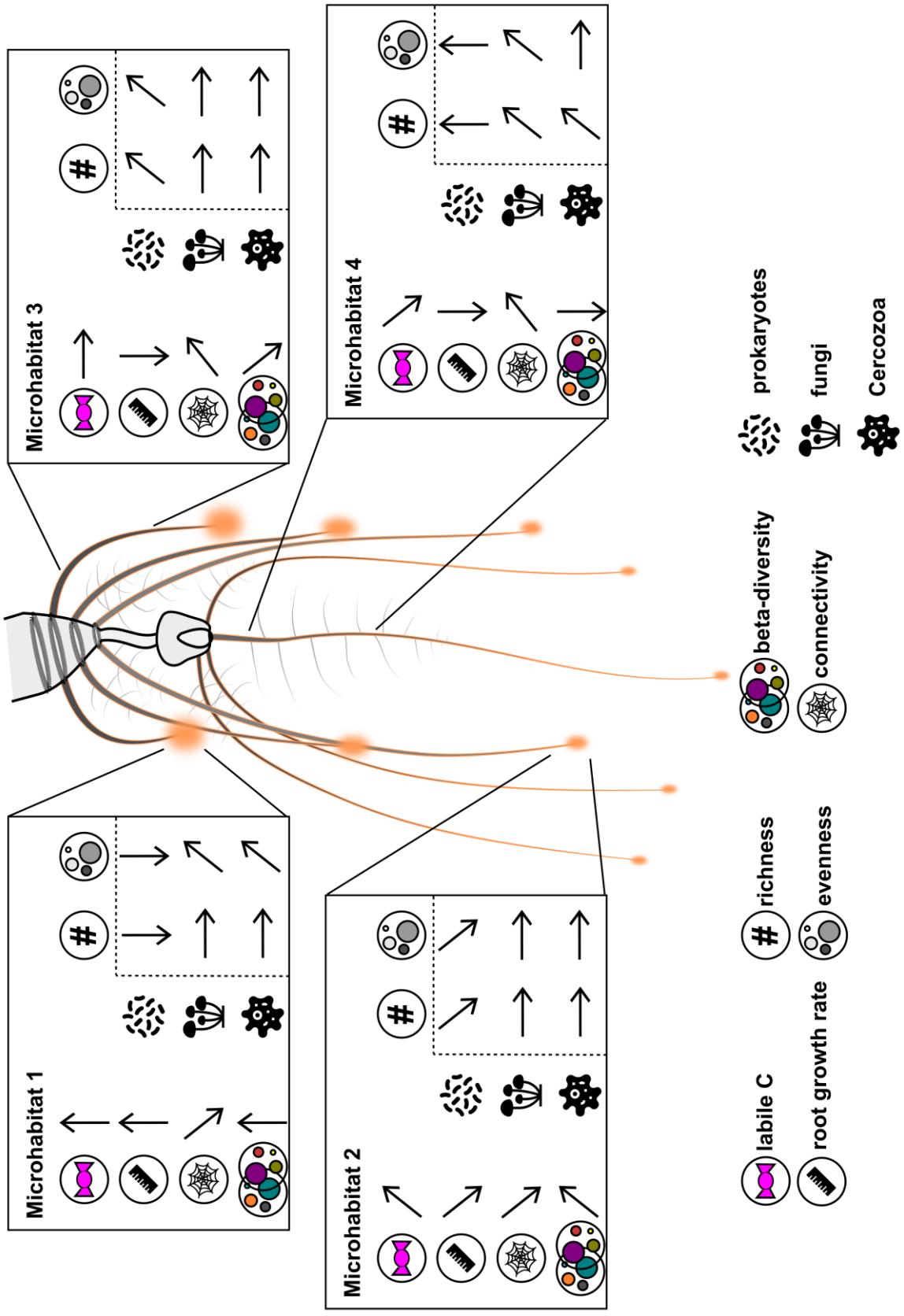

Fig. 1 Overview of study results. Conceptual illustration of photosynthate allocation as observed by PET and microbial colonization of the resulting microhabitats.

3.6. Additional factors contributing to microbial spatial variation

The rhizosphere, as a self-organized system, forms spatiotemporal patterns through numerous dynamic feedbacks among rhizosphere processes (Vetterlein et al., 2020). While this thesis primarily explores the role of photosynthate and root architecture in microbiome assembly, additional factors must be considered. Water availability and soil properties directly influence root development, rhizodeposition rates and thus also microbial colonization. Here, we discuss how their interaction with rhizodeposition creates spatial heterogeneity in the rhizosphere and contributes to the reproducible microbial colonization patterns observed in the maize root system.

Gradients in water availability are an important factor causing spatial heterogeneity in the rhizosphere, as almost all water and nutrients utilized by the plant pass through the rhizosphere, and roots take up water unevenly. Generally, lateral roots contribute most to plant water uptake in maize (Ahmed et al., 2016) and their branching capacity allows them to grow towards wetter areas of the soil (hydrotropism). When axial root types are compared, shoot-borne crown roots generally take up more water than seed-borne roots in maize (Ahmed et al., 2018) and barley (Schneider et al., 2020). This is attributed to their direct connection to the shoot, which favors xylem tension and thus water uptake (Ahmed et al., 2018). These differences in water uptake capability might have contributed to the variation in microbial community composition between seed-borne and shoot-borne roots (Chapter 2.2 Fig. S5, S12). Water availability is closely associated with rhizodeposition. In their ^{14}C labeling study, Zhang et al. (2023) found higher exudation levels under optimum water content than under drought. Also, enzymatic hotspots of microbial activity were more colocalized with root exudate hotspots under optimal moisture, while they showed higher colocalization with water hotspots under drought (Zhang et al., 2023). Tiziani et al. (2022) found that maize roots increasingly exuded citramalic acid, malonic acid, and 4-hydroxycoumarin under drought and heat stress. At root tips, mucilage is reported to help retain water in the rhizosphere and make it hydraulically well conductive, facilitating water flow from dry bulk soil towards the root (Ahmed et al., 2014). This would make the root tips an environment with both high moisture and high photosynthate availability, which might even amplify the high bacterial colonization observed at root tips (Chapter 2.2 Fig. S8), especially under drought. Water availability was shown to be the main determinant of rhizosphere extent, rather than root exudates (Zhang et al., 2023). In line, water availability was reported to significantly influence the diffusion of root exudates through the soil and their microbial decomposition (Holz et al., 2018), which might reinforce microbial spatial patterns in the rhizosphere. This highlights the central position of water availability in influencing spatial microbial colonization in the rhizosphere.

Water availability does also interact with soil parameters. Fine-textured soils, like clay, retain more water, while sandy soils drain quickly; affecting the mobility of microorganisms that often depend on water films for their movement (Hinsinger et al., 2009). This moisture continuity in fine-textured soils enables microorganisms to move more easily, while sandy soils have larger, more disconnected pores, which tend to dry out quickly and make it more difficult for microorganisms to unlock new root areas. Soil-dependent differences in water retention might buffer root-induced heterogeneity in community composition in the case of fine-textured soils, or enhance it in case of sandy soils. Indeed, we found that the effect of root growth rate on bacterial Shannon diversity was insignificant in loam, while the bacterial diversity was strongly reduced around fast-growing roots in sandy soils (Chapter 2.1 Fig. 4), even though the root growth rates at the timepoint of destructive sample collection did not differ between the sandy and loamy substrates (Chapter 2.1 Fig. 2c). Although not investigated in this thesis, there are indications that protists, and thus predator-prey relationships, are similarly affected by soil porosity and water availability (Stefan et al., 2014). As many protists cannot enter smaller pore spaces, we would expect a lowered network connectivity in loamy as compared to sandy soils. In contrast, soil textures might only have a mitigated effect on hyphal fungi due to their ability to quickly bridge spaces with their hyphal system. Indeed, we observed that spatial patterns in both fungal alpha and beta diversity in the rhizosphere were less pronounced than that of bacteria (Chapter 2.2 Fig. S5, S7a – S7c, Table 1). This would be in line with results by Bourceret et al. (2022) who found that the maize fungal community was less responsive to root metabolite changes than the bacterial community. Hence, to fully grasp the complexity of rhizosphere spatiotemporal organization, our findings on the impact of photosynthate distribution will have to be integrated with measurements of water availability as well as soil traits like porosity. The non-invasive measurement of root water uptake along with root system architecture would be possible using MRI scans (Müllers et al., 2022; van Dusschoten et al., 2020).

3.7. Practical relevance for plant breeding, microbiome engineering and modeling

Our results contribute to the understanding of the association between maize root system architecture and rhizodeposition, which might aid decisions in plant breeding. Spatial root system traits have long been overlooked in breeding programs due to the challenges of non-destructive phenotyping. However, they are now receiving increased attention with the availability of advanced non-invasive imaging technologies such as MRI. In recent years, the root system of maize is increasingly considered a promising breeding target, as its functional complexity enables breeding for efficient water and nutrient uptake, as well as for stability and abiotic stress tolerance

(Hochholdinger et al., 2024). In maize, different root phenotypes have been proposed, e.g. the “steep – cheap – deep” concept for optimizing nitrogen and water uptake (Lynch, 2013) or the notion that root cortical aerenchyma might increase maize growth by up to 70% under phosphorus deficiency (Postma & Lynch, 2011). Optimizing photosynthate allocation patterns might also be useful during breeding efforts, as they determine resource utilization and the metabolic cost of soil exploration. Breeding for increased rhizodeposition could, although with a considerable cost for yield, enhance belowground soil organic carbon storage and aid in the mitigation of climate change. Calculations suggest that a 0.4 % increase in soil organic carbon stocks in the top 1 m of global agricultural soil could possibly compensate for 20–35% of global CO_2 emissions (Minasny et al., 2017).

A better understanding of microbial colonization processes in the rhizosphere of the complex maize root system is key in paving the way towards microbiome engineering for improved plant health. Although microbiome engineering is still in its infancy, three approaches can roughly be distinguished: firstly, the manipulation of the already existent microbiome by adapting management strategies (e.g. reduced tillage), secondly, the direct inoculation with beneficial microbial strains or even synthetic consortia and lastly, the steering of microbiome establishment by choosing specific host plants (e.g. genetically engineered to attract beneficial taxa) (Bano et al., 2021). Here, our approach can help to identify potentially beneficial taxa that directly interact with the plant host by consuming rhizodeposits. Stable isotope labeling might also help to determine whether inoculation with beneficials actually leads to an improved plant nutrient acquisition (Giller et al., 2024). Also, identifying the preferential habitat of beneficial taxa within a complex root system might help to determine their competitiveness in interactions with other microorganisms and aid their establishment in different soil types.

Through the combination of different isotopic (imaging) and molecular techniques, our work also highlights the added value of combined methods for modeling spatiotemporal aspects of rhizodeposition and microbial colonization in the rhizosphere. Functional-structural root and rhizosphere models assist in forecasting plant responses to abiotic stress and agricultural practices. However, attempts to model interconnected processes like root growth, rhizodeposition, microbial colonization and water/nutrient uptake in root systems are often impeded by the quality of experimental studies. Model parameterizations need to be validated with experimental data, but many experimental rhizosphere studies are conducted in a low spatial resolution and results are often not comparable between studies. Schnepf et al. (2022) highlights that the missing link between processes within roots and their effect in the rhizosphere currently hampers the modeling of processes like root exudation. Here, our study and potential follow-up studies might be able to provide some insights, as we linked root-internal to root external photosynthate levels and related

them to rhizosphere community dynamics. Generally, holistic experimental designs featuring not only a high spatiotemporal resolution based on root functions but also combinatory measurements of multiple parameters from the same plants might be a valuable contribution to future modeling approaches. Other authors emphasize the need for combinatorial approaches, especially non-invasive imaging technology, to unravel plant rhizosphere processes and capture their spatiotemporal complexity (Oburger & Schmidt, 2016; Vetterlein et al., 2020).

3.8. Conclusion

The research presented in this thesis demonstrates that root photosynthate allocation in the maize root system and its rhizosphere is highly heterogeneous between root types, along the root longitudinal axis, and in time. We reveal that this heterogeneity fuels spatial assembly patterns of the rhizosphere microbiome by driving microhabitat formation and thus niche differentiation, and contributing to microbial food web establishment. Thus, this research establishes the first direct link between spatial heterogeneity in rhizodeposition and the assembly of the rhizosphere microbiome. Our findings on root type-dependent photosynthate partitioning and microbiome assembly add another layer of complexity to but also improve our understanding of the spatiotemporal organization of the rhizosphere. This advanced understanding could aid future efforts to model rhizodeposition and rhizosphere microbial colonization, as well as guide strategies to manipulate the rhizosphere microbiome for enhanced crop yield and resilience.

4. Appendix

4.1. Curriculum vitae

Personal data

Name	Sina Rosemarie Schultes
Date of birth	[redacted]1995
Location of birth	[redacted]

Education and experience

04/2023 – present	**Agricultural Scientist** at AgPrime GmbH
02/2019 – 10/2025	**PhD Candidate** Molecular Biology of the Rhizosphere at University of Bonn and Enabling Technologies at Jülich Research Centre
2016 – 2018	**MSc Plant Biotechnology** (specialization phytopathology) at Wageningen University & Research **MSc thesis** at Tropical Phytopathology: Fusarium Wilt of banana **Industry internship** at Bayer CropScience: Black Sigatoka of banana
2013 – 2016	**BSc Biology** at Radboud University Nijmegen

Conference activities

Best talk award at miCROPe – Microbe-Assisted Crop Production conference, Vienna, 2022

Talk at International Conference of the German Society for Plant Sciences, Bonn, 2022

Talk at Plant Biology Europe, Turin, 2021

Poster at DGHM & VAAM Conference, Leipzig, 2020

Poster at Rhizosphere 5 Conference, Saskatoon (CA), 2019

4.2. Danksagung

Zunächst gilt mein herzlicher Dank Claudia Knief, die mir die Möglichkeit zur Promotion gegeben hat. Auch als wegen kaputter Refraktometer und nicht lieferbarem CsTFA / $^{13}CO_2$ nichts mehr zu laufen schien, konnte ich immer zu dir kommen. Robert Koller möchte ich für seine Betreuung am FZ Jülich danken, mit deiner begeisterten Art konntest du bisher jedes Meeting auflockern.

Mein besonderer Dank gilt Katharina Frindte für ihre zahlreichen Ratschläge, ihre langjährige Expertise und Unterstützung bei der Laborarbeit. Besonders gegen Ende dieser Thesis hast du mich immer wieder motiviert, weiterzumachen. Kein „Experimentator“ kann dich je ersetzen. Ohne meinen Kollegen Max Becker wären mir viele Aspekte der Bioinformatik völlig verschlossen geblieben. Danke für all deine investierte Zeit, die „24h Hilfshotline“ und vor allem deine Geduld. Bei meiner Kollegin Janina Zierul möchte ich mich besonders für ihre Fähigkeit, mich an langen Labortagen zu Ertragen und ihre Hilfsbereitschaft bedanken. Marius Röder und Merle Noschinski-Reetz möchte ich besonders für ihre tatkräftige Unterstützung bei der Laborarbeit danken.

Michael Bonkowski, Lioba Rüger, Daniela Niedeggen und Jule Freudenthal: Ihr habt viel Zeit investiert, um diese Arbeit noch um Analysen der Cercozoa zu ergänzen - danke für die großartige Zusammenarbeit. Vielen Dank auch an Michael für die Übernahme der Position des Zweitprüfers. An nächster Stelle bedanke ich mich herzlich bei Andrea Schnepf und Wulf Amelung für die Übernahme der Positionen der mündlichen Prüferin und des Vorsitzenden in meiner Prüfungskommission.

Mein herzlicher Dank gilt auch Antonia Chlubek, Carsten Hinz, Ralf Metzner, Daniel Pflugfelder, Dagmar von Dusschoten, Esther Breuer und Marco Dautzenberg für ihre Unterstützung während der Experimente am FZ Jülich. Danke für euren unermüdlichen Einsatz während der Durchführung der Messungen. Auch bei den Mitarbeitern der Bonner Bodenkunde, Sara Bauke und Kirsten Unger möchte ich mich herzlich für ihre Unterstützung bei den IRMS Messungen bedanken.

Bei Caspar Langenbach möchte ich mich dafür bedanken, dass ich vorrübergehend meine Arbeitszeit reduzieren konnte, um diese Dissertation fertig zu stellen.

Meinen talentierten Studentinnen Juliane Zaunick und Lika Kudrjasova möchte ich herzlich für die Bearbeitung zahlreicher Proben danken. Zudem möchte ich Lisa Koszak fürs Munter Machen danken.

Zu guter Letzt möchte ich der wichtigsten Person in meinem Leben danken. Jan Weinkaemmerer, ohne dich, deinen Zuspruch und dein regelmäßiges Wieder-Aufbauen hätte ich es nie geschafft ❤️.

Bibliography

Abarenkov, K., Nilsson, R. H., Larsson, K.-H., Taylor, A. F., May, T. W., Frøslev, T. G., Pawlowska, J., Lindahl, B., Põldmaa, K., & Truong, C. (2024). The UNITE database for molecular identification and taxonomic communication of fungi and other eukaryotes: sequences, taxa and classifications reconsidered. *Nucleic acids research*, *52*(D1), D791-D797.

Adedayo, A. A., & Babalola, O. O. (2023). Fungi that promote plant growth in the rhizosphere boost crop growth. *Journal of Fungi*, *9*(2), 239.

Afzal, M. Y., Das, B. K., Valappil, V. T., Scaria, J., & Brözel, V. S. (2024). Root exudate compounds change the bacterial community in bulk soil. *Rhizosphere*, *30*, 100885.

Ahmad, M., Hussain, A., Dar, A., Luqman, M., Ditta, A., Iqbal, Z., Ahmad, H. T., Nazli, F., Soufan, W., & Almutairi, K. (2023). Combating iron and zinc malnutrition through mineral biofortification in maize through plant growth promoting Bacillus and Paenibacillus species. *Frontiers in plant science*, *13*, 1094551.

Ahmed, M. A., Kroener, E., Holz, M., Zarebanadkouki, M., & Carminati, A. (2014). Mucilage exudation facilitates root water uptake in dry soils. *Functional Plant Biology*, *41*(11), 1129-1137.

Ahmed, M. A., Zarebanadkouki, M., Kaestner, A., & Carminati, A. (2016). Measurements of water uptake of maize roots: the key function of lateral roots. *Plant and Soil*, *398*, 59-77.

Ahmed, M. A., Zarebanadkouki, M., Meunier, F., Javaux, M., Kaestner, A., & Carminati, A. (2018). Root type matters: measurement of water uptake by seminal, crown, and lateral roots in maize. *Journal of Experimental Botany*, *69*(5), 1199-1206.

Asiloglu, R., Bodur, S. O., Samuel, S. O., Aycan, M., Murase, J., & Harada, N. (2024). Trophic modulation of endophytes by rhizosphere protists. *The ISME journal*, *18*(1), wrae235.

Assenov, Y., Ramírez, F., Schelhorn, S.-E., Lengauer, T., & Albrecht, M. (2008). Computing topological parameters of biological networks. *Bioinformatics*, *24*(2), 282-284.

Atkinson, J. A., Pound, M. P., Bennett, M. J., & Wells, D. M. (2019). Uncovering the hidden half of plants using new advances in root phenotyping. *Current opinion in biotechnology*, *55*, 1-8.

Aulakh, M., Wassmann, R., Bueno, C., Kreuzwieser, J., & Rennenberg, H. (2001). Characterization of root exudates at different growth stages of ten rice (Oryza sativa L.) cultivars. *Plant biology*, *3*(02), 139-148.

Badri, D. V., & Vivanco, J. M. (2009). Regulation and function of root exudates. *Plant, Cell & Environment*, *32*(6), 666-681.

Bag, S., Mondal, A., Majumder, A., Mondal, S. K., & Banik, A. (2022). Flavonoid mediated selective cross-talk between plants and beneficial soil microbiome. *Phytochemistry Reviews*, *21*(5), 1739-1760.

Bano, S., Wu, X., & Zhang, X. (2021). Towards sustainable agriculture: rhizosphere microbiome engineering. *Applied Microbiology and Biotechnology*, 1-20.

Becker, M. F., Hellmann, M., & Knief, C. (2022). Spatio-temporal variation in the root-associated microbiota of orchard-grown apple trees. *Environmental microbiome*, *17*(1), 1-21.

Beirinckx, S., Viaene, T., Haegeman, A., Debode, J., Amery, F., Vandenabeele, S., Nelissen, H., Inzé, D., Tito, R., & Raes, J. (2020). Tapping into the maize root microbiome to identify bacteria that promote growth under chilling conditions. *Microbiome*, *8*, 1-13.

Berg, G., & Smalla, K. (2009). Plant species and soil type cooperatively shape the structure and function of microbial communities in the rhizosphere. *FEMS microbiology ecology*, *68*(1), 1-13.

Biesgen, D., Frindte, K., Maarastawi, S., & Knief, C. (2020). Clay content modulates differences in bacterial community structure in soil aggregates of different size. *Geoderma*, *376*, 114544.

Blacutt, A. A., Gold, S. E., Voss, K. A., Gao, M., & Glenn, A. E. (2018). Fusarium verticillioides: Advancements in understanding the toxicity, virulence, and niche adaptations of a model mycotoxigenic pathogen of maize. *Phytopathology*, *108*(3), 312-326.

Blagodatskaya, E., Yuyukina, T., Blagodatsky, S., & Kuzyakov, Y. (2011). Turnover of soil organic matter and of microbial biomass under C3–C4 vegetation change: consideration of 13C fractionation and preferential substrate utilization. *Soil Biology and Biochemistry*, *43*(1), 159-166.

Bolyen, E., Rideout, J. R., Dillon, M. R., Bokulich, N. A., Abnet, C. C., Al-Ghalith, G. A., Alexander, H., Alm, E. J., Arumugam, M., & Asnicar, F. (2019). Reproducible, interactive, scalable and extensible microbiome data science using QIIME 2. *Nature biotechnolgy*, *37*(8), 852-857.

Bonkowski, M. (2004). Protozoa and plant growth: the microbial loop in soil revisited. *New Phytol*, *162*(3), 617-631.

Bonkowski, M., & Brandt, F. (2002). Do soil protozoa enhance plant growth by hormonal effects? *Soil Biology and Biochemistry*, *34*(11), 1709-1715.

Bonkowski, M., Tarkka, M., Razavi, B. S., Schmidt, H., Blagodatskaya, E., Koller, R., Yu, P., Knief, C., Hochholdinger, F., & Vetterlein, D. (2021). Spatiotemporal Dynamics of Maize (*Zea mays* L.) Root Growth and Its Potential Consequences for the Assembly of the Rhizosphere Microbiota. *Frontiers in microbiology*, *12*, 461.

Bosshard, P. P., Zbinden, R., & Altwegg, M. (2002). Paenibacillus turicensis sp. nov., a novel bacterium harbouring heterogeneities between 16S rRNA genes. *International journal of systematic and evolutionary microbiology*, *52*(6), 2241-2249.

Bourceret, A., Guan, R., Dorau, K., Mansfeldt, T., Omidbakhshfard, A., Medeiros, D. B., Fernie, A. R., Hofmann, J., Sonnewald, U., & Mayer, J. (2022). Maize field study reveals covaried microbiota and metabolic changes in roots over plant growth. *MBio*, *13*(2), e02584-02521.

Brown, S. P., Grillo, M. A., Podowski, J. C., & Heath, K. D. (2020). Soil origin and plant genotype structure distinct microbiome compartments in the model legume Medicago truncatula. *Microbiome*, *8*(1), 1-17.

Bulgarelli, D., Schlaeppi, K., Spaepen, S., Van Themaat, E. V. L., & Schulze-Lefert, P. (2013). Structure and functions of the bacterial microbiota of plants. *Annual review of plant biology*, *64*(1), 807-838.

Callahan, B. J., McMurdie, P. J., Rosen, M. J., Han, A. W., Johnson, A. J. A., & Holmes, S. P. (2016). DADA2: high-resolution sample inference from Illumina amplicon data. *Nature methods*, *13*(7), 581.

Camacho, C., Coulouris, G., Avagyan, V., Ma, N., Papadopoulos, J., Bealer, K., & Madden, T. L. (2009). BLAST+: architecture and applications. *BMC bioinformatics*, *10*, 1-9.

Canarini, A., Kaiser, C., Merchant, A., Richter, A., & Wanek, W. (2019). Root exudation of primary metabolites: mechanisms and their roles in plant responses to environmental stimuli. *Frontiers in plant science*, *10*, 157.

Caporaso, J. G., Lauber, C. L., Walters, W. A., Berg-Lyons, D., Lozupone, C. A., Turnbaugh, P. J., Fierer, N., & Knight, R. (2011). Global patterns of 16S rRNA diversity at a depth of millions of sequences per sample. *PNAS*, *108*, 4516-4522.

Carson, J. K., Gonzalez-Quiñones, V., Murphy, D. V., Hinz, C., Shaw, J. A., & Gleeson, D. B. (2010). Low pore connectivity increases bacterial diversity in soil. *Applied and Environmental Microbiology*, *76*(12), 3936-3942.

Cavaglieri, L., Orlando, J., & Etcheverry, M. (2009). Rhizosphere microbial community structure at different maize plant growth stages and root locations. *Microbiological research*, *164*(4), 391-399.

Ceolin, S., Schymanski, S. J., van Dusschoten, D., Koller, R., & Klaus, J. (2024). Root growth dynamics and allocation as a response to rapid and local changes in soil moisture. *EGUsphere*, *2024*, 1-23.

Chaparro, J. M., Badri, D. V., & Vivanco, J. M. (2014). Rhizosphere microbiome assemblage is affected by plant development. *The ISME journal*, *8*(4), 790-803.

Chau, J. F., Bagtzoglou, A. C., & Willig, M. R. (2011). The effect of soil texture on richness and diversity of bacterial communities. *Environmental Forensics*, *12*(4), 333-341.

Chen, J., Wang, Z., Tan, K., Huang, W., Shi, J., Li, T., Hu, J., Wang, K., Wang, C., & Xin, B. (2023). A complete telomere-to-telomere assembly of the maize genome. *Nature Genetics*, *55*(7), 1221-1231.

Cooper, J. E. (2004). Multiple responses of rhizobia to flavonoids during legume root infection. In *Advances in botanical research* (Vol. 41, pp. 1-62). Elsevier.

Cotton, T. A., Pétriacq, P., Cameron, D. D., Al Meselmani, M., Schwarzenbacher, R., Rolfe, S. A., & Ton, J. (2019). Metabolic regulation of the maize rhizobiome by benzoxazinoids. *The ISME journal*, *13*(7), 1647-1658.

Darwent, M. J., Paterson, E., McDonald, A. J. S., & Tomos, A. D. (2003). Biosensor reporting of root exudation from *Hordeum vulgare* in relation to shoot nitrate concentration. *Jorunal of Experimental Botany*, *54*(381), 325-334.

De Moraes, M. T., Debiasi, H., Franchini, J. C., Bonetti, J. d. A., Levien, R., Schnepf, A., & Leitner, D. (2019). Mechanical and hydric stress effects on maize root system development at different soil compaction levels. *Frontiers in plant science*, *10*, 1358.

DeAngelis, K. M., Brodie, E. L., DeSantis, T. Z., Andersen, G. L., Lindow, S. E., & Firestone, M. K. (2009). Selective progressive response of soil microbial community to wild oat roots. *The ISME journal*, *3*(2), 168-178.

Delgado-Baquerizo, M., Oliverio, A. M., Brewer, T. E., Benavent-González, A., Eldridge, D. J., Bardgett, R. D., Maestre, F. T., Singh, B. K., & Fierer, N. (2018). A global atlas of the dominant bacteria found in soil. *Science*, *359*(6373), 320-325.

Dennis, P. G., Miller, A. J., & Hirsch, P. R. (2010). Are root exudates more important than other sources of rhizodeposits in structuring rhizosphere bacterial communities? *FEMS Microbiolgy Ecology*, *72*(3), 313-327.

Dixon, P. (2003). VEGAN, a package of R functions for community ecology. *Journal of Vegetation Science*, *14*(6), 927-930.

Doan, T. H., Doan, T. A., Kangas, M. J., Ernest, A. E., Tran, D., Wilson, C. L., Holmes, A. E., Doyle, E. L., & Durham Brooks, T. L. (2017). A low-cost imaging method for the temporal and spatial colorimetric detection of free amines on maize root surfaces. *Frontiers in plant science*, *8*, 1513.

Drigo, B., Pijl, A. S., Duyts, H., Kielak, A. M., Gamper, H. A., Houtekamer, M. J., Boschker, H. T., Bodelier, P. L., Whiteley, A. S., & Van Veen, J. A. (2010). Shifting carbon flow from roots into associated microbial communities in response to elevated atmospheric CO2. *Proc. Natl. Acad. Sci. U.S.A*, *107*(24), 10938-10942.

Dumack, K., & Bonkowski, M. (2021). Protists in the plant microbiome: an untapped field of research. *The Plant Microbiome: Methods and Protocols*, 77-84.

Dumack, K., Fiore-Donno, A. M., Bass, D., & Bonkowski, M. (2020). Making sense of environmental sequencing data: ecologically important functional traits of the protistan groups Cercozoa and Endomyxa (Rhizaria). *Molecular ecology resources*, *20*(2), 398-403.

Dunford, E. A., & Neufeld, J. D. (2010). DNA stable-isotope probing (DNA-SIP). *Journal of visualized experiments: JoVE*(42).

Dupuy, L. X., & Silk, W. K. (2016). Mechanisms of early microbial establishment on growing root surfaces. *Vadose Zone Journal*, *15*(2).

Edgar, R. C., Haas, B. J., Clemente, J. C., Quince, C., & Knight, R. (2011). UCHIME improves sensitivity and speed of chimera detection. *Bioinformatics*, *27*(16), 2194-2200.

Edwards, J., Johnson, C., Santos-Medellín, C., Lurie, E., Podishetty, N. K., Bhatnagar, S., Eisen, J. A., & Sundaresan, V. (2015). Structure, variation, and assembly of the root-associated microbiomes of rice. *Proceedings of the National Academy of Sciences*, *112*(8), E911-E920.

el Zahar Haichar, F., Marol, C., Berge, O., Rangel-Castro, J. I., Prosser, J. I., Balesdent, J. m., Heulin, T., & Achouak, W. (2008). Plant host habitat and root exudates shape soil bacterial community structure. *The ISME journal*, *2*(12), 1221.

Enns, L. C., McCully, M. E., & Canny, M. J. (2006). Branch roots of young maize seedlings, their production, growth, and phloem supply from the primary root. *Functional Plant Biology*, *33*(4), 391-399.

Farrar, J., Hawes, M., Jones, D., & Lindow, S. (2003). How roots control the flux of carbon to the rhizosphere. *Ecology*, *84*(4), 827-837.

Fierer, N. (2017). Embracing the unknown: disentangling the complexities of the soil microbiome. *Nature Reviews Microbiology*, *15*(10), 579-590.

Figueiredo dos Santos, L., Fernandes Souta, J., de Paula Soares, C., Oliveira da Rocha, L., Luiza Carvalho Santos, M., Grativol, C., Fernando Wurdig Roesch, L., & Lopes Olivares, F. (2021). Insights into the structure and role of seed-borne bacteriome during maize germination. *FEMS microbiology ecology*, *97*(4), fiab024.

Fiore-Donno, A. M., Richter-Heitmann, T., & Bonkowski, M. (2020). Contrasting responses of protistan plant parasites and phagotrophs to ecosystems, land management and soil properties. *Frontiers in microbiology*, *11*, 1823.

Fiore-Donno, A. M., Richter-Heitmann, T., Degrune, F., Dumack, K., Regan, K. M., Marhan, S., Boeddinghaus, R. S., Rillig, M. C., Friedrich, M. W., & Kandeler, E. (2019). Functional traits and spatio-temporal structure of a major group of soil protists (Rhizaria: Cercozoa) in a temperate grassland. *Frontiers in microbiology*, *10*, 1332.

Fischer, H., Eckhardt, K. U., Meyer, A., Neumann, G., Leinweber, P., Fischer, K., & Kuzyakov, Y. (2010). Rhizodeposition of maize: Short-term carbon budget and composition. *Journal of plant nutrition and soil science*, *173*(1), 67-79.

Flues, S., Bass, D., & Bonkowski, M. (2017). Grazing of leaf-associated Cercomonads (Protists: Rhizaria: Cercozoa) structures bacterial community composition and function. *Environmental microbiology*, *19*(8), 3297-3309.

Folman, L. B., Postma, J., & Veen, J. v. (2001). Ecophysiological characterization of rhizosphere bacterial communities at different root locations and plant developmental stages of cucumber grown on rockwool. *Microbial Ecology*, *42*, 586-597.

Frindte, K., Lehndorff, E., Vlaminck, S., Werner, K., Kehl, M., Khormali, F., & Knief, C. (2020). Evidence for signatures of ancient microbial life in paleosols. *Scientific Reports*, *10*(1), 1-11.

Frindte, K., Pape, R., Werner, K., Löffler, J., & Knief, C. (2019). Temperature and soil moisture control microbial community composition in an arctic–alpine ecosystem along elevational and micro-topographic gradients. *ISME J*, *13*(8), 2031-2043.

Gamalei, Y. V. (2002). Assimilate transport and partitioning in plants: approaches, methods, and facets of research. *Russian Journal of Plant Physiology*, *49*, 16-31.

Ganther, M., Vetterlein, D., Heintz-Buschart, A., & Tarkka, M. T. (2021). Transcriptome sequencing analysis of maize roots reveals the effects of substrate and root hair formation in a spatial context. *Plant and Soil*, 1-18.

Gao, Y., Yang, Y., Ling, W., Kong, H., & Zhu, X. (2011). Gradient distribution of root exudates and polycyclic aromatic hydrocarbons in rhizosphere soil. *Soil Science Society of America Journal*, *75*(5), 1694-1703.

Gao, Z., Karlsson, I., Geisen, S., Kowalchuk, G., & Jousset, A. (2018). Protists: Puppet Masters of the Rhizosphere Microbiome. *Trends Plant Sci*.

Gardes, M., & Bruns, T. D. (1993). ITS primers with enhanced specificity for basidiomycetes-application to the identification of mycorrhizae and rusts. *Molecular ecology*, *2*(2), 113-118.

Gebauer, L., Bouffaud, M.-L., Ganther, M., Yim, B., Vetterlein, D., Smalla, K., Buscot, F., Heintz-Buschart, A., & Tarkka, M. T. (2021). Soil texture, sampling depth and root hairs shape the structure of ACC deaminase bacterial community composition in maize rhizosphere. *Frontiers in microbiology*, *12*, 616828.

Giller, K. E., James, E. K., Ardley, J., & Unkovich, M. J. (2024). Science losing its way: examples from the realm of microbial N2-fixation in cereals and other non-legumes. *Plant and Soil*, 1-24.

Glücksman, E., Bell, T., Griffiths, R. I., & Bass, D. (2010). Closely related protist strains have different grazing impacts on natural bacterial communities. *Environmental microbiology*, *12*(12), 3105-3113.

Griffiths, B. S., Christensen, S., & Bonkowski, M. (2007). Microfaunal interactions in the rhizosphere, how nematodes and protozoa link above-and belowground processes. In Z. G. Cardon & J. L. Whitbeck (Eds.), *The Rhizosphere - An Ecological Perspective* (pp. 57-71). Elsevier.

Guillou, L., Bachar, D., Audic, S., Bass, D., Berney, C., Bittner, L., Boutte, C., Burgaud, G., de Vargas, C., & Decelle, J. (2012). The Protist Ribosomal Reference database (PR2): a catalog of unicellular eukaryote small sub-unit rRNA sequences with curated taxonomy. *Nucleic acids research*, *41*(D1), D597-D604.

Guo, J., Ling, N., Li, Y., Li, K., Ning, H., Shen, Q., Guo, S., & Vandenkoornhuyse, P. (2021). Seed-borne, endospheric and rhizospheric core microbiota as predictors of plant functional traits across rice cultivars are dominated by deterministic processes. *New Phytologist*, *230*(5), 2047-2060.

Hafner, S., Wiesenberg, G. L., Stolnikova, E., Merz, K., & Kuzyakov, Y. (2014). Spatial distribution and turnover of root-derived carbon in alfalfa rhizosphere depending on top-and subsoil properties and mycorrhization. *Plant and Soil*, *380*, 101-115.

Haichar, F. e. Z., Roncato, M.-A., & Achouak, W. (2012). Stable isotope probing of bacterial community structure and gene expression in the rhizosphere of Arabidopsis thaliana. *FEMS microbiology ecology*, *81*(2), 291-302.

Hamasaki, Y., Watanabe, Y., Kotoura, S., Fuchu, H., Sugiyama, M., Hashizume, K., & Morita, H. (2005). Paenibacillus macerans possesses two types of 16S rDNA copies in a genome with a length difference of twelve base pairs. *Bioscience, biotechnology, and biochemistry*, *69*(10), 1995-1998.

Hannula, S., Morrien, E., Van der Putten, W., & De Boer, W. (2020). Rhizosphere fungi actively assimilating plant-derived carbon in a grassland soil. *Fungal Ecology*, *48*, 100988.

Hannula, S. E., Morriën, E., de Hollander, M., Van Der Putten, W. H., van Veen, J. A., & De Boer, W. (2017). Shifts in rhizosphere fungal community during secondary succession following abandonment from agriculture. *The ISME journal*, *11*(10), 2294-2304.

Hartmann, A., Schmid, M., Tuinen, D. v., & Berg, G. (2009). Plant-driven selection of microbes. In: Springer.

Hartmann, M., & Six, J. (2023). Soil structure and microbiome functions in agroecosystems. *Nature Reviews Earth & Environment*, *4*(1), 4-18.

He, P., Sun, A., Jiao, X., Ren, P., Li, F., Wu, B., He, J. Z., & Hu, H. W. (2024). National-scale distribution of protists associated with sorghum leaves and roots. *Environmental microbiology reports*, *16*(5), e70024.

Hemkemeyer, M., Dohrmann, A. B., Christensen, B. T., & Tebbe, C. C. (2018). Bacterial preferences for specific soil particle size fractions revealed by community analyses. *Frontiers in microbiology*, *9*, 149.

Heyer, J., Galchenko, V. F., & Dunfield, P. F. (2002). Molecular phylogeny of type II methane-oxidizing bacteria isolated from various environments. *Microbiology*, *148*(9), 2831-2846.

Hinsinger, P., Bengough, A. G., Vetterlein, D., & Young, I. M. (2009). Rhizosphere: biophysics, biogeochemistry and ecological relevance. In: Springer.

Hinz, C., Jahnke, S., Metzner, R., Pflugfelder, D., Scheins, J., Streun, M., & Koller, R. (2024). Setup and characterisation according to NEMA NU 4 of the phenoPET scanner, a PET system dedicated for plant sciences. *Physics in Medicine & Biology*, *69*(5), 055019.

Ho, A., Di Lonardo, D. P., & Bodelier, P. L. J. F. m. e. (2017). Revisiting life strategy concepts in environmental microbial ecology. *93*(3), fix006.

Hochholdinger, F., Park, W. J., Sauer, M., & Woll, K. (2004). From weeds to crops: genetic analysis of root development in cereals. *Trends in plant science*, *9*(1), 42-48.

Hochholdinger, F., & Tuberosa, R. (2009). Genetic and genomic dissection of maize root development and architecture. *Curr. Opin. Plant Biol*, *12*(2), 172-177.

Hochholdinger, F., Woll, K., Sauer, M., & Dembinsky, D. (2004). Genetic dissection of root formation in maize (Zea mays) reveals root-type specific developmental programmes. *Annals of botany*, *93*(4), 359-368.

Hochholdinger, F., Yu, P., & Feix, G. (2024). 11 Genetic Analysis of Maize. *Plant roots: The hidden half*, 185.

Holz, M., Zarebanadkouki, M., Carminati, A., & Kuzyakov, Y. (2019). Visualization and quantification of root exudation using 14 C imaging: challenges and uncertainties. *Plant and Soil*, *437*, 473-485.

Holz, M., Zarebanadkouki, M., Kaestner, A., Kuzyakov, Y., & Carminati, A. (2018). Rhizodeposition under drought is controlled by root growth rate and rhizosphere water content. *Plant and Soil*, *423*, 429-442.

Hu, L., Robert, C. A., Cadot, S., Zhang, X., Ye, M., Li, B., Manzo, D., Chervet, N., Steinger, T., & Van Der Heijden, M. G. (2018). Root exudate metabolites drive plant-soil feedbacks on growth and defense by shaping the rhizosphere microbiota. *Nature communications*, *9*(1), 1-13.

Hubeau, M., & Steppe, K. (2015). Plant-PET scans: in vivo mapping of xylem and phloem functioning. *Trends in plant science*, *20*(10), 676-685.

Hungate, B. A., Marks, J. C., Power, M. E., Schwartz, E., van Groenigen, K. J., Blazewicz, S. J., Chuckran, P., Dijkstra, P., Finley, B. K., & Firestone, M. K. (2021). The functional significance of bacterial predators. *MBio*, *12*(2), 10.1128/mbio. 00466-00421.

Hungate, B. A., Mau, R. L., Schwartz, E., Caporaso, J. G., Dijkstra, P., van Gestel, N., Koch, B. J., Liu, C. M., McHugh, T. A., & Marks, J. C. (2015). Quantitative microbial ecology through stable isotope probing. *Applied and Environmental Microbiology*, *81*(21), 7570-7581.

Hünninghaus, M., Dibbern, D., Kramer, S., Koller, R., Pausch, J., Schloter-Hai, B., Urich, T., Kandeler, E., Bonkowski, M., & Lueders, T. (2019). Disentangling carbon flow across microbial kingdoms in the rhizosphere of maize. *Soil Biology and Biochemistry*, *134*, 122-130.

Hütsch, B. W., Augustin, J., & Merbach, W. (2002). Plant rhizodeposition—an important source for carbon turnover in soils. *J. Plant. Nutr. Soil Sci*, *165*(4), 397-407.

Ikenaga, M., & Sakai, M. (2014). Application of locked nucleic acid (LNA) oligonucleotide–PCR clamping technique to selectively PCR amplify the SSU rRNA genes of bacteria in investigating the plant-associated community structures. *Microbes and environments*, ME14061.

Jaeger, C. H., Lindow, S. E., Miller, W., Clark, E., & Firestone, M. (1999). Mapping of sugar and amino acid availability in soil around roots with bacterial sensors of sucrose and tryptophan. *Applied and Environmental Microbiology*, *65*(6), 2685-2690.

Jahnke, S., Menzel, M. I., Van Dusschoten, D., Roeb, G. W., Bühler, J., Minwuyelet, S., Blümler, P., Temperton, V. M., Hombach, T., & Streun, M. (2009). Combined MRI–PET dissects dynamic changes in plant structures and functions. *The Plant Journal*, *59*(4), 634-644.

Jones, D. L., Hodge, A., & Kuzyakov, Y. (2004). Plant and mycorrhizal regulation of rhizodeposition. *New Phytologist*, *163*(3), 459-480.

Jones, D. L., Nguyen, C., & Finlay, R. D. (2009). Carbon flow in the rhizosphere: carbon trading at the soil–root interface. *Plant and Soil*, *321*(1-2), 5-33.

Jorda, H., Ahmed, M. A., Javaux, M., Carminati, A., Duddek, P., Vetterlein, D., & Vanderborght, J. (2022). Field scale plant water relation of maize (Zea mays) under drought–impact of root hairs and soil texture. *Plant and Soil*, *478*(1), 59-84.

Katoh, K., & Standley, D. M. (2013). MAFFT multiple sequence alignment software version 7: improvements in performance and usability. *Molecular biology and evolution*, *30*(4), 772-780.

Kawasaki, A., Dennis, P. G., Forstner, C., Raghavendra, A. K., Richardson, A. E., Watt, M., Mathesius, U., Gilliham, M., & Ryan, P. R. (2021). The microbiomes on the roots of wheat (*Triticum aestivum* L.) and rice (*Oryza sativa* L.) exhibit significant differences in structure between root types and along root axes. *Functional Plant Biology*, *48(9)*, 871-888.

Kawasaki, A., Donn, S., Ryan, P. R., Mathesius, U., Devilla, R., Jones, A., & Watt, M. (2016). Microbiome and exudates of the root and rhizosphere of *Brachypodium distachyon*, a model for wheat. *PloS one*, *11*(10).

Kawasaki, A., Okada, S., Zhang, C., Delhaize, E., Mathesius, U., Richardson, A. E., Watt, M., Gilliham, M., & Ryan, P. R. (2018). A sterile hydroponic system for characterising root exudates from specific root types and whole-root systems of large crop plants. *Plant methods*, *14*(1), 1-13.

Keel, S. G., Campbell, C. D., Högberg, M. N., Richter, A., Wild, B., Zhou, X., Hurry, V., Linder, S., Näsholm, T., & Högberg, P. (2012). Allocation of carbon to fine root compounds and their residence times in a boreal forest depend on root size class and season. *New Phytologist*, *194*(4), 972-981.

Keyes, S. D., Zygalakis, K. C., & Roose, T. (2017). An explicit structural model of root hair and soil interactions parameterised by synchrotron X-ray computed tomography. *Bulletin of Mathematical Biology*, *79*, 2785-2813.

Khanipour Roshan, S., Dumack, K., Bonkowski, M., Leinweber, P., Karsten, U., & Glaser, K. (2021). Taxonomic and functional diversity of heterotrophic protists (Cercozoa and endomyxa) from biological soil crusts. *Microorganisms*, *9*(2), 205.

Koller, R., Rodriguez, A., Robin, C., Scheu, S., & Bonkowski, M. (2013). Protozoa enhance foraging efficiency of arbuscular mycorrhizal fungi for mineral nitrogen from organic matter in soil to the benefit of host plants. *New Phytologist*, *199*(1), 203-211.

Kong, X., Han, Z., Tai, X., Jin, D., Ai, S., Zheng, X., & Bai, Z. (2020). Maize (Zea mays L. Sp.) varieties significantly influence bacterial and fungal community in bulk soil, rhizosphere soil and phyllosphere. *FEMS microbiology ecology*, *96*(3), fiaa020.

Kuznetsova, A., Christensen, R. H. B., & Brockhoff, P. B. (2013). Different tests on lmer objects (of the lme4 package): Introducing the lmerTest package. The R User Conference, useR,

Kuzyakov, Y., & Blagodatskaya, E. (2015). Microbial hotspots and hot moments in soil: concept & review. *Soil Biology and Biochemistry*, *83*, 184-199.

Kuzyakov, Y., Domanski, G. J. J. o. P. N., & Science, S. (2000). Carbon input by plants into the soil. Review. *163*(4), 421-431.

Kuzyakov, Y., & Razavi, B. S. (2019). Rhizosphere size and shape: temporal dynamics and spatial stationarity. *Soil Biology and Biochemistry*, *135*, 343-360.

Lahti, L., & Shetty, S. (2018). Introduction to the microbiome R package. *Preprint at https://microbiome. github. io/tutorials*.

Landl, M., Haupenthal, A., Leitner, D., Kroener, E., Vetterlein, D., Bol, R., Vereecken, H., Vanderborght, J., & Schnepf, A. (2021). Simulating rhizodeposition patterns around growing and exuding root systems. *in silico Plants*, *3*(2), diab028.

Lennon, J. T., & Jones, S. E. (2011). Microbial seed banks: the ecological and evolutionary implications of dormancy. *Nature Reviews Microbiology*, *9*(2), 119.

Lenth, R. (2022). emmeans: Estimated Marginal Means, aka Least-Squares Means, R package version 1.8.3. https://CRAN.R-project.org/package=emmeans

Li, F., Qing, T., Wu, F., Yue, K., Zhu, J., & Ni, X. (2024). Trade-off in the partitioning of recent photosynthate carbon under global change. *Global Change Biology*, *30*(1), e17110.

Li, J., Van Gerrewey, T., & Geelen, D. (2022). A meta-analysis of biostimulant yield effectiveness in field trials. *Frontiers in plant science*.

Li, X., Rui, J., Mao, Y., Yannarell, A., & Mackie, R. (2014). Dynamics of the bacterial community structure in the rhizosphere of a maize cultivar. *Soil Biology and Biochemistry*, *68*, 392-401.

Liljeroth, E., Burgers, S., & Van Veen, J. (1991). Changes in bacterial populations along roots of wheat (*Triticum aestivum* L.) seedlings. *Biol. Fertil. Soils*, *10*(4), 276-280.

Ling, N., Wang, T., & Kuzyakov, Y. (2022). Rhizosphere bacteriome structure and functions. *Nature communications*, *13*(1), 836.

Lippold, E., Phalempin, M., Schlüter, S., & Vetterlein, D. (2021). Does the lack of root hairs alter root system architecture of Zea mays? *Plant and Soil*, *467*(1), 267-286.

Liu, S., He, F., Kuzyakov, Y., Xiao, H., Hoang, D. T. T., Pu, S., & Razavi, B. S. (2022). Nutrients in the rhizosphere: A meta-analysis of content, availability, and influencing factors. *Science of the Total Environment*, *826*, 153908.

Liu, X., Zhao, H., & Chen, S. (2006). Colonization of maize and rice plants by strain Bacillus megaterium C4. *Current microbiology*, *52*, 186-190.

Loo, E. P.-I., Durán, P., Pang, T. Y., Westhoff, P., Deng, C., Durán, C., Lercher, M., Garrido-Oter, R., & Frommer, W. B. (2024). Sugar transporters spatially organize microbiota colonization along the longitudinal root axis of Arabidopsis. *Cell Host & Microbe*, *32*(4), 543-556. e546.

Lopez, G., Ahmadi, S. H., Amelung, W., Athmann, M., Ewert, F., Gaiser, T., Gocke, M. I., Kautz, T., Postma, J., & Rachmilevitch, S. (2023). Nutrient deficiency effects on root architecture and root-to-shoot ratio in arable crops. *Frontiers in plant science*, *13*, 1067498.

Love, M. I., Huber, W., & Anders, S. (2014). Moderated estimation of fold change and dispersion for RNA-seq data with DESeq2. *Genome biology*, *15*(12), 1-21.

Lueders, T. (2010). Stable isotope probing of hydrocarbon-degraders. In *Handbook of hydrocarbon and lipid microbiology*.

Lynch, J. P. (2013). Steep, cheap and deep: an ideotype to optimize water and N acquisition by maize root systems. *Annals of botany*, *112*(2), 347-357.

Lynch, J. P. (2015). Root phenes that reduce the metabolic costs of soil exploration: opportunities for 21st century agriculture. *Plant, Cell & Environment*, *38*(9), 1775-1784.

Maloney, P., Van Bruggen, A., & Hu, S. (1997). Bacterial community structure in relation to the carbon environments in lettuce and tomato rhizospheres and in bulk soil. *Microbial Ecology*, *34*(2), 109-117.

Manter, D. K., & Vivanco, J. M. (2007). Use of the ITS primers, ITS1F and ITS4, to characterize fungal abundance and diversity in mixed-template samples by qPCR and length heterogeneity analysis. *Journal of Microbiological Methods*, *71*(1), 7-14.

Marschner, P., Crowley, D., & Rengel, Z. (2011). Rhizosphere interactions between microorganisms and plants govern iron and phosphorus acquisition along the root axis–model and research methods. *Soil Biology and Biochemistry*, *43*(5), 883-894.

Marschner, P., Yang, C.-H., Lieberei, R., & Crowley, D. E. (2001). Soil and plant specific effects on bacterial community composition in the rhizosphere. *Soil Biology and Biochemistry*, *33*(11), 1437-1445.

Martin, M. (2011). Cutadapt removes adapter sequences from high-throughput sequencing reads. *EMBnet Journal*, *17*(1), 10-12.

Massalha, H., Korenblum, E., Malitsky, S., Shapiro, O. H., & Aharoni, A. (2017). Live imaging of root–bacteria interactions in a microfluidics setup. *Proceedings of the National Academy of Sciences*, *114*(17), 4549-4554.

McMurdie, P. J., & Holmes, S. (2013). phyloseq: an R package for reproducible interactive analysis and graphics of microbiome census data. *PloS one*, *8*(4).

Mendes, R., Garbeva, P., & Raaijmakers, J. M. (2013). The rhizosphere microbiome: significance of plant beneficial, plant pathogenic, and human pathogenic microorganisms. *FEMS microbiology reviews*, *37*(5), 634-663.

Metzner, R., Chlubek, A., Bühler, J., Pflugfelder, D., Schurr, U., Huber, G., Koller, R., & Jahnke, S. (2022). In vivo imaging and quantification of carbon tracer dynamics in nodulated root systems of pea plants. *Plants*, *11*(5), 632.

Metzner, R., Eggert, A., Van Dusschoten, D., Pflugfelder, D., Gerth, S., Schurr, U., Uhlmann, N., & Jahnke, S. (2015). Direct comparison of MRI and X-ray CT technologies for 3D imaging of root systems in soil: potential and challenges for root trait quantification. *Plant methods*, *11*(1), 17.

Micallef, S. A., Channer, S., Shiaris, M. P., & Colón-Carmona, A. (2009). Plant age and genotype impact the progression of bacterial community succession in the Arabidopsis rhizosphere. *Plant signaling & behavior*, *4*(8), 777-780.

Minasny, B., Malone, B. P., McBratney, A. B., Angers, D. A., Arrouays, D., Chambers, A., Chaplot, V., Chen, Z.-S., Cheng, K., & Das, B. S. (2017). Soil carbon 4 per mille. *Geoderma*, *292*, 59-86.

Modrzewska, M., Bryła, M., Kanabus, J., & Pierzgalski, A. (2022). Trichoderma as a biostimulator and biocontrol agent against Fusarium in the production of cereal crops: Opportunities and possibilities. *Plant Pathology*, *71*(7), 1471-1485.

Monteiro, R. A., Schmidt, M. A., Baura, V. A. d., Balsanelli, E., Wassem, R., Yates, M. G., Randi, M. A., Pedrosa, F. O., & Souza, E. M. d. (2008). Early colonization pattern of maize (Zea mays L. Poales, Poaceae) roots by Herbaspirillum seropedicae (Burkholderiales, Oxalobacteraceae). *Genetics and Molecular Biology*, *31*, 932-937.

Müllers, Y., Postma, J. A., Poorter, H., Kochs, J., Pflugfelder, D., Schurr, U., & Van Dusschoten, D. (2022). Shallow roots of different crops have greater water uptake rates per unit length than deep roots in well-watered soil. *Plant and Soil*, *481*(1), 475-493.

Munoz-Ucros, J., Zwetsloot, M. J., Cuellar-Gempeler, C., & Bauerle, T. L. (2021). Spatiotemporal patterns of rhizosphere microbiome assembly: From ecological theory to agricultural application. *Journal of Applied Ecology*, *58*(5), 894-904.

Nagel, K. A., Putz, A., Gilmer, F., Heinz, K., Fischbach, A., Pfeifer, J., Faget, M., Blossfeld, S., Ernst, M., & Dimaki, C. (2012). GROWSCREEN-Rhizo is a novel phenotyping robot enabling simultaneous measurements of root and shoot growth for plants grown in soil-filled rhizotrons. *Functional Plant Biology*, *39*(11), 891-904.

Neufeld, J. D., Vohra, J., Dumont, M. G., Lueders, T., Manefield, M., Friedrich, M. W., & Murrell, J. C. (2007). DNA stable-isotope probing. *Nature protocols*, *2*(4), 860.

Nguyen, C. (2003). Rhizodeposition of organic C by plants: mechanisms and controls. *Agronomie*, *23*(5-6), 375-396.

Nguyen, C. (2009). Rhizodeposition of organic C by plants: mechanisms and controls. In E. Lichtfouse, M. Navarrete, P. Debaeke, S. Véronique, & C. Alberola (Eds.), *Sustainable Agriculture* (pp. 375-396). Springer, Dordrecht.

Nuccio, E. E., Starr, E., Karaoz, U., Brodie, E. L., Zhou, J., Tringe, S., Malmstrom, R. R., Woyke, T., Banfield, J. F., & Firestone, M. K. J. b. (2019). Niche differentiation is spatially and temporally regulated in the rhizosphere. 611863.

Oburger, E., & Jones, D. L. (2018). Sampling root exudates–mission impossible? *Rhizosphere*, *6*, 116-133.

Oburger, E., & Schmidt, H. (2016). New methods to unravel rhizosphere processes. *Trends in plant science*, *21*(3), 243-255.

Okello, P. N., Petrović, K., Kontz, B., & Mathew, F. M. (2019). Eight species of Fusarium cause root rot of corn (Zea mays) in South Dakota. *Plant Health Progress*, *20*(1), 38-43.

Orman-Ligeza, B., Parizot, B., Gantet, P. P., Beeckman, T., Bennett, M. J., & Draye, X. (2013). Post-embryonic root organogenesis in cereals: branching out from model plants. *Trends in plant science*, *18*(8), 459-467.

Pandey, B. K., & Bennett, M. J. (2024). Uncovering root compaction response mechanisms: new insights and opportunities. *Journal of Experimental Botany*, *75*(2), 578-583.

Park, W. J., Hochholdinger, F., & Gierl, A. (2004). Release of the benzoxazinoids defense molecules during lateral-and crown root emergence in Zea mays. *Journal of Plant Physiology*, *161*(8), 981-985.

Paterson, E., Gebbing, T., Abel, C., Sim, A., & Telfer, G. (2007). Rhizodeposition shapes rhizosphere microbial community structure in organic soil. *New Phytologist*, *173*(3), 600-610.

Pausch, J., & Kuzyakov, Y. (2011). Photoassimilate allocation and dynamics of hotspots in roots visualized by ^{14}C phosphor imaging. *Journal of plant nutrition and soil science*, *174*(1), 12-19.

Pausch, J., & Kuzyakov, Y. (2018). Carbon input by roots into the soil: Quantification of rhizodeposition from root to ecosystem scale. *Global Change Biology*, *24*(1), 1-12.

Peiffer, J. A., Spor, A., Koren, O., Jin, Z., Tringe, S. G., Dangl, J. L., Buckler, E. S., & Ley, R. E. (2013). Diversity and heritability of the maize rhizosphere microbiome under field conditions. *Proceedings of the National Academy of Sciences*, *110*(16), 6548-6553.

Pett-Ridge, J., & Firestone, M. K. (2017). Using stable isotopes to explore root-microbe-mineral interactions in soil. *Rhizosphere*, *3*, 244-253.

Pflugfelder, D., Metzner, R., Dusschoten, D., Reichel, R., Jahnke, S., & Koller, R. (2017). Non-invasive imaging of plant roots in different soils using magnetic resonance imaging (MRI). *Plant methods*, *13*(1), 102.

Philippot, L., Raaijmakers, J. M., Lemanceau, P., & Van Der Putten, W. H. (2013). Going back to the roots: the microbial ecology of the rhizosphere. *Nature Reviews Microbiology*, *11*(11), 789.

Poorter, H., Niklas, K. J., Reich, P. B., Oleksyn, J., Poot, P., & Mommer, L. (2012). Biomass allocation to leaves, stems and roots: meta-analyses of interspecific variation and environmental control. *New Phytologist*, *193*(1), 30-50.

Postma, J. A., & Lynch, J. P. (2011). Theoretical evidence for the functional benefit of root cortical aerenchyma in soils with low phosphorus availability. *Annals of botany*, *107*(5), 829-841.

Qian, X., Li, H., Wang, Y., Wu, B., Wu, M., Chen, L., Li, X., Zhang, Y., Wang, X., & Shi, M. (2019). Leaf and root endospheres harbor lower fungal diversity and less complex fungal co-occurrence patterns than rhizosphere. *Frontiers in microbiology*, *10*, 1015.

Qiao, Y., Miao, S., Han, X., Yue, S., & Tang, C. (2017). Improving soil nutrient availability increases carbon rhizodeposition under maize and soybean in Mollisols. *Science of the Total Environment*, *603*, 416-424.

Quast, C., Pruesse, E., Yilmaz, P., Gerken, J., Schweer, T., Yarza, P., Peplies, J., & Glöckner, F. O. (2012). The SILVA ribosomal RNA gene database project: improved data processing and web-based tools. *Nucleic acids research*, *41*(D1), D590-D596.

Rattray, E. A., Paterson, E., & Killham, K. (1995). Characterisation of the dynamics of C-partitioning within *Lolium perenne* and to the rhizosphere microbial biomass using ^{14}C pulse chase. *Biology and Fertility of Soils*, *19*(4), 280-286.

Razavi, B. S., Zarebanadkouki, M., Blagodatskaya, E., & Kuzyakov, Y. (2016). Rhizosphere shape of lentil and maize: spatial distribution of enzyme activities. *Soil Biology and Biochemistry*, *96*, 229-237.

Remus, R., & Augustin, J. (2016). Dynamic linking of 14 C partitioning with shoot growth allows a precise determination of plant-derived C input to soil. *Plant and Soil*, *408*, 493-513.

Rich, S. M., & Watt, M. (2013). Soil conditions and cereal root system architecture: review and considerations for linking Darwin and Weaver. *Journal of Experimental Botany*, *64*(5), 1193-1208.

Rogers, E. D., Monaenkova, D., Mijar, M., Nori, A., Goldman, D. I., & Benfey, P. N. (2016). X-ray computed tomography reveals the response of root system architecture to soil texture. *Plant Physiology*, *171*(3), 2028-2040.

Rognes, T., Flouri, T., Nichols, B., Quince, C., & Mahé, F. (2016). VSEARCH: a versatile open source tool for metagenomics. *PeerJ*, *4*, e2584.

Röttjers, L., & Faust, K. (2018). From hairballs to hypotheses–biological insights from microbial networks. *FEMS microbiology reviews*, *42*(6), 761-780.

Rüger, L., Feng, K., Chen, Y., Sun, R., Sun, B., Deng, Y., Vetterlein, D., & Bonkowski, M. (2022). Responses of Root Architecture and the Rhizosphere Microbiome Assembly of Maize (Zea Mays L.) to a Soil Texture Gradient. *Available at SSRN 4273732*.

Rüger, L., Feng, K., Dumack, K., Freudenthal, J., Chen, Y., Sun, R., Wilson, M., Yu, P., Sun, B., & Deng, Y. (2021). Assembly patterns of the rhizosphere microbiome along the longitudinal root axis of maize (*Zea mays* L.). *Frontiers in microbiology*, *12*, 237.

Rüger, L., Ganther, M., Freudenthal, J., Jansa, J., Heintz-Buschart, A., Tarkka, M. T., & Bonkowski, M. (2023). Root cap is an important determinant of rhizosphere microbiome assembly. *New Phytologist*, *239*(4), 1434-1448.

Sasse, J., Martinoia, E., & Northen, T. J. T. i. p. s. (2018). Feed your friends: do plant exudates shape the root microbiome? , *23*(1), 25-41.

Sasvári, Z., Hornok, L., & Posta, K. (2011). The community structure of arbuscular mycorrhizal fungi in roots of maize grown in a 50-year monoculture. *Biology and Fertility of Soils*, *47*, 167-176.

Schimel, J. P., & Weintraub, M. N. (2003). The implications of exoenzyme activity on microbial carbon and nitrogen limitation in soil: a theoretical model. *Soil Biology and Biochemistry*, *35*(4), 549-563.

Schloss, P. D., Westcott, S. L., Ryabin, T., Hall, J. R., Hartmann, M., Hollister, E. B., Lesniewski, R. A., Oakley, B. B., Parks, D. H., & Robinson, C. J. (2009). Introducing mothur: open-source, platform-independent, community-supported software for describing and comparing microbial communities. *Applied and Environmental Microbiology*, *75*(23), 7537-7541.

Schneider, H. M., Postma, J. A., Kochs, J., Pflugfelder, D., Lynch, J. P., & van Dusschoten, D. (2020). Spatio-temporal variation in water uptake in seminal and nodal root systems of barley plants grown in soil. *Frontiers in plant science*, *11*, 1247.

Schnepf, A., Carminati, A., Ahmed, M. A., Ani, M., Benard, P., Bentz, J., Bonkowski, M., Knott, M., Diehl, D., & Duddek, P. (2022). Linking rhizosphere processes across scales: Opinion. *Plant and Soil*, *478*(1), 5-42.

Schütz, V., Frindte, K., Cui, J., Zhang, P., Hacquard, S., Schulze-Lefert, P., Knief, C., Schulz, M., & Dörmann, P. (2021). Differential impact of plant secondary metabolites on the soil microbiota. *Frontiers in microbiology*, *12*, 666010.

Seaton, F. M., George, P. B., Lebron, I., Jones, D. L., Creer, S., & Robinson, D. A. (2020). Soil textural heterogeneity impacts bacterial but not fungal diversity. *Soil Biology and Biochemistry*, *144*, 107766.

Sessitsch, A., Weilharter, A., Gerzabek, M. H., Kirchmann, H., & Kandeler, E. (2001). Microbial population structures in soil particle size fractions of a long-term fertilizer field experiment. *Applied and Environmental Microbiology*, *67*(9), 4215-4224.

Shannon, P., Markiel, A., Ozier, O., Baliga, N. S., Wang, J. T., Ramage, D., Amin, N., Schwikowski, B., & Ideker, T. (2003). Cytoscape: a software environment for integrated models of biomolecular interaction networks. *Genome research*, *13*(11), 2498-2504.

Shiferaw, B., Prasanna, B. M., Hellin, J., & Bänziger, M. (2011). Crops that feed the world 6. Past successes and future challenges to the role played by maize in global food security. *Food security*, *3*, 307-327.

Sible, C. N., Seebauer, J. R., & Below, F. E. (2021). Plant biostimulants: A categorical review, their implications for row crop production, and relation to soil health indicators. *Agronomy*, *11*(7), 1297.

Sivasithamparam, K., Parker, C., & Edwards, C. (1979). Rhizosphere micro-organisms of seminal and nodal roots of wheat grown in pots. *Soil Biology and Biochemistry*, *11*(2), 155-160.

Somasundaram, S., P. Rao, T., Tatsumi, J., & Iijima, M. (2009). Rhizodeposition of mucilage, root border cells, carbon and water under combined soil physical stresses in Zea mays L. *Plant Production Science*, *12*(4), 443-448.

Stefan, G., Cornelia, B., Jörg, R., & Michael, B. (2014). Soil water availability strongly alters the community composition of soil protists. *Pedobiologia*, *57*(4-6), 205-213.

Steinkellner, S., Lendzemo, V., Langer, I., Schweiger, P., Khaosaad, T., Toussaint, J.-P., & Vierheilig, H. (2007). Flavonoids and strigolactones in root exudates as signals in symbiotic and pathogenic plant-fungus interactions. *Molecules*, *12*(7), 1290-1306.

Stelpflug, S. C., Sekhon, R. S., Vaillancourt, B., Hirsch, C. N., Buell, C. R., de Leon, N., & Kaeppler, S. M. (2016). An expanded maize gene expression atlas based on RNA sequencing and its use to explore root development. *The plant genome*, *9*(1), plantgenome2015.2004.0025.

Tackmann, J., Rodrigues, J. F. M., & von Mering, C. (2019). Rapid inference of direct interactions in large-scale ecological networks from heterogeneous microbial sequencing data. *Cell systems*, *9*(3), 286-296. e288.

Taerum, S. J., Micciulla, J., Corso, G., Steven, B., Gage, D. J., & Triplett, L. R. (2022). 18S rRNA gene amplicon sequencing combined with culture-based surveys of maize rhizosphere protists reveal dominant, plant-enriched and culturable community members. *Environmental microbiology reports*, *14*(1), 110-118.

Tai, H., Lu, X., Opitz, N., Marcon, C., Paschold, A., Lithio, A., Nettleton, D., & Hochholdinger, F. (2016). Transcriptomic and anatomical complexity of primary, seminal, and crown roots highlight root type-specific functional diversity in maize (*Zea mays* L.). *J. Exp. Bot*, *67*(4), 1123-1135.

Thoenen, L., Kreuzer, M., Pestalozzi, C., Florean, M., Mateo, P., Züst, T., Wei, A., Giroud, C., Rouyer, L., & Gfeller, V. (2024). The lactonase BxdA mediates metabolic specialisation of maize root bacteria to benzoxazinoids. *Nature communications*, *15*(1), 6535.

Tiziani, R., Miras-Moreno, B., Malacrinò, A., Vescio, R., Lucini, L., Mimmo, T., Cesco, S., & Sorgonà, A. (2022). Drought, heat, and their combination impact the root exudation patterns and rhizosphere microbiome in maize roots. *Environmental and Experimental Botany*, *203*, 105071.

Tournier, E., Amenc, L., Pablo, A.-L., Legname, E., Blanchart, E., Plassard, C., Robin, A., & Bernard, L. (2015). Modification of a commercial DNA extraction kit for safe and rapid recovery of DNA and RNA simultaneously from soil, without the use of harmful solvents. *MethodsX*, *2*, 182-191.

Trachsel, S., Kaeppler, S. M., Brown, K. M., & Lynch, J. P. (2011). Shovelomics: high throughput phenotyping of maize (Zea mays L.) root architecture in the field. *Plant and Soil*, *341*, 75-87.

Trap, J., Bonkowski, M., Plassard, C., Villenave, C., & Blanchart, E. (2016). Ecological importance of soil bacterivores for ecosystem functions. *Plant and Soil*, *398*, 1-24.

USDA. (2017). The Soil Survey Manual. 120. https://www.nrcs.usda.gov/sites/default/files/2022-09/The-Soil-Survey-Manual.pdf

Van Bruggen, A., Semenov, A., & Zelenev, V. (2000). Wavelike distributions of microbial populations along an artificial root moving through soil. *Microbial Ecology*, *40*(3), 250-259.

Van Diepeningen, A. D., De Vos, O. J., Zelenev, V. V., Semenov, A. M., & Van Bruggen, A. H. (2005). DGGE fragments oscillate with or counter to fluctuations in cultivable bacteria along wheat roots. *Microbial Ecology*, *50*, 506-517.

van Dusschoten, D., Kochs, J., Kuppe, C. W., Sydoruk, V. A., Couvreur, V., Pflugfelder, D., & Postma, J. A. (2020). Spatially resolved root water uptake determination using a precise soil water sensor. *Plant Physiology*, *184*(3), 1221-1235.

van Dusschoten, D., Metzner, R., Kochs, J., Postma, J. A., Pflugfelder, D., Bühler, J., Schurr, U., & Jahnke, S. (2016). Quantitative 3D analysis of plant roots growing in soil using magnetic resonance imaging. *Plant Physiology*, pp. 01388.02015.

Van Vuurde, J., & Schippers, B. (1980). Bacterial colonization of seminal wheat roots. *Soil Biology and Biochemistry*, *12*(6), 559-565.

Vanhees, D. J., Schneider, H. M., Sidhu, J. S., Loades, K. W., Bengough, A. G., Bennett, M. J., Pandey, B. K., Brown, K. M., Mooney, S. J., & Lynch, J. P. (2022). Soil penetration by maize roots is negatively related to ethylene-induced thickening. *Plant, Cell & Environment*, *45*(3), 789-804.

Veach, A. M., Morris, R., Yip, D. Z., Yang, Z. K., Engle, N. L., Cregger, M. A., Tschaplinski, T. J., & Schadt, C. W. (2019). Rhizosphere microbiomes diverge among Populus trichocarpa plant-host genotypes and chemotypes, but it depends on soil origin. *Microbiome*, *7*(1), 1-15.

Vetterlein, D., Carminati, A., Kögel-Knabner, I., Bienert, G. P., Smalla, K., Oburger, E., Schnepf, A., Banitz, T., Tarkka, M. T., & Schlüter, S. (2020). Rhizosphere spatiotemporal organization–a key to rhizosphere functions. *Frontiers in agronomy*, *2*, 8.

Vetterlein, D., Lippold, E., Schreiter, S., Phalempin, M., Fahrenkampf, T., Hochholdinger, F., Marcon, C., Tarkka, M., Oburger, E., & Ahmed, M. (2021). Experimental platforms for the investigation of spatiotemporal patterns in the rhizosphere - laboratory and field scale. *Jorunal of Plant Nutrition and Soil Science*, *184*(1), 35-50.

Waarde, A. v. (2012). Introduction on pet: Description of basics and principles. In *Trends On The Role Of Pet In Drug Development* (pp. 1-13). World Scientific.

Wagner, M. R., Lundberg, D. S., Del Rio, T. G., Tringe, S. G., Dangl, J. L., & Mitchell-Olds, T. (2016). Host genotype and age shape the leaf and root microbiomes of a wild perennial plant. *Nature communications*, *7*(1), 12151.

Wallace, J. G., & May, G. (2018). Endophytes: The other maize genome. *The maize genome*, 213-246.

Waller, S., Wilder, S. L., Schueller, M. J., Housh, A. B., & Ferrieri, R. A. (2020). Quantifying plant-borne carbon assimilation by root-associating bacteria. *Microorganisms*, *8*(5), 700.

Watt, M., Hugenholtz, P., White, R., & Vinall, K. (2006). Numbers and locations of native bacteria on field-grown wheat roots quantified by fluorescence in situ hybridization (FISH). *Environmental microbiology*, *8*(5), 871-884.

Watt, M., Kirkegaard, J., & Passioura, J. (2006). Rhizosphere biology and crop productivity—a review. *Soil Research*, *44*(4), 299-317.

Watt, M., Silk, W., & Passioura, J. (2006). Rates of root and organism growth, soil conditions, and temporal and spatial development of the rhizosphere. *Annals of botany*, *97*(5), 839-855.

Wen, T., Xie, P., Penton, C. R., Hale, L., Thomashow, L. S., Yang, S., Ding, Z., Su, Y., Yuan, J., & Shen, Q. (2022). Specific metabolites drive the deterministic assembly of diseased rhizosphere microbiome through weakening microbial degradation of autotoxin. *Microbiome*, *10*(1), 177.

Wendel, A. S., Bauke, S. L., Amelung, W., & Knief, C. (2022). Root-rhizosphere-soil interactions in biopores. *Plant and Soil*, *475*(1), 253-277.

Werner, L. M., Knott, M., Diehl, D., Ahmed, M. A., Banfield, C., Dippold, M., Vetterlein, D., & Wimmer, M. A. (2022). Physico-chemical properties of maize (Zea mays L.) mucilage differ with the collection system and corresponding root type and developmental stage of the plant. *Plant and Soil*, *478*(1-2), 103-117.

Werth, M., & Kuzyakov, Y. (2006). Assimilate partitioning affects ^{13}C fractionation of recently assimilated carbon in maize. *Plant Soil*, *284*(1), 319-333.

Werth, M., & Kuzyakov, Y. (2010). 13C fractionation at the root–microorganisms–soil interface: a review and outlook for partitioning studies. *Soil Biology and Biochemistry*, *42*(9), 1372-1384.

Wheatley, R. M., & Poole, P. S. (2018). Mechanisms of bacterial attachment to roots. *FEMS microbiology reviews*, *42*(4), 448-461.

White, T. J., Bruns, T., Lee, S., & Taylor, J. (1990). Amplification and direct sequencing of fungal ribosomal RNA genes for phylogenetics. In Innis MA, Gelfand DH, Sninsky JJ, & W. TJ (Eds.), *PCR protocols: a guide to methods and applications* (pp. 315-322). Academic Press, London.

Wickham, H. (2016). Data analysis. In *ggplot2* (pp. 189-201). Springer.

Xia, Q., Rufty, T., & Shi, W. (2020). Soil microbial diversity and composition: Links to soil texture and associated properties. *Soil Biology and Biochemistry*, *149*, 107953.

Yamawaki, M., Kanno, S., Ishibashi, H., Noda, A., Hirose, A., Tanoi, K., & Nakanishi, T. (2011). A study of 32P-phosphate uptake in a plant by a real-time RI imaging system. *Proceedings in Radiochemistry*, *1*(1), 287-291.

Yao, H., Chapman, S. J., Thornton, B., & Paterson, E. (2015). 13 C PLFAs: a key to open the soil microbial black box? *Plant and Soil*, *392*, 3-15.

Ye, J., Guo, Y., Zhang, D., Zhang, N., Wang, C., & Xu, M. (2013). Cytological and molecular characterization of quantitative trait locus qRfg1, which confers resistance to Gibberella stalk rot in maize. *Molecular plant-microbe interactions*, *26*(12), 1417-1428.

Yim, B., Ibrahim, Z., Rüger, L., Ganther, M., Maccario, L., Sørensen, S. J., Heintz-Buschart, A., Tarkka, M. T., Vetterlein, D., & Bonkowski, M. (2022). Soil texture is a stronger driver of the maize rhizosphere microbiome and extracellular enzyme activities than soil depth or the presence of root hairs.

Youngblut, N. D., Barnett, S. E., & Buckley, D. H. (2018). HTSSIP: an R package for analysis of high throughput sequencing data from nucleic acid stable isotope probing (SIP) experiments. *PloS one*, *13*(1), e0189616.

Yu, P., Gutjahr, C., Li, C., & Hochholdinger, F. (2016). Genetic control of lateral root formation in cereals. *Trends in plant science*, *21*(11), 951-961.

Yu, P., He, X., Baer, M., Beirinckx, S., Tian, T., Moya, Y. A., Zhang, X., Deichmann, M., Frey, F. P., & Bresgen, V. (2021). Plant flavones enrich rhizosphere Oxalobacteraceae to improve maize performance under nitrogen deprivation. *Nature Plants*, *7*(4), 481-499.

Yu, P., Hochholdinger, F., & Li, C. (2019). Plasticity of lateral root branching in maize. *Frontiers in plant science*, *10*, 363.

Yu, P., Li, C., Li, M., He, X., Wang, D., Li, H., Marcon, C., Li, Y., Perez-Limón, S., & Chen, X. (2024). Seedling root system adaptation to water availability during maize domestication and global expansion. *Nature Genetics*, *56*, 1245-1256.

Yu, P., Wang, C., Baldauf, J. A., Tai, H., Gutjahr, C., Hochholdinger, F., & Li, C. (2018). Root type and soil phosphate determine the taxonomic landscape of colonizing fungi and the transcriptome of field-grown maize roots. *New Phytologist*, *217*(3), 1240-1253.

Yu, P., White, P. J., Hochholdinger, F., & Li, C. (2014). Phenotypic plasticity of the maize root system in response to heterogeneous nitrogen availability. *Planta*, *240*(4), 667-678.

Yue, Y., Liu, C., Xu, B., Wang, Y., Lv, Q., Zhou, Z., Li, R., Kowalchuk, G. A., Jousset, A., & Shen, Q. (2023). Rhizosphere shapes the associations between protistan predators and bacteria within microbiomes through the deterministic selection on bacterial communities. *Environmental microbiology*, *25*(12), 3623-3629.

Zai, X., Luo, W., Bai, W., Li, Y., Xiao, X., Gao, X., Wang, E., Wei, G., & Chen, W. (2021). Effect of root diameter on the selection and network interactions of root-associated bacterial microbiomes in Robinia pseudoacacia L. *Microbial Ecology*, 1-12.

Zelenev, V., Van Bruggen, A., & Semenov, A. (2005). Modeling wave-like dynamics of oligotrophic and copiotrophic bacteria along wheat roots in response to nutrient input from a growing root tip. *Ecological modeling*, *188*(2-4), 404-417.

Zhang, X., Bilyera, N., Fan, L., Duddek, P., Ahmed, M. A., Carminati, A., Kaestner, A., Dippold, M. A., Spielvogel, S., & Razavi, B. S. (2023). The spatial distribution of rhizosphere microbial activities under drought: water availability is more important than root-hair-controlled exudation. *New Phytologist*, *237*(3), 780-792.

Zou, Y., Zhang, Y., & Testerink, C. (2022). Root dynamic growth strategies in response to salinity. *Plant, Cell & Environment*, *45*(3), 695-704.

Zuur, A. F., Ieno, E. N., Walker, N. J., Saveliev, A. A., & Smith, G. M. (2009). *Mixed effects models and extensions in ecology with R* (Vol. 574). Springer.